The cytochrome P450 reductase enzyme contributes to normal cardiovascular function

Dissertation

zur Erlangung des Doktorgrades

der Naturwissenschaften

vorgelegt beim Fachbereich

Biochemie, Chemie und Pharmazie

der Johann Wolfgang Goethe-Universität

in Frankfurt am Main

von Frau Melina López Sciarra

aus Lausanne, Switzerland

Frankfurt am Main, 2023

(D30)

vom Fachbereich Biochemie, Chemie und Pharmazie (FB14) der
Johann Wolfgang Goethe-Universität als Dissertation angenommen.

Dekan:	Prof. Dr. Clemens Glaubitz (Johann Wolfgan Goethe-Universität, Frankfurt)
Gutachter:	Prof. Dr. Robert Fürst (Johann Wolfgan Goethe-Universität, Frankfurt)
	Prof. Dr. Ralf P. Brandes (Johann Wolfgan Goethe-Universität, Frankfurt)

Datum der Disputation: 07.09.2023

Contents

1 Introduction

1.1 Cytochrome P450 enzymes and cytochrome P450 reductase

1.1.1 The CYP450 enzymes

Cytochrome P450 (CYP450) enzymes are a superfamily of membrane-bound heme-containing monooxygenases present in all three kingdoms of life[1,2]. They are mainly localized to the endoplasmic reticulum (ER)[3]. Regarding their nomenclature, CYP450 enzymes are designated by “CYP” followed by an Arabic numeral for the family. The subfamily is represented with a letter and an end number depicts a member within a specific subfamily. As an example, the CYP3A1 refers to the CYP family 3, subfamily A and protein 1 of that subfamily[4,5]. CYP450 enzymes play two main roles in living organisms: oxidative metabolism of endogenous substrates (steroids, fatty acids, prostaglandins) and oxidative biotransformation of xenobiotics substrates such as drugs[6,7]. Although CYP450 enzymes catalyze a great number of reactions such as hydroxylation, dealkylation and epoxidation among others, they all incorporate one atom of oxygen to X-H bonds of substrate together with the concomitant reduction of an oxygen to water[5].

CYP450 enzymes are virtually expressed in all tissues with the highest expression being found in the liver and intestines[5,8]. Different factors influence CYP450 enzymes expression and their function such as genetic polymorphism, drugs, sex, fat distribution, age, diet as well as diseases[9]. These parameters are of importance in particular in the liver where about 15 isoforms belonging to the CYP families 1, 2 and 3 are part of the Phase I of drug metabolism[8–10]. In fact, several reports focus on the clinical impact of genetic variations and drug-drug interactions on drug-metabolizing CYP450[8,9]. Although the highest level of CYP450 isoenzymes is found in the liver, the cardiovascular expression is not negligible[11–13]. Vascular cells mainly express CYP2C and CYP2J epoxygenases as well as CYP4A ω-hydroxylase[11,14]. Those arachidonic acid metabolizing CYP450 enzymes generate epoxyeicosatrienoic acids (EETs) and hydroxyeicosatrienoic acids (HETEs), which are involved in vascular homeostasis[14]. The heart also expresses CYP450 enzymes and cardiomyocyte-derived EETs are associated with a cardioprotective role[15]. Thus, the role of CYP450 enzymes in cardiovascular diseases (hypertension, cardiomyopathy)[14] has been extensively studied.

1.1.2 The cytochrome P450 reductase

The enzymatic activity of all microsomal CYP450 isoenzymes depends on the cytochrome P450 reductase (POR). The ratio of CYP450:POR has been suggested to range between 5:1 and 20:1. CYP450 enzymes arrange in clusters, with a central POR surrounded by multiple CYP450 molecules[16,17]. POR is a membrane-bound diflavin reductase bound to the endoplasmic reticulum membrane by a N-terminal hydrophobic anchor[17]. Only two mammalian enzymes use FAD and FMN as cofactors, POR being one and the other being the nitric oxide synthase (NOS) enzymes[18]. Structurally, POR is composed of three domains: a nicotinamide adenine dinucleotide phosphate (NADPH)-binding domain, a flavin adenine dinucleotide (FAD)-binding domain and a flavin mononucleotide (FMN)-binding domain (**Figure 1**).

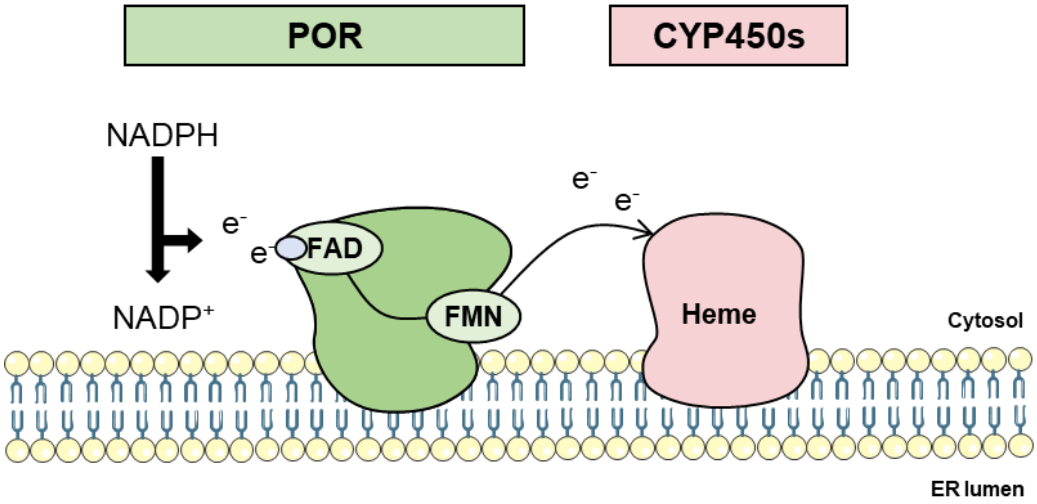

Figure 1: The cytochrome P450 reductase – cytochrome P450 system in endoplasmic reticulum. NADPH binds to the NADPH-binding domain (in blue) of POR and electrons are first transferred to the FAD domain, then flow through the FMN domain and distributed, one at the time, to CYP450 enzymes. In total, a cycle consists of the transfer of two electrons. Figure adapted from Mukherjee *et al.* (2021)[19] and Pandian *et al.* (2020)[20].
POR: cytochrome P450 reductase; CYP450: cytochrome P450 enzymes; NADPH: nicotinamide adenine dinucleotide phosphate; FAD: flavin adenine dinucleotide; FMN: flavin mononucleotide. ER: reticulum endoplasmic.

The electron transfer is initiated with the transfer of two electrons from NADPH to the redox cofactor FAD. Then, the electrons pass through the FMN domain which then transfers electrons, one a the time, to the redox partners of POR: CYP450 enzymes and hemeoxygenases (HO-1/2)[17,21]. Cytochrome b_5 enzymes can also accept electrons from POR and further deliver them to CYP450 enzymes[22].

Such electron transfers allow for the different functions of CYP450, like fatty acid anabolism, drugs metabolism, heme degradation and sterol biosynthesis (**Figure 2**).

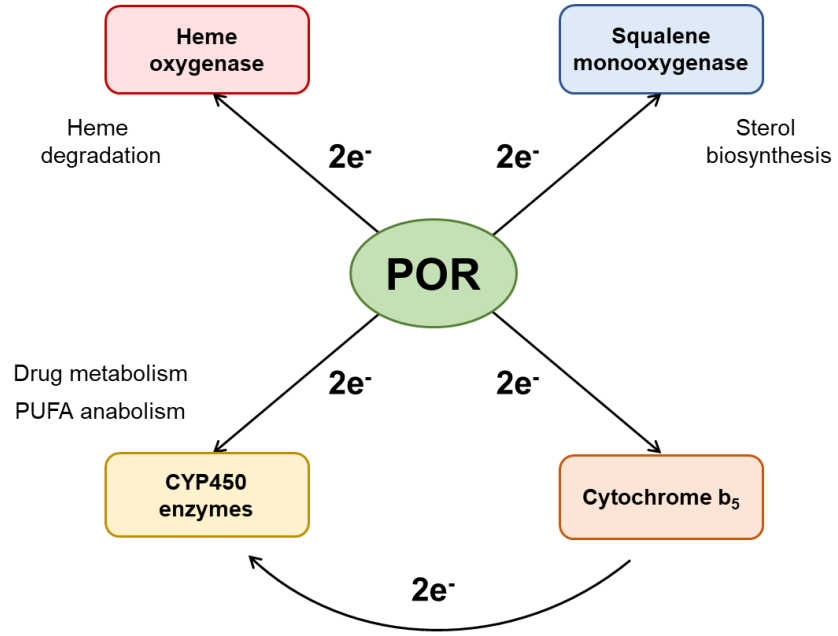

Figure 2. POR and its redox partners
POR is involved in different oxidative metabolic processes by distributing electrons to heme oxygenases, CYP450 enzymes and cytochrome b_5.
POR: cytochrome P450 reductase; e^-: electron; PUFA: polyunsaturated fatty acid.

The cytochrome P450 reductase POR is broadly expressed, as shown by Tabula Muris, a compendium of single cell transcriptome data from mice (https://tabula-muris.ds.czbiohub.org/). POR is virtually expressed in all organs with a distinct expression pattern across them (**Figure 3**). Moreover, POR is ubiquitously expressed in the cardiovascular system[23,24].

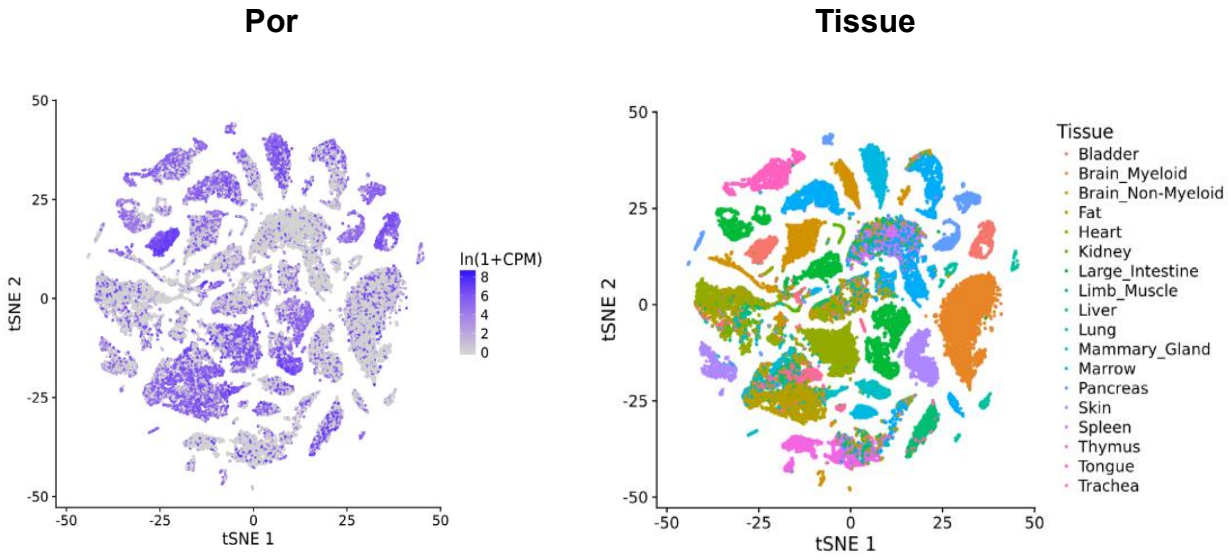

Figure 3. Expression of POR in murine tissues.
Generated from Tabula Muris website: https://tabula-muris.ds.czbiohub.org/.

Given that POR is essential for the activity of CYP450 and HO enzymes, its loss of function by mutations has consequences in multiple organ systems[25]. In fact, in the early stages of mammalian development microsomal deletion of POR leads to embryonic lethality explained by neural, eye, limb and cardiac abnormalities[26,27]. POR deficiency (PORD) is an autosomal recessive disorder causing steroidogenic disorders such as skeletal malformations known as Antley-Bixler syndrome (ABS) and insufficient glucocorticoid production[28]. A study published in 2004 by Arlt and collaborators reported congenital adrenal hyperplasia as an example of steroidogenic disorders caused by mutations in the encoding gene of POR[29].

So far most studies focused on single nucleotide polymorphisms (SNPs) in genes encoding drugs transporters and drug-metabolizing enzymes, such as CYP450 enzymes[30]. Interestingly, most drugs are metabolized by CYP450 enzymes, whose activity is POR-dependent (electron transfer), but genetic variations of POR in metabolism of drugs have not been evaluated yet[30]. SNPs in coding regions of POR and differences in SNP frequencies could potentially lead to variations within the population in metabolizing drugs[30]. In addition to its function in the metabolism of drug, the POR/CYP450 system is also important in the vasculature, where genetic variants of POR are associated with congestive heart failure and peripheral vascular diseases[31,32].

Whereas there are over 50 different CYP450 coding genes in humans and over 90 in mice, there is only one gene coding for POR[33,34]. Given that CYP450 enzymes have overlapping functions and similar tissue distribution profiles, lack of specific inhibitors or compensatory expression is a large limitation in the CYP450 research. Thus, targeting specific individual CYP450 for inhibition is almost impractible[35,36]. Knocking out POR makes it then a valuable strategy to switch off all CYP450 enzymes, in a cell-specific manner[37].

1.2 Endothelial nitric oxide synthase

Nitric oxide (NO) is a versatile molecule produced enzymatically by mammalian cells with a half-life of 3-5 seconds[38–40]. There are three isoforms of the nitric oxide synthase enzyme with endothelial nitric oxide synthase (eNOS), also called nitric oxide synthase 3 (NOS3), being one of these isoforms[41]. Structurally, eNOS is composed of a reductase domain, highly homologous to POR, and an oxygenase domain[42]. The C-terminal site contains the reductase activity of eNOS, which is composed of a FAD-binding domain, a FMN-binding domain and NADPH-binding domain. The N-terminal site contains the oxygenase activity of the enzyme which is composed of domains that bind a prosthetic heme group, a molecular oxygen, (6R-)5,6,7,8-tetrahydrobiopterin, and the substrate L-arginine[41,43,44].

The electron transfer is initiated in the carboxy-terminal reductase domain with the transfer of electrons from NADPH to the redox cofactor FAD. Electrons pass through the FMN domain and are distributed to the heme in the amino-terminal oxygenase domain. The electrons are used to reduce the molecular oxygen and oxidize L-arginine to L-citrulline and NO[43].

At the posttranslational level, the activity of eNOS is regulated by numerous mechanisms[44], among them phosphorylation on Ser^{1177} and Thr^{495}. Binding of molecules such as acetylcholine or bradykinin to their receptor increases intracellular levels of calcium, allowing the formation of a calcium-calmodulin complex which interacts with eNOS[45]. Binding of the calcium-calmodulin complex facilitates the electron transfer from the reductase domain to the oxygenase domain of eNOS[43,44]. Protein kinase C (PKC) is responsible for the basal phosphorylation of Thr^{495}, which blocks the interaction between the calcium-calmodulin complex and eNOS. Stimulation of a phosphatase (protein phosphatase 1; PP1) leads to dephosphorylation of Thr^{495}, facilitating the calcium-calmodulin complex binding to eNOS[44–46]. Conversely, AMP-activated protein kinase (AMPK) promotes eNOS phosphorylation at the Ser^{1177}. In addition, shear stress as well as binding of insulin and growth factors, such as VEGF, to their receptor activates both Akt and PKA (protein kinase A) pathways, resulting in Ser^{1177} phosphorylation[44,45,47]. Overall, phosphorylation of eNOS at the Ser^{1177} facilitates its activity hence, NO production (**Figure 4**).

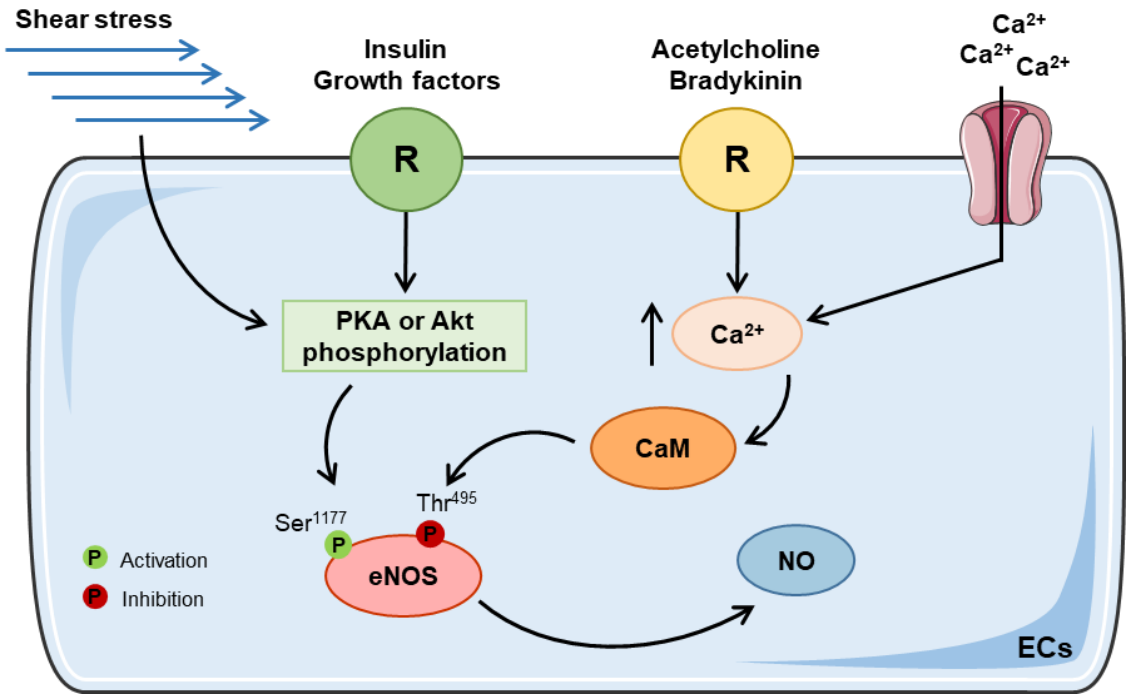

Figure 4. Activation of endothelial nitric oxide synthase.
Binding of agonists such as acetylcholine and bradykinin to their specific receptor expressed on the endothelial cell membrane increases the intracellular concentration of calcium. This leads to the formation of calcium-calmodulin complex which binds to eNOS, resulting in NO production. Shear stress and binding of insulin or growth factors activate Akt and PKA pathways. This leads to the phosphorylation of eNOS at the activation site Ser^{1177}, resulting in NO production. Figure adapted from Zhao *et al.* (2015)[48].
P: phosphorylation site; R: receptor; PKA: protein kinase A; CaM: calmodulin; eNOS endothelial nitric oxide synthase; NO nitric oxide; ECs: endothelial cells.

Nitric oxide is produced in the endothelial layer of vessels and diffuses to the underlying vascular smooth muscle layer where it activates the soluble guanylyl cyclase (sCG) and the cGMP-protein kinase G (PKG) pathway inducing relaxation. Thus, NO produced by eNOS regulates local vascular tone and blood flow[41,44]. Besides controlling vascular tone, NO exerts a great number of additional functions in the cardiovascular system such as inhibition of smooth muscle cell proliferation, platelet aggregation, leucocyte adhesion and vascular inflammation[38].

Dysregulation of eNOS activity can result in endothelial dysfunction. Uncoupling of eNOS contributes to endothelial dysfunction as a consequence of an excess production of superoxide and hydrogen peroxide that can accelerate degradation of NO. Therefore, dysregulation of the enzyme contributes markedly to pathological cardiovascular events[42].

1.3 Organic nitrates

1.3.1 Mechanism of action

Nitrovasodilators (**Table 1**) are a diverse group of agents releasing or producing nitric oxide (NO) or related compounds, thus leading to vascular relaxation[49]. Organic nitrate esters such as nitroglycerin (NTG), isosorbide dinitrate (ISDN), isosorbide mononitrate (ISMN) and pentaerythritol tetranitrate (PETN) contain a -ONO_2 group. Their nitrate ester bond distinguishes them from nitro compounds and nitric oxide-containing compounds such as sodium nitroprusside[50,51].

Nitrovasodilators	Clinical use	Side effects	References
Nitroglycerin (NTG)	Angina , chest pain, acute heart failure	Nitrate tolerance, headache, flushing, postural hypotension	DrugBank; Divakaran and Loscalzo, 2017[52]
Pentaerythritol tetranitrate (PETN)	Angina	Headache, nausea, skin irritation, postural hypotension	DrugBank; Divakaran and Loscalzo, 2017[52]
Isosorbide dinitrate (ISDN)	Angina	Nitrate tolerance, headache, postural hypotension	DrugBank; Divakaran and Loscalzo, 2017[52]
Isosorbide mononitrate (ISMN)	Angina	Nitrate tolerance, headache, postural hypotension	DrugBank; Divakaran and Loscalzo, 2017[52]
Molsidomine	Ischemic heart disease, angina, chronic heart failure and pulmonary hypertension	Headache, nausea, postural hypotension, hypersensitivity	DrugBank

Table 1. Summary of clinical organic nitrate drugs and other NO-donors and their application. Table published in Lopez *et al.* (2021)[53].

Organic nitrates are among the oldest drugs used in the treatment of cardiovascular diseases. Although the use of organic nitrates for prophylaxis and relief of acute angina attacks started as early as in 1878, their mechanism of action was just elucidated in the 1970s and 1980s[54]. As prodrugs, organic nitrates are enzymatically bio-activated to release nitric oxide (NO) or similar reactive nitrogen species[55]. Their metabolite(s) activates the soluble guanylyl cyclase (sGC) with the subsequent increased level of the second messenger, cyclic GMP (cGMP), thus activating the

cGMP-protein kinase G (PKG) pathway[56,57]. PKG can reduce the entry of calcium (Ca^{2+}) into the cell by phosphorylating the voltage-dependent Ca^{2+} channels, thus perturbing the constrictor function. Phosphorylation of the potassium (K^+) channels by PKG results in a K^+ efflux, i.e. membrane hyperpolarization. PKG can also inhibit the myosin light chain kinase (MLCK) and activate the myosin light chain phosphatase (MLCP) resulting in vascular relaxation[58,59] (**Figure 5**).

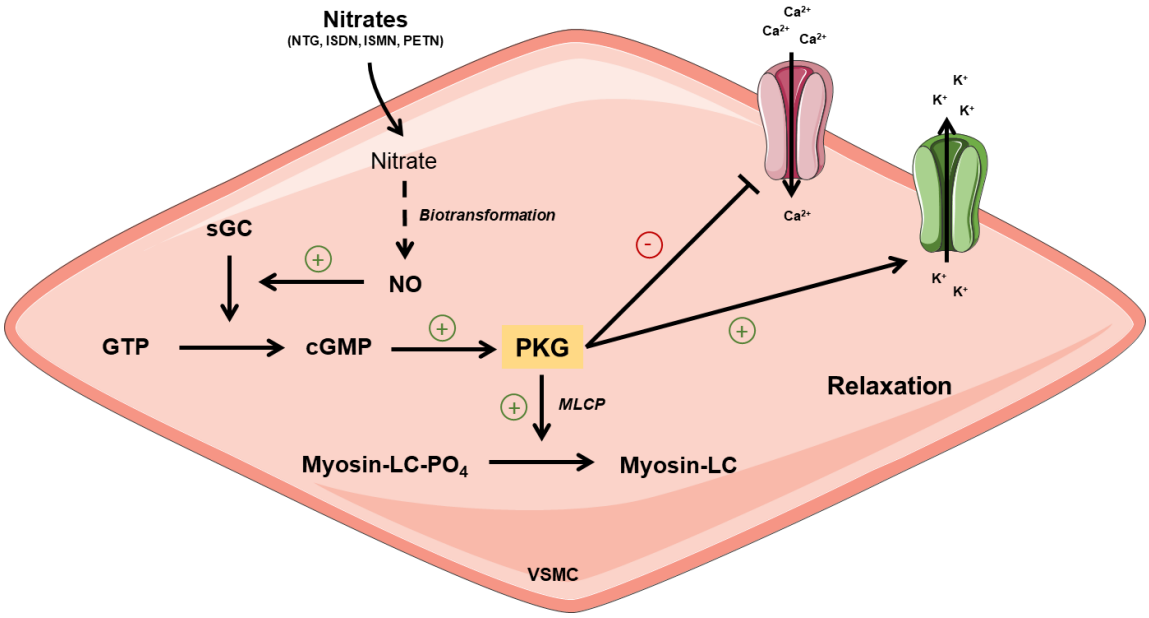

Figure 5. Mechanism of action of organic nitrates.
Organic nitrates such as NTG or PETN are enzymatically bio-activated to release NO which stimulates sGC. In turn, sGC generates cGMP which activates PKG. PKG activation results in vascular relaxation through inhibition of voltage-dependent Ca^{2+} channels, activation of K^+ channels and activation of MLCP. Figure adapted from Katzung (2017)[60].
NTG: nitroglycerin; ISDN: isosorbide dinitrate; ISMN: isosorbide mononitrate; PETN: pentaerythritol tetranitrate; NO: nitric oxide; sGC: soluble guanylyl cyclase; GTP: guanosine-5'-triphosphate; cGMP: Cyclic guanosine monophosphate; Ca^{2+}: calcium; K^+: potassium; MLCP: myosin light chain phosphatase; Myosin-LC: myosin light chain; Myosin-LC-PO_4: myosin-LC phosphorylated; VSMC: vascular smooth muscle cell.

Upon chronic administration of organic nitrates, i.e. NTG, ISMN and ISDN, the clinical effects become progressively more blunted because of the development of nitrate tolerance[61,62]. Nitrate tolerance is defined as an absence of vascular response to organic nitrates and numerous hypothesis have been proposed to explain the development of nitrate tolerance. One explanation is an increase in NO-inactiving reactive oxygen species (ROS) in response to NTG. In fact, increases in ROS have been observed in numerous model of nitrate tolerance condition[62,63]. Further studies demonstrated that the vascular production of peroxynitrite was increased in animals

treated with NTG[62,64]. Increased ROS production was observed as well in arterial segments and blood samples from patients exhibiting tolerance towards NTG[62,65,66]. Desensitization of the sGC by S-nitrosylation has been suggested as another mechanism of tolerance. Different studies reported that S-nitrosylation of sGC leads to a reduction in responsiveness to NO, potentially explained by a phenomenon of NO memory kept in the smooth muscle cells[62,67]. Treatment with ISMN, the most frequently used oral organic nitrate, was associated with an increase in the endothelin-1 (ET-1) expression in the endothelium and increased sensitivity of the vessels to vasoconstricting agents[62,68]. Numerous studies provided evidences for endothelial dysfunction in animals and humans caused by prolonged organic nitrate therapy[62,69–71]. Endothelial dysfunction may be caused by dysfunction of the endothelial nitric oxide synthase (eNOS), i.e. decreased expression, reduced activity and/or uncoupling of the enzyme[62].

1.3.2 Biotranformation pathway of organic nitrates

As prodrugs, organic nitrates are enzymatically activated to release their nitrovasodilator species. The biotransformation pathway differs according to the concentrations used: therapeutic (low) and pharmacological (high) concentrations (**Figure 6**)[61,72]. The mitochondrial aldehyde dehydrogenase (ALDH2) has been identified as the main enzyme responsible for the bioactivation of NTG and PETN at therapeutic concentrations[61,73–75]. Inhibition or deletion of ALDH2 impairs NTG- and PETN-dependent relaxation without affecting ISDN vasodilator potency[72]. Furthermore, the function of ALDH2 in the bioactivation of NTG was also observed in human studies[76].

The hepatic biotransformaton is important for activation or degradation of a large panel of drugs[4]. Several studies have demonstrated the importance of the hepatic CYP450 enzymes in the bioactivation of NTG[56,77–79]. The role of cytochrome P450 enzymes in the bioactivation of NTG and PETN at pharmacological concentrations has been reported in vascular tissues[72,77,79,80]. In addition, vascular cytochrome P450 enzymes are favorable candidates for the biotransformation of ISDN and ISMN, i.e. less reactive organic nitrates[72,81]. However, the validation of these observations using an *in vivo* model is still missing. In order to investigate whether the vascular POR/CYP450 can bio-activate organic nitrates, NTG- and PETN-dependent relaxation was studied here using a smooth muscle cell specific, inducible knockout of POR.

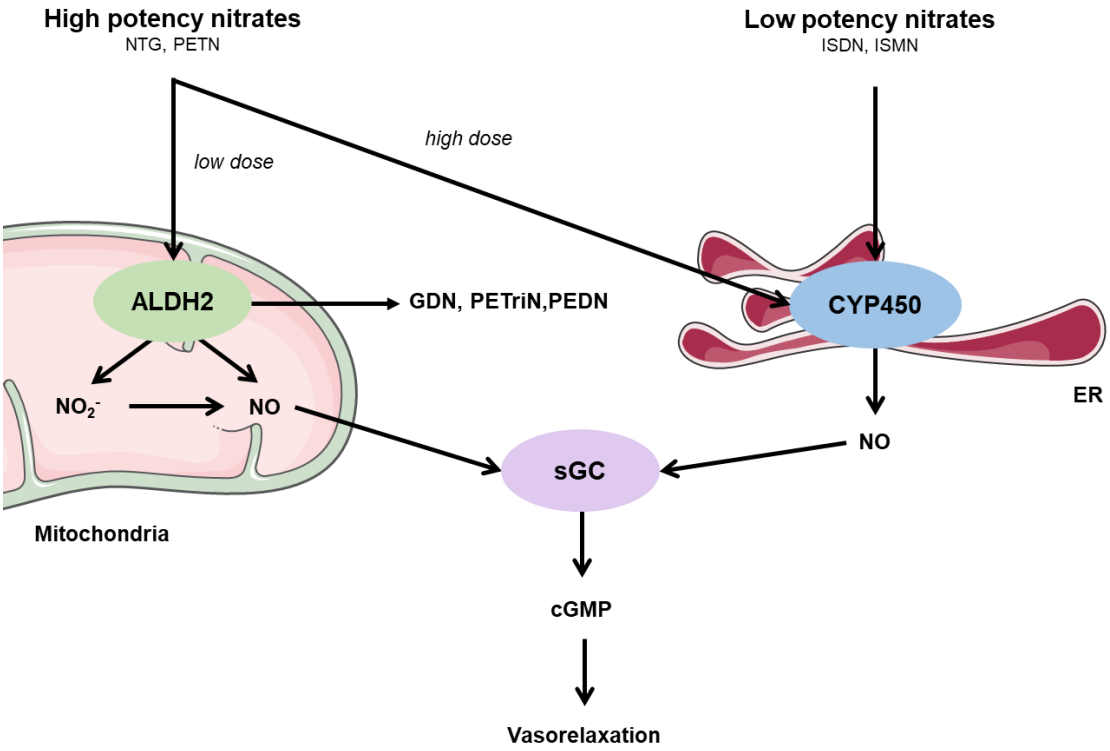

Figure 6. Proposed pathways for biotransformation of organic nitrates in vessels.
The left part depicts the bioactivation of high potency nitrates, i.e. NTG and PETN, by ALDH2 in mitochondria when administrated at therapeutic concentration (< 1 µM). ALDH2 converts NTG and PETN to nitrite, NO and their dinitrated metabolites (1,2-glyceril dinitrate, PETriN and PEDN). Nitrite can be further bio-activated to NO or a related species (NOx). The right part depicts the bioactivation of high potency nitrates when administrated at pharmaceutical concentration (> 1 µM) and of low potency nitrates (ISDN, ISMN) by the CYP450 enzymes in the ER. The CYP450 system converts these prodrugs into NO. Nitric oxide activates sGC leading to an increase in cGMP concentration which results then in vasodilatation. Figure adapted from Daiber *et al.* (2008)[72].
NTG: nitroglycerin; PETN: pentaerythritol tetranitrate; ISDN: isosorbide dinitrate; ISMN: isosorbide mononitrate; GDN: 1,2-glyceryl dinitrate; PETriN: pentaerithrityl trinitrate; PEDN: pentaerithrityl dinitrate; ALDH2: mitocondrial aldehyde dehydrogenase; NO_2^-: nitrite; NO: nitric oxide; sGC: soluble guanylyl cyclase; cGMP: cyclic GMP; ER: endoplasmic reticulum.

1.4 Endothelial cell-cardiomyocyte crosstalk

Several cell populations constitute the heart forming a complex network of intercellular communication[82,83]. While cardiomyocytes (CMs) contribute to most of cardiac tissue volume, they only represent 25-35% of all the cells in the heart. In term of absolute number, endothelial cells (ECs) are the most prevalent cell type (>60% of the non-myocyte population) in the heart[82,84]. The distribution of oxygen and metabolic substrates to CMs is facilitated by capillaries, so that each cardiomyocyte is in contact with several capillaries, resulting in a ratio EC:CM of 3:1. This architectural arrangement also allows for an autocrine and paracrine crosstalk between cardiomyocytes and endothelial cells[82] (**Figure 7**).

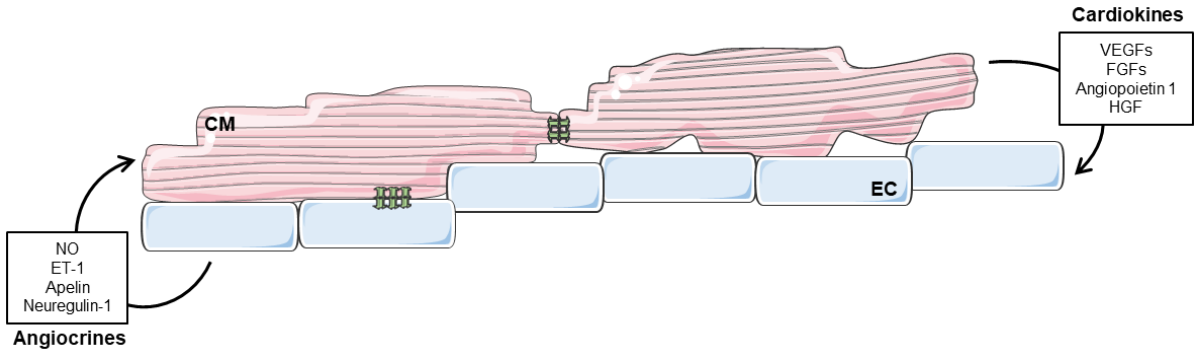

Figure 7. Paracrine factors mediating endothelial–cardiomyocyte crosstalk.
Illustration of selected known angiocrines and cardiokines mediating endothelial cell-cardiomyocyte crosstalk. Endothelial cells and cardiomyocytes can also communicate through direct cell-to-cell contact (gap junctions, as depicted in green). Figure adapted from Colliva *et al.* (2020)[85].
CM: cardiomyocyte; EC: endothelial cell; NO: nitric oxide; ET-1: endothelin-1; VEGFs: vascular growth factors; FGFs: fibroblast growth factors; HGF: hepatocyte growth factor.

Cardiomyocytes produce and secrete various molecules for paracrine signaling which are called cardiokines. These comprise growth factors, endocrine hormones, cytokines or peptides. The vascular growth factor (VEGF) is the main cardiokine and regulates EC activation and proliferation. VEGF binds to VEGFR2 (VEGF receptor 2) in ECs, activating its signaling cascade which induces angiogenesis (formation of new vessels from a pre-existing vessel). This allows for a better oxygen and nutrients supply in deprived areas to match the need of cardiomyocytes in situations like such as hypertrophy or increased transmural pressure (physiological growth)[83]. Angiopoietin-1 (Ang1) is an oligomeric-secreted glycoprotein and binds to Tie2, a tyrosine kinase receptor expressed on ECs. Ang1 is required for the maturation of the neovasculature and vascular integrity[86]. The myocardium-derived Ang1 is reported to

be essential for coronary vein formation in the developing heart, by promoting migration, proliferation and venous differentiation of immature ECs[87].

Endothelial cells secrete a set of factors called angiocrines acting on the neighboring cells. NO, well known for inducing vasodilation in SMCs, is one of EC-derived factors regulating the cardiac contractility by inducing ventricular relaxation[83]. The relaxant effects of NO have been attributed to phosphorylation of troponin I by the cGMP-PKG pathway, which results (among other pathways) in a reduction of myofilament Ca^{2+} sensitivity[85]. In contrast, endothelin-1 (ET-1) acts as a potent vasoconstrictor by binding to ET_B receptors expressed by CMs. This induces cell contraction by increasing intracellular levels of calcium in CMs[85]. Neuregulin-1 (NRG-1), a member of the epidermal growth factor (EGF) family, is produced and secreted by microvascular ECs and endocardium in the heart. NRG-1 binds to its receptor ErbB (tyrosine kinase receptor), expressed on the surface of CMs, and promotes cardioprotection and regeneration[83,88]. In fact, it has been shown that endothelium-derived NRG-1 protects the CMs during ischemia/reperfusion against apopotosis[88,89].

Thus, cardiac ECs and CMs communicate through paracrine signals and there are evidences suggesting that the pathogenesis of several heart diseases involves perturbation in the endothelial cell-cardiomyocyte crosstalk. However, very little is known about how the cardiac ECs secretome affects CMs in response to physiological or pathological stimuli[83,84].

1.5 EETs in the cardiovascular system

1.5.1 Arachidonic acid: a precursor of vasoactive molecules

Arachidonic acid (AA) is a ω-6 polyunsaturated fatty acid (PUFA) and plays an important role in the cardiovascular system. In mammal cells, AA ester is a constituent of the inner surface of cell membrane and cytosolic phospholipids and is usually incorporated in the glycerol backbone sn-2 position. It confers membrane fluidity and flexibility, which is necessary for the function of all cells[90].

Prior to be further metabolized, AA is hydrolyzed and released from the membrane phospholipids by the phospholipase A2 (PLA2)[90,91]. Various pathways can activate the hydrolysis of AA by the PLA2 enzyme such as inflammation, activation of Toll-like receptor 4 (TLR4), purinergic receptors, or activation of P75 and P55 (tumor necrosis factor alpha (TNF-α) receptor)[92]. Three distinct enzyme systems can metabolize AA, generating a great number of fatty acid mediators with multiple functions: cyclooxygenases (COXs), lipoxygenases (LOXs) and CYP450 enzymes (ω-hydroxylases and epoxygenases) (**Figure 8**)[13,91].

In the cardiovascular system, ω-hydroxylases (CYP4A and CYP4F subfamilies) and epoxygenases (CYP2C and CYP2J subfamilies) use AA to respectively generate the vasoconstrictor 20-hydroxyeicosatetraenoic acid (20-HETE) and the vasodilators epoxyeicosatrienoic acids (EETs)[36,93]. The vascular synthesis of 20-HETE occurs in vascular smooth muscle cells where it induces vasoconstriction through several mechanisms[93]. As for EETs, they are synthesized and released from the endothelium where they reach the vascular smooth muscle layer inducing vasorelaxation[94].

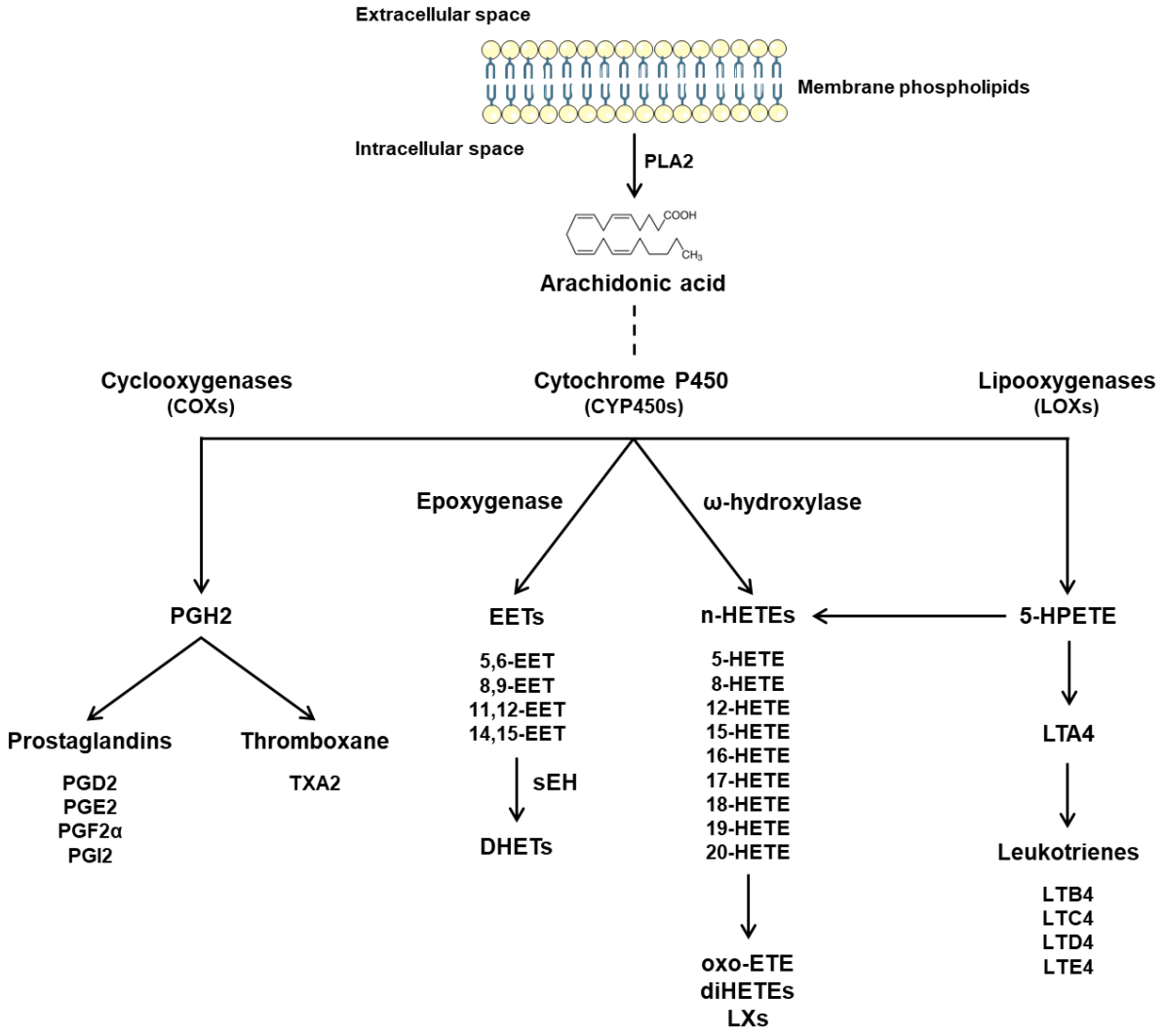

Figure 8. Overview of the arachidonic acid metabolism pathways and its fatty acid mediators. Arachidonic acid is released from membrane-bound phospholipid stores by the phospholipase A2. It is further metabolized by three enzymatic systems (cyclooxygenases, lipoxygenases and cytochrome P450 enzymes) to prostaglandins, prostacyclin, thromboxane A2, leukotrienes, hydroxyeicosatetraenoic acids and epoxyeicosatrienoic acids. The latter are further metabolized by the soluble epoxide hydrolase (sEH) to dihydroxyeicosatetraenoic acids. Figure adapted from Wang *et al.* (2021)[13].

PLA2: phospholipase A2; PGs: prostaglandins; PGI2: prostacyclin; TXA2: thromboxane A2; EETs: epoxyeicosatrienoic acids; HETEs: hydroxyeicosatetraenoic acids; sEH: soluble epoxide hydrolase; LTs: leukotrienes.

1.5.2 EETs and vascular function

EETs are AA-derived epoxyeicosatrienoic acid products of epoxygenases. Epoxygenases target the double bonds of AA resulting in the production of four region-isomeric cis-epoxyeicosatrienoic acids: 5,6-EET; 8,9-EET; 11,12-EET and 14,15-EET (**Figure 9**). Each of these may exist as either two stereoisomers (S,R and R,S)[94,95]. In the vascular system, human endothelial cells express CYP2C8, CYP2C9 and CYP2J2 as the isoforms responsible for the production of EETs, whereas murine endothelial cells express diverse isoforms of the CYP2C subfamily[96,97]. Although epoxygenases produce all four EETs, they are regio-selective, with 11,12- and 14,15-EET being the main products[98].

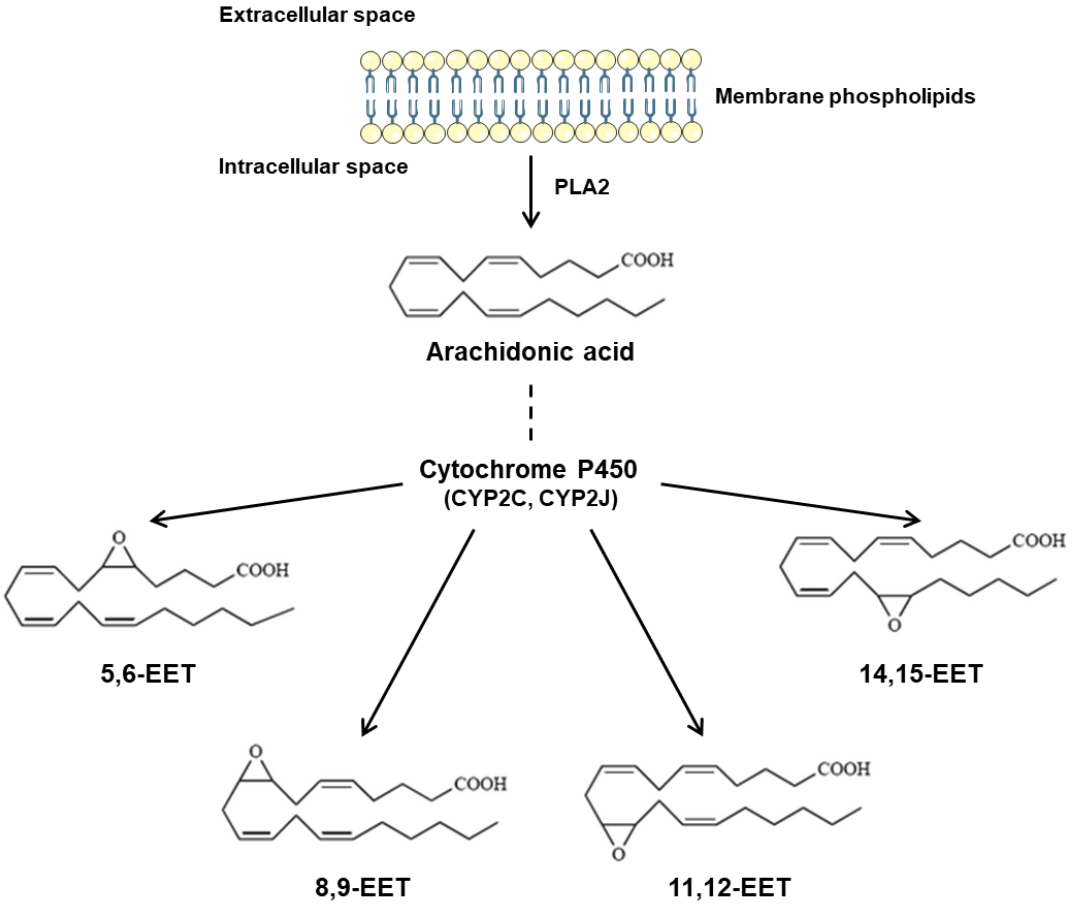

Figure 9. Overview of EETs produced by CYP450 epoxygenases.
Arachidonic acid is metabolized by CYP450 epoxygenases into one of the four EETs: 5,6-EET; 8,9-EET; 11,12-EET and 14,15-EET. Figure adapted from Sudhabar *et al.* (2010)[99].

EETs are potent autocrine and paracrine metabolites with a great number of biological functions in different tissues and cells: anti-inflammatory properties, cardioprotective effects, induction of mitogenesis in renal epithelial cells, stimulation of hormones secretion and inhibition of platelet aggregation[100]. In the vascular system, endothelial

produced EETs function as an endothelium-dependent hyperpolarizing factor (EDHF) [98]. There are two possible mechanisms by which EETs may function as an EDHF: transferable factors or autocrine function[94]. As transferable factors, EETs are released from the endothelium and bind to G-protein coupled receptors on the smooth muscle layer. This causes the activation of large conductance, calcium-activated potassium (BK_{Ca}) channels, resulting in a K^+ efflux, an increase in the membrane potential or hyperpolarization and relaxation[101–103]. As autocrine factors, EETs promote an endothelial calcium influx through activation of a transient receptor potential channel (TRPV4). This causes the activation of small conductance (SK) and intermediate-conductance calcium-dependent K^+ (IK) channels, resulting in the release of K^+ into intracellular space. The change in K^+ elicits either endothelial hyperpolarization which can be spread to smooth muscle cell through gap junction communication or activation of inwardly rectifying K^+ channels or Na/K-ATPase on the smooth muscle layer, resulting in hyperpolarization and relaxation[94,101,102].

Although intracellular levels of EETs are tightly regulated by soluble epoxide hydrolase (sEH) and converted to dihydroxyeicosatetraenoic acids (DHETEs), EETs can be subjected to β-oxidation and chain elongation[36]. Furthermore, there are evidences that EETs can also be incorporated into the sn-2 position of phospholipids by the acyl coenzyme A (CoA). This function may result an intracellular storage of EETs, whose release upon cellular activation is CYP450-independent[36,98].

1.5.3 EETs and cardioprotective function

Although the largest expression of CYP450 enzymes occurs in the liver, the cardiac expression of CYP450 epoxygenases (CYP2C8, CYP2C9 and CYP2J2) and ω-hydroxylases (CYP4A and CYP4F subfamilies) is substantial[12].

As in the vascular system, cardiac epoxygenases generate four regioisomeric cis-epoxyeicosatrienoic acids: 5,6-EET; 8,9-EET; 11,12-EET and 14,15-EET. A great number of publications demonstrated cardioprotection by EETs. Cardiac L-type Ca^{2+} channel phosphorylation is modulated by 11,12-EET, a CYP2J2-derived metabolite, via a cAMP-PKA-dependent mechanism[104]. Activation of K_{ATP} channels can be modulated by 8,9-EET and 11,12-EET by decreasing its overall sensitive to ATP inhibition[105]. Furthermore, CYP2J2-derived metabolites have shown cardioprotection during myocardial ischemia-reperfusion (I/R) in CYP2J2 transgenic animals by activating mitoK_{ATP} channel and p42/p44 MAPK[106]. TAC-operated (transverse aortic constriction) mice showed an impaired cardiac function which was rescued by overexpressing CYP2J2 in cardiomyocytes or treatment of the mice with 11,12-EET. As previously stated, EETs are converted into their less active forms, DHETEs, by sEH. Inhibition of sEH increases the bio-availavility of EETs which then improve the cardiac function as shown in heart failure murine models such as in myocardial I/R injury or myocardial infarction (MI)[107,108]. Specific CYP-producing EETs isoforms in cardiac endothelial cells impact cardiac function[109,110]. However, the putative cardioprotective role of cardiac endothelial EETs remains unclear[110].

Cardiac ω-hydroxylases, i.e. CYP4A and CYP4F, are responsible for the generation of 20-HETE from AA. Based on recent human population studies, a polymorphism in the human CYP4A11 gene is associated with increased incidence of myocardial infarction (MI)[111]. Expression of CYP4A and CYP4F, together with the stimulation of 20-HETE production, has been shown to increase in response to IR in animal models. These effects were suppressed with administration of DDMS (dibromo-dodecenyl-methylsulfimide), an inhibitor of 20-HETE synthesis[111].

These studies highlight the importance of CYP450 enzymes in the regulation of cardiac contractily in healthy and diseased state[12].

2 Aim

Cytochrome P450 enzymes are important for the metabolism of endogenous (steroids, fatty acids) and xenobiotic molecules (polluant, drugs)[6,7]. The highest levels of CYP450 isoenzymes are found in the liver, however, the cardiovascular expression is substantial[11–13].

The first part of the study focuses on the metabolism of organic nitrates. For over a century, angina or ischemic heart disease were treated with nitroglycerin (NTG) or pentaerythritol tetranitrate (PETN)[112]. As prodrugs, these compounds have to be enzymatically bio-activated to release their nitrovasodilator by either aldehyde dehydrogenase (ALDH2) or cytochrome P450 enzymes[72]. Albeit ALDH2 has been named as the main enzyme to locally activate organic nitrates in human and murine vessels, the role of vascular cytochrome P450 enzymes on the biotransformation of organic nitrates remains unclear. The aim of the present study was to determine whether the POR/CYP450 system locally contributes to the vascular biotransformation of organic nitrates. For that purpose, the bio-activation of organic nitrates by recombinant CYP450 microsomes was determined by nitrite measurements. Furthermore, the dilator response induced by organic nitrates was studied using a smooth muscle-cell specific, inducible knockout mouse of POR (smcPOR$^{-/-}$), in presence or absence of benomyl (an ALDH2 inhibitor).

The second part of the study focuses on the cardiac function of the cytochrome P450 reductase. The POR/CYP450 system produces epoxyeicosatrienoic acids (EETs) and hydroxyeicosarrienoic acids (HETEs)[113,114] which have been shown to maintain vascular homeostasis and have cardioprotective effects in cardiomyocytes (CMs)[36]. However, the cardiac relevance of the endothelial POR/CYP450 system is still unclear. The main aim of the present study was to evaluate whether endothelial deletion of POR had any physiological consequence for the cardiac function. This was explored by using an endothelial cell-specific, tamoxifen-inducible knockout of POR to reveal morphological and functional changes in the heart and uncover differences in gene expression profiles. Transverse aortic constriction (TAC) was employed as a pressure-overload model to further examine the role of the endothelial POR/CYP450 system on the cardiac function.

3 Materials

3.1 Chemicals

Table 2. List of Chemicals

Chemicals	Company
2-acrylamido-2methylpropane sulfonic acid (AMPS)	Applichem, Darmstadt, Germany
4′,6-diamidino-2-phenylindole dihydrochloride (DAPI)	Sigma Aldrich, Taufkirchen, Germany
Acetic acid	Applichem, Darmstadt, Germany
Acetylcholine	Sigma Aldrich, Taufkirchen, Germany
Acrylamid-biacrylamid rotiphorese gel 30	Roth, Karlsruhe, Germany
Benomyl	Sigma Aldrich, Taufkirchen, Germany
Bepanthen eye ointment	Bayer, Leverkusen, Germany
Betadine (Braunol)	B. Braun, Melsungen, Germany
Bouin's solution	Sigma Aldrich, Taufkirchen, Germany
Bovine serum albumin (BSA) 7.5%	Gibco Life Technologies, Carlsbad, USA
Bromphenol blue	Applichem, Darmstadt, Germany
Buprenorphine	Indivior Europe Limited, Dublin, Ireland
Calcium triplex-dihydrate	Merck, Darmstadt, Germany
CHAPS	Applichem, Darmstadt, Germany
Collagenase type II	Worthington Biochemical, Lakewood, USA
D-(+)-Glucose monohydrate	Sigma Aldrich, Taufkirchen, Germany
Dako fluorescence mounting medium	Agilent Technologies, Waldbronn, Germany
Deoxyribose nucleotides (dNTPs)	Bioline, London, UK
DETA NONOate	Enzo Life Sciences GmbH, Lörrach, Germany
Dimethyl sulfoxide (DMSO)	Sigma Aldrich, Taufkirchen, Germany
Direct Red 80	Sigma Aldrich, Taufkirchen, Germany
Dispase	Roche Diagnostics, Mannheim, Germany
Dithiothreitol (DTT)	Invitrogen, Carlsbad, USA
DRAQ5	BioLegend, Amsterdam, The Netherlands
Dulbecco's Modified Eagle Medium (DMEM)	Gibco Life Technologies, Carlsbad, USA
DynaBeads sheep anti-rat IgG	Thermo Fisher, Darmstadt, Germany

Elastase	Worthington Biochemical, Lakewood, USA
Eosin	Merck, Darmstadt, Germany
Ethanol EtOH) absolute	Sigma Aldrich, Taufkirchen, Germany
Ethidium bromide	Roth, Karlsruhe, Germany
Ethylene diamine tetraacetic acid (EDTA)	Applichem, Darmstadt, Germany
FastGreen FCF	Sigma Aldrich, Taufkirchen, Germany
Fetal Calf Serum (FCS)	Sigma Aldrich, Taufkirchen, Germany
First Strand Buffer, 5x	Invitrogen, Carlsbad, USA
Formaldehyde 4%, ROTI Histofix	Roth, Karlsruhe, Germany
Glycerol 86%	Roth, Karlsruhe, Germany
Glycine	Roth, Karlsruhe, Germany
Hank's balanced salted solution (HBSS)	Sigma Aldrich, Taufkirchen, Germany
Hematoxylin Mayer's	Applichem, Darmstadt, Germany
HEPES	Sigma Aldrich, Taufkirchen, Germany
Hydrochloric acid (HCl)	Roth, Karlsruhe, Germany
Isoflurane	Abbvie, North Chicago, USA
Isopropanol	Sigma Aldrich, Taufkirchen, Germany
Isosorbide dinitrate (ISDN)	Andreas Daiber, Universitätklinik Mainz, Germany
Isosorbide mononitrate (ISMN)	Merck, Darmstadt, Germany
iTaq™ Universal SYBR® Green Supermix	Bio-Rad, Munich, Germany
Magnesium chlorid ($MgCl_2$)	Sigma Aldrich, Taufkirchen, Germany
Magnesium sulphate heptahydrate	Sigma Aldrich, Taufkirchen, Germany
Methanol	Sigma Aldrich, Taufkirchen, Germany
Molsidomine	Merck, Darmstadt, Germany
Monobasic sodium phosphate (NaH_2PO_4)	Sigma Aldrich, Taufkirchen, Germany
Nicotinamide adenine dinucleotide phosphate (NADPH)	Applichem, Darmstadt, Germany
Nitro blue tetrazolium (NBT)	Merck, Darmstadt, Germany
Nitroglycerin (NTG)	Andreas Daiber, Universitätklinik Mainz, Germany
Novaminsulfon (Novalgin)	Zentiva, Berlin, Germany
Nω-Nitro-L-arginine methyl ester hydrochloride (L-NAME)	Sigma Aldrich, Taufkirchen, Germany
O.C.T compound	Tissue Tek Satura, Osaka, Japan

Okadaic acid (OA)	Applichem, Darmstadt, Germany
Orthovanadate (OV)	Applichem, Darmstadt, Germany
Pentaerythritol tetranitrate (PETN)	Andreas Daiber, Universitätsklinik Mainz, Germany
Phenylmethanesulfonylfluoride (PMSF)	Sigma Aldrich, Taufkirchen, Germany
Picric acid-saturated solution 1.3%	Sigma Aldrich, Taufkirchen, Germany
Potassium chloride (KCl)	Roche Diagnostics, Mannheim, Germany
Potassium phosphate monobasic	Sigma Aldrich, Taufkirchen, Germany
Proadifen hydrochloride (SKF525)	Sigma Aldrich, Taufkirchen, Germany
Protein-inhibitor mix (PIM)	Sigma Aldrich, Taufkirchen, Germany
Random Primers	Promega, Madison, USA
Reverse Transkriptase Superscript III	Invitrogen, Carlsbad, USA
Roti GelStain	Roth, Karlsruhe, Germany
Roti-block	Roth, Karlsruhe, Germany
Rotiphorese Gel 30	Roth, Karlsruhe, Germany
Roti-Quant	Roth, Karlsruhe, Germany
Sodium bicarbonate ($NaHCO_3$)	Sigma Aldrich, Taufkirchen, Germany
Sodium chloride (NaCl)	Sigma Aldrich, Taufkirchen, Germany
Sodium dodecyl sulfate (SDS)	Roth, Karlsruhe, Germany
Sodium fluoride (NaF)	Sigma Aldrich, Taufkirchen, Germany
Sodium iodide	Applichem, Darmstadt, Germany
Sodium nitrite	Merck, Darmstadt, Germany
SYTOX® Green dye	Life Technologies, Carlsbad, USA
Tetramethylethylenediamine (TEMED)	Applichem, Darmstadt, Germany
TRIS	Roth, Karlsruhe, Germany
Trisodium citrate (dehydrate)	Roth, Karlsruhe, Germany
Triton X-100	Roth, Karlsruhe, Germany
Tween 20	Sigma Aldrich, Taufkirchen, Germany
U46619	Sigma Aldrich, Taufkirchen, Germany
Wheat germ agglutinin (WGA)	Life Technologies, Carlsbad, USA
Xylene cyanol	Sigma Aldrich, Taufkirchen, Germany
Xylol	Roth, Karlsruhe, Germany

3.2 Material

Table 3. List of Material

Materials	Company
0.1 mL 8-strip PCR tubes	STARLAB International GmbH, Hamburg, Germany
0.2 mL 8-strip PCR tubes	STARLAB International GmbH, Hamburg, Germany
8-strip domed PCR capes	STARLAB International GmbH, Hamburg, Germany
8-strip flat PCR tubes	STARLAB International GmbH, Hamburg, Germany
Aquagel®, lubricating gel	Parker Laboratories, Almelo, The Netherlands
Aquasonic® 100, ultrasound transmission gel	Parker Laboratories, Almelo, The Netherlands
Cover slips	Roth, Karlsruhe, Germany
Cryomolds	Tissue Tek Sakura, Osaka, Japan
DynaMag-2 Magnet	Thermo Scientific, Waltham, USA
Ethilon 7-0	Ethicon, Somerville, USA
Membrane slide 1mm PEN	Zeiss, Oberkochen, Germany
Microtome blades N35	Feather, Osaka, Japan
MiniVent ventilator for mice	HSE Hugo Sachs Eletronik, March-Hugstetten, Germany
NextSeq2000	Illumina, San Diego, USA
Nitrocellulose transfer membrane	NeoLab, Heidelberg, Germany
O-ring aortic banding (ORAB) 0.5mm	Apple Rubber, NY, USA
Prolene 6-0	Ethicon, Somerville, USA
Signa gel® Electrode gel	Parker Laboratories, The Netherlands
Super frost ultra plus slides	Thermo Scientific, Waltham, USA
Vasofix® Safety IV catheter, 22G, 0.9 x 25 mm	B. Braun, Melsungen, Germany
Whatman paper/ gel-blotting paper	A. Hartenstein, Würzburg, Germany

3.3 Equipment

Table 4. List of Equipment

Equipment	Company
AriaMx Real-Time PCR	Agilent Technologies, California, USA
Centrifuge (rotor)	Eppendorf, Hamburg, Germany
Confocal microscope LSM 510	Zeiss, Göttingen, Germany
Confocal microscope TCS SP5 II	Leica, Wetzlar, Germany
Cryostat HM550	Thermo Scientific, Schwerte, Germany
Electrophoresis device	Bio-Rad, Münich, Germany
Freezer HERAfreeze basic (-80°C)	Heraeus Instruments, Hanau, Germany
Heating block Thermomixer compact	Eppendorf, Hamburg, Germany
Heating plate and control unit	Minitüb, Tiefenbach, Germany
Infrared scanner Odyssey	LI-COR, Bad Homburg, Germany
Isoflurane vapor 19.3	Drägerwerk AG, Lübeck, Germany
LabChip Gx Touch 24	Perkin Elmer, Rodgau, Germany
Laminar flow Heraguard ECO	Thermo Scientific, Schwerte, Germany
Microplate Reader, Infinite 200 PRO	Tecan, Männedorf, Germany
Microscope AxioObserver.Z1	Zeiss, Jena, Germany
Microscope Axiovert 40 ETL	Zeiss, Göttingen, Germany
Microscope Leica M651	Leica, Wetzlar, Germany
Nitric Oxide Analyser, Sievers NOA-280	FMI GmbH, Seeheim, Germany
PCR device Eppendorf Mastercycler Gradient	Eppendorf, Hamburg, Germany
pH meter	Sartorius, Göttingen, Germany
Pipette	Eppendorf, Hamburg, Germany
Power supply CS – 300V	Roth, Karlsruhe, Germany
PowerPac HC	Bio-Rad, Munich, Germany
Scale analytical balance	Sartorius, Göttingen, Germany
Spectrophotometer NanoDrop ND-1000	PEQLAB Biotechnologie, Erlangen, Germany
Steril bench laminar flow HB 2448	Heraeus Instruments, Hanau, Germany
Tissue lyser	Qiagen, Hilden, Germany
Vevo 3100	Visualsonics, Toronto, Canada
Vortex mixer vortex genie 2	Scientific Industries, New York, USA
Water purification system Milli-Q	Millipore, Billerica, USA
Western blot chamber	Bio-Rad, Munich, Germany

3.4 Buffers and solutions

Table 5. Recipes for buffers and solutions

Buffer	Recipe
Hank's buffer	4 mM Na_2CO_3 in Hank's salt
HEPES tyrode buffer (HT buffer)	19g Thyrodes' salt 4.77g HEPES Fil up to 2L ddH_2O, pH 7.4 at 37°C
Krebs-Henseleit solution (Stock solution I) (Organ bath)	40 mM $CaCl_2$ dihydrate 2.97 M NaCl 30 mM $MgSO_4 \cdot 7H_2O$ 120 mM KCl
Potassium-enriched Krebs-Henseleit solution (Stock solution I KCl) (Organ bath)	112 mM NaCl 1.97 M KCl 40 mM $CaCl_2$ dihydrate 30 mM $MgSO_4 \cdot 7H_2O$
Stock solution II (Organ bath)	0.63 M $NaHCO_3$ 30 mM KH_2PO_4
4.1% Ca-EDTA solution (Organ bath)	4.1g Ca-Titriplex Fil up to 100mL ddH_2O
Krebs-Henseleit wash buffer (Organ bath)	12 mM Glucose 80mL Stock solution I 80mL Stock solution II 520µL Ca-EDTA Fil up to 2L ddH_2O
Potassium-enriched buffer (Organ bath)	12 mM Glucose 40mL Stock solution I KCl 40mL Stock solution II 260µL Ca-EDTA Fil up to 1L ddH_2O

Triton lysis buffer (Western blot)	20 mM Tris/HCl, pH 7.5 150 mM NaCl 20 mM sodium fluoride 1% Triton X-100 2 mM orthovanadate (OV) 10 mM okadaic acid (OA) 10 nM protein inhibitor mix 40 µg/mL phenylmethlysulfonyl fluoride (PMSF)
1x Wash buffer (Western blot)	0.3% Tween-20 50 mM Tris/HCl, pH 7.5 150 mM NaCl
1x Running buffer (Western blot)	25 mM Tris 190 mM Glycine 0.1% SDS
1x Transfer buffer (Western blot)	25 mM Tris 190 mM Glycine 20% methanol
Washing buffer	0.5% bovine serum albumine (BSA) 50mL HBSS 2 mM EDTA
Digestion mix for heart	1.2 U/mL Dispase (0.9 U/mg) 2 mg/mL Collagenase type II (230 U/mg) 0.03 mg/mL Elastase (4.92 U/mg) in DMEM
Stop solution	10% FCS (filtered) in DMEM
FACS buffer 1	0.5% bovine serum albumine (BSA) 2 mM EDTA in DPBS
FACS buffer 2	10% FCS (filtered)

	3 mM EDTA 25 mM HEPES in DPBS
Endothelium-removal solution	1% CHAPS 5g Glucose in HT buffer
0.01% Sirius Red (Sirius Red staining)	50mg Direct Red80 15mL ddH_2O 485mL Picric acid-saturated solution 1.3%
0.1% Fast Green (Sirius Red staining)	500mg FastGreen FCF Fil up to 500mL ddH_2O
1% acetic acid solution (Sirius Red staining)	1mL acetic acid glacial Fil up tp 99mL ddH_2O
10mM sodium-citrate-buffer pH 6.0 (WGA staining)	2.94g trisodium citrate (dehydrate) 0.5 mL Tween 20 Fil up to 1L ddH_2O

3.5 Animals

Table 6. Mouse lines

Genotype	Source/Generation
C57BL/6J	Charles River, Deisenhofen
$CPR^{flox/flox}$-CMV-GT-Rosa-$CreERT2^{TG/0}$	Lopez *et al.* 2021[53,115]
$CPR^{flox/flox}$-Smmhc-CreERT2	Lopez *et al*. 2021[53,115,116]
$CPR^{flox/flox}$-Cdh5-$CreERT2^{+/0}$	Malacarne *et al*. 2022[115,117,118]

Table 7. List of diet used for animal experiments

Diet	Company
Breeding diet, 10 mm	Ssniff, Soest
Maintenance diet, 10 mm	Ssniff, Soest
Tamoxifen diet, CreActive T400, 10 mm	Genobios, Laval

3.6 Synthetic oligonucleotides

Table 8. List of Primer sequences

Gene	Forward Primer (5'-3')	Reverse Primer (5'-3')
mNppa	TCTGATGGATTTCAAGAACCTGC	ATCTATCGGAGGGGTCCCAG
mNppb	TCCTAGCCAGTCTCCAGAGCAA	GGTCCTTCAAGAGCTGTCTCTG
mMyh6	GCTGGAAGATGAGTGCTCAGAG	CCAGCCATCTCCTCTGTTAGGT
mMyh7	CAGGTCTGGCTCTGAGCATTC	CCAGGCCTGTAGAAGAGCTGTA
mPostn	AAGACTGCTTCAGGGAGACAC	CTGGCCTCTGGGTTTTCACT
mBgn	TGTCCCTCCCCAGGAACATT	GGTGAGATCTCCTTGGGCAC
mGlut4	GCCCGGACCCTATACCCTAT	GGTTCCCCATCGTCAGAGC
mβ-actin	AGATCAAGATCATTGCTCCTCCT	ACGCAGCTCAGTAACAGTCC

3.7 Antibodies

3.7.1 Primary antibodies

Table 9. List of Primary antibodies

Protein	Order No	Species	Dilution	Company
β-actin	A1978	Mouse	1:10000 (WB)	Sigma
Caldesmon-1	12503	Rabbit	1:200 (IF)	Cell Signaling
CD144	555289	Rat	1:1000	BD Bioscences
CYP51A1	13431-1-AP	Rabbit	1:1000 (WB)	Proteintech
eNOS	610297	Mouse	1:1000 (WB)	BD Bioscences
ERK1/2	4696	Mouse	1:2000 (WB)	Cell Signaling
GAPDH	PA1-16777	Rabbit	1:2000 (WB)	Thermo Scientific
Lectin-FITC conjugate	L9381-2MG	*Bandieraea simplicifolia*	1:100 (FACS)	Sigma
POR	sc-25270	Mouse	1:500 (WB)	Santa Cruz
αSM-actin-Cy3	C6198	Rabbit	1:300 (IF)	Sigma
WGA-647 conjugate	W32466	Wheat germ	1:100 (IF)	Life Technologies

3.7.2 Secondary antibodies

Table 10. List of Secondary antibodies

Reactivity	Order No	Species	Dilution	Company
Anti-mouse IgG 800 nm	926-32212	Donkey	1:10000	LI-COR
Anti-mouse IgG 680 nm	926-68072	Donkey	1:10000	LI-COR

Anti-rabbit IgG 800 nm	926-32213	Donkey	1:10000	LI-COR
Anti-rabbit IgG 680 nm	926-68073	Donkey	1:10000	LI-COR
Anti-rabbit IgG Alexa546	A10040	Donkey	1:500	LI-COR

3.8 Reaction systems

Table 11. List of Reagents

Name	Company
Debris removal solution	Miltenyi Biotec, Bergisch Gladbach, Germany
Red blood cell (RBC) lysis buffer for mouse	Alfa Aesa, Kandel, Germany
RNeasy micro kit (50)	Qiagen, Hilden, Germany
RNeasy fibrous tissue mini kit (50)	Qiagen, Hilden, Germany
SMART-seq® v4 Ultra® Low Input RNA kit	Takara Bio, Saint-German-en-Laye, France
VAHTS Stranded mRNA-seq Library	Vazyme, Münich, Germany

3.9 Surgical tools

Table 12. List of Surgical tools

Tool	Order No	Company
Castroviejo needle holder	12565-14	Fine Science Tools, Heidelberg, Germany
Dumont SS forceps	11203-25	Fine Science Tools, Heidelberg, Germany
Extra fine graefe forceps	11151-10	Fine Science Tools, Heidelberg, Germany
Mouse retractor set	13-005-180	Kent Scientific, Bad Homburg, Germany
Scissors	10162-12	Fine Science Tools, Heidelberg, Germany
Spatula for intubation	-	Homemade, Heidelberg, Germany
Spinal cord hook	10162	Fine Science Tools, Heidelberg, Germany

3.10 Software

Table 13. List of Software

Name	Company
Agilent Aria MX 1.7	Agilent Technologies, California, USA
Citavi 6	Swiss Academic Software, Wädenswil, Switzerland
GraphPadPrism 8	GraphPad Software, San Diego, USA
Image J	National Institutes of Health, Bethesda, USA
Image studio 5.2	LI-COR, Bad Homburg, Germany
LabChart 8	ADInstruments, Oxford, UK

Nanodrop, 2000/200c	Thermo Scientific, Waltham, USA
R	https://www.r-project.org
R Studio	Rstudio Inc., Boston, USA
Vevo LAB 5.6.0	Visualsonics, Toronto, Canada
Zen blue edition	Zeiss, Oberkochen, Germany

Table 14. List of R packages

Name	Source
DESeq2 (1.32.0)	Bioconductor
ggplot2 (3.3.5)	CRAN
Stats (4.1.1)	RStudio Inc., Boston, USA

4 Methods

4.1 *In vivo* experiments

4.1.1 Animal breeding and housing

All animal experiments were performed in accordance with the University's Animal Care Committee and the Federal Authorities for Animal Research (Regierungspräsidium Darmsadt; approval number FU1188). Mice were housed in groups in a specified pathogen-free facility with a 12h day/12h night cycle with free access to chow and water.

C57BL/6J mice were purchased from Charles River. In this study, three lines of inducible knockout mice of POR have been generated:

1. smooth muscle cell-specific tamoxifen-inducible knockout mice of POR (smcPOR$^{-/-}$) were generated as previously described[53]. Briefly, CPR$^{flox/flox}$ mice[115] were crossed with Smmhc-CreERT2 (Myh11, smooth muscle myosin heavy chain) mice[116]. Since CreERT2 is under the control of the Myh11 promoter/enhancer region on the BAC transgene, which is carried by the Y chromosome, only male mice could be utilized from this line. Control animals (CTL) are defined as carrying the Cre-recombinase as well as the floxed POR gene but without tamoxifen treatment.
2. endothelial cell-specific tamoxifen-inducible knockout mice of POR (ecPOR$^{-/-}$) were generated as previously described[117]. CPR$^{flox/flox}$ were[115] crossed with Cdh5-CreERT2 transgenic animals[118]. Control animals (CTL) are denoted here as CPR$^{flox/flox}$-Cdh5-CreERT2$^{0/0}$ littermates (i.e. no cre expression) with tamoxifen treatment.
3. global inducible knockout mice of POR (POR$^{-/-}$) were generated by crossing CPR$^{flox/flox}$ mice[115] with CMV-GT-Rosa-CreERT2$^{TG/0}$.

Deletion of POR was induced by feeding mice with tamoxifen (400 mg/kg) for 10 days when they were 8 weeks old. Both POR$^{-/-}$ and smcPOR$^{-/-}$ underwent a washout of 10 days, whereas a washout of 30 days was applied to ecPOR$^{-/-}$ animals.

4.1.2 Nitrite measurements

4.1.2.1 CYP450-containing microsomes

Nitric oxide (NO) is a colorless gas with a half-life of 3-5 seconds in biological tissue[39]. Nitrite (NO_2^-) is the major oxidation product of NO in absence of oxyhemoglobin or superoxide anion and is produced by the reaction of NO with oxygen. Hence, nitrite can be used as a footprint of NO. Nitrite levels in plasma samples were measured with the Nitric Oxide Analyser (NOA, Sievers NOA-280) in a nitrogen atmosphere using acetic acid and sodium iodide.

Vascular CYP enzymes (CYP2C8, 2C9, 3A4 and 1B1) were purchased in the form of recombinant Supersomes™ (Corning). Each POR/CYP combination was individually incubated with NO prodrugs: NTG, PETN, ISDN, ISMN and molsidomine. POR+CypB5, i.e. without the catalytic CYP unit, was used as a negative control. DETA-NONOate (100 µM), a spontaneous NO donor, was used as a positive donor. CYPs inactivation was induced by SKF525 (100 µM), a non-selective CYP suicide inhibitor. CYP enzymes (10 µg of total protein) were incubated in HEPES in the presence of NO prodrugs (100 µM) and nitric oxide release was measured 3, 10, 30 and 60 min after adding NADPH (100 µM).

4.1.2.2 Plasma samples and aortic rings

Mice received low nitrite water for 5 days before the measurements. Blood was collected from the right ventricle into heparin tubes. Samples were centrifuged for 10 min at 2000g at 4°C. Plasma was separated and further cleared by centrifugal filter units (Microcon®-10) for 70 min at 13,000rpm at 4°C. Nitrite plasma levels were measured by loading 50 µL to the NOA and sodium nitrite (100 nM to 10 µM) was used as reference curve.

Nitrite production of vessels was measured from the supernatant of aortic rings. For that purpose, 1 mm rings of $smcPOR^{-/-}$ and CTL animals were incubated in a 96 wells plate with NTG or PETN (100 µM) for 30 min at 37°C. In selected experiments, CYPs and ALDH2 were inhibited with SKF525 (100 µM) or benomyl (10 and 100 µM) respectively. Aortic rings were pre-treated with those inhibitors for 5 min followed by 25 min incubation with NTG or PETN.

4.1.3 Echocardiography

Cardiac function and structure of the left ventricle (LV) were assessed by ultrasound imaging using the Vevo 3100 device. Body temperature and heart rate were kept at 37°C and 450-500 beats per minute (BPM), respectively.

Anesthesia was induced with 4% Isoflurane in an induction chamber. Anesthesia was maintained throughout the procedure with 1.5-2% Isoflurane provided in 1L/min O_2. Eye ointment protection was applied before animal was placed on the heated platform (straight, 0°) on supine position. Electrocardiogram (ECG) gel was applied on each of the electrodes and mouse's paws were taped down to the table electrodes (**Figure 10A**). Hair removal cream was applied on the mouse's chest and after 1 minute was wiped away using wet gauze swabs (**Figure 10B**). Body temperature was controlled through a rectal thermometer and gel was smeared over the chest before positioning the transducer (**Figure 10C**).

The vevo ultrasound cardiovascular package was used in both B- and M-modes. Cardiac structures were first assessed in B-mode parasternal long axis view (PSLAX). For that purpose, the transducer was first turned sagital to the mouse, the table tilted to the left and the mouse's limbs brought down. Afterwards, the transducer was angled pointing toward the center of the mouse and toward the observer (**Figure 10D**). Finally, the transducer was rotated 45° counterclockwise in order to line up with the angle in the mouse heart (**Figure 10E**). For the short-axis view (SAX), the transducer was turned 90° clockwise (**Figure 10F**) and M-mode was selected to evaluate the motion of the heart over time.

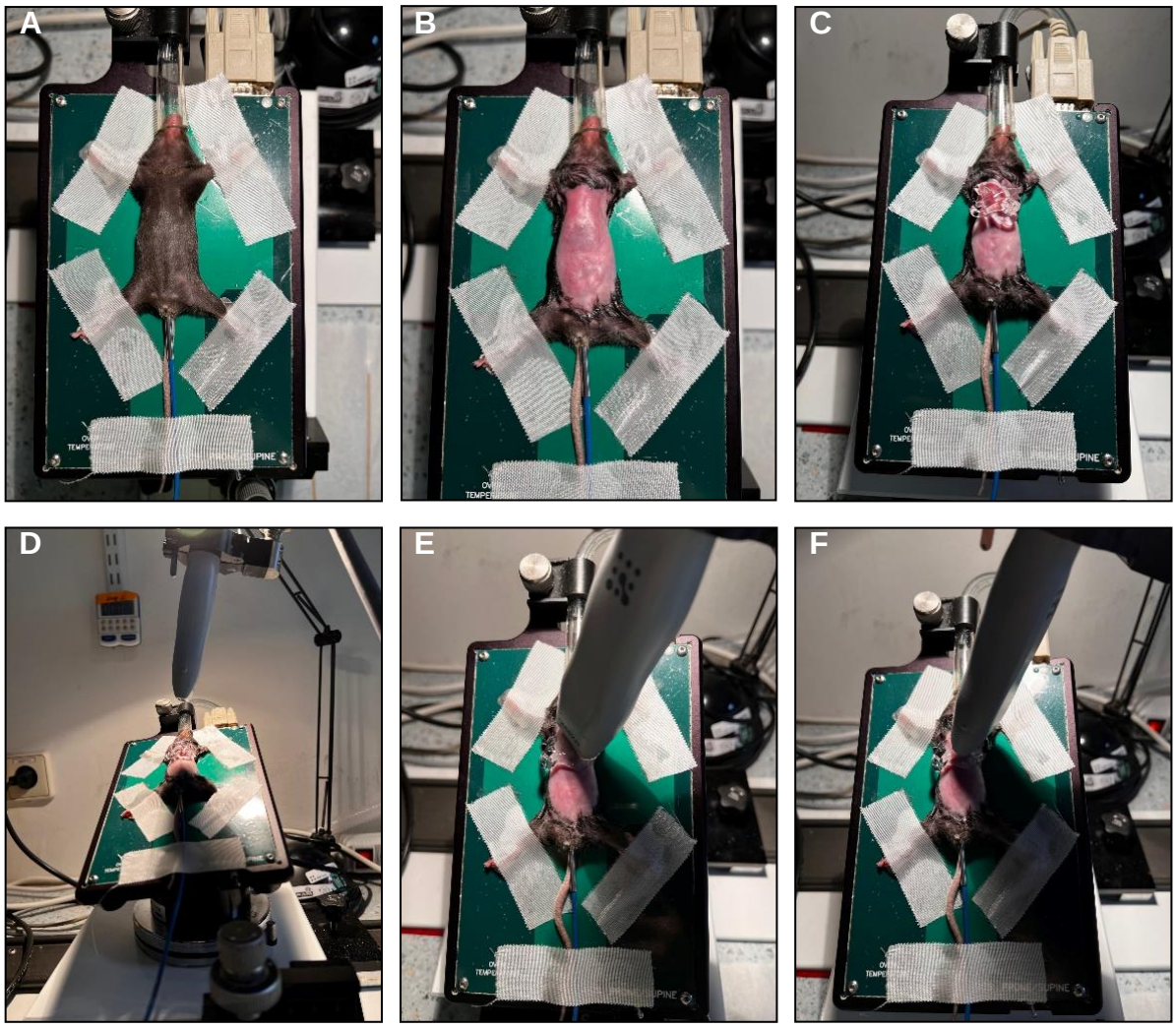

Figure 10. Echocardiography setup.
A: Animal in supine position with paws taped down to electrode tables. **B:** Naked chest after hair removal. **C:** Ultrasound gel applied on mouse chest. **D:** Tilted table to the left with mouse's limbs brought down. **E:** Transducer rotated 45° counter clockwise for PSLAX. **F:** Transducer rotated 90° clockwise for SAX. PSLAX: parasternal long axis view; SAX: short axis view.

Pictures and recordings were taken in both B-mode PSLAX and M-mode SAX (**Figure 11A**, **Figure 11B**).The analysis of the data was performed with the Vevo LAB desktop software. The Cardiac Package and SAX were selected. Cardiac measurements were obtained from M-mode images.

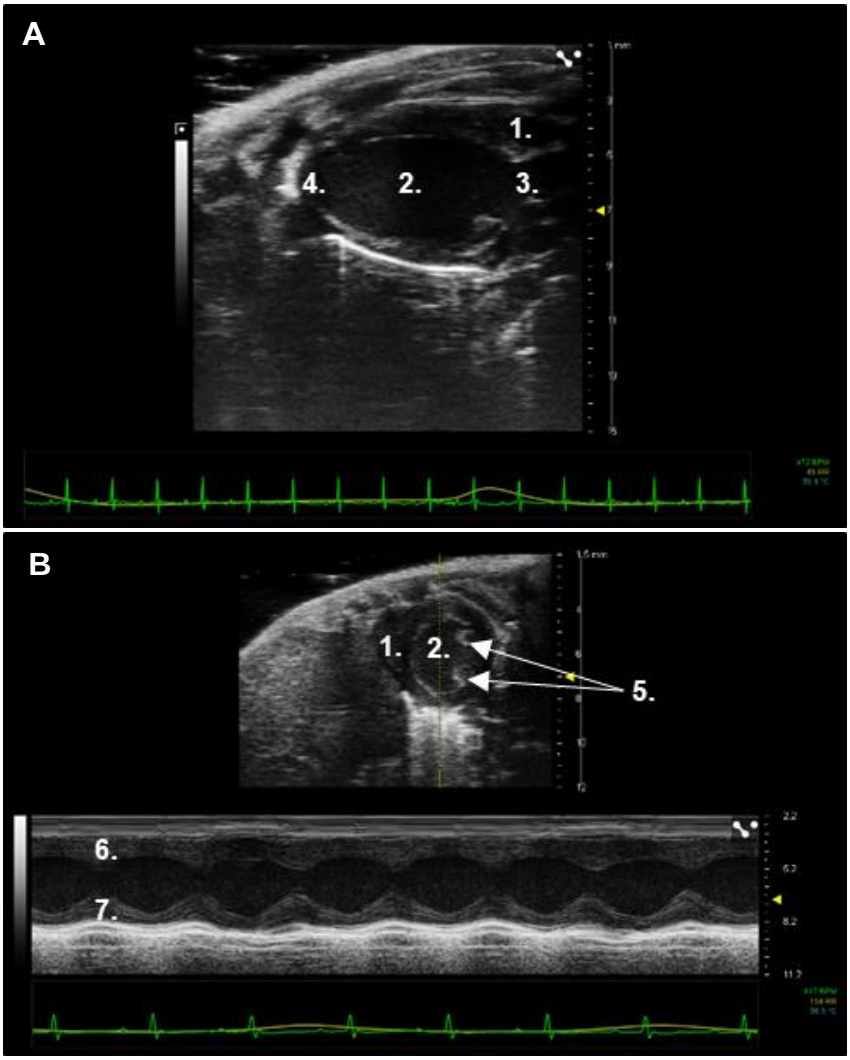

Figure 11. Representative images in B-mode PSLAX and M-mode SAX.
A: Representative image taken in B-mode PSLAX. **B:** Representative image taken in M-mode SAX. 1: right ventricle; 2: left ventricle; 3: aorta; 4: apex; 5: papillary muscles; 6: anterior wall; 7: posterior wall.

4.1.4 Transverse aortic constriction

Transverse aortic constriction (TAC) is a cardiac pressure-overload model resulting in left ventricular hypertrophy[119]. This is helpful to study the molecular pathways involved in the transition from cardiac hypertrophy to heart failure[120]. The surgery used in this project utilizes O-rings for constriction and was implemented through a collaboration with the group of Prof. Johannes Backs, University of Heidelberg. This O-ring method[121] reduces the variability imposed by the original constriction method utilizing a needle and a guide.

TAC surgery was performed in 8 weeks old mice with a body weight of 20-23 g. One day before the surgery, metamizol (2 mg/mL) was provided in the drinking water and maintained for four days post-surgery. O-ring aortic bandings (ORAB, inner diameter

of 0.50mm) were used to constrict the aorta and prepared as following (**Figure 12A**): First, a lateral incision was made with a scalpel (**Figure 12B**) and a non-absorbable 7-0 ethicon suture was passed through the ends of the opening cut (**Figure 12C**). Sutures of 2 cm were left on each side of the ring ends and the suture ends from the same side of the o-ring were passed through the hole of the spinal cord hook (**Figure 12D**).

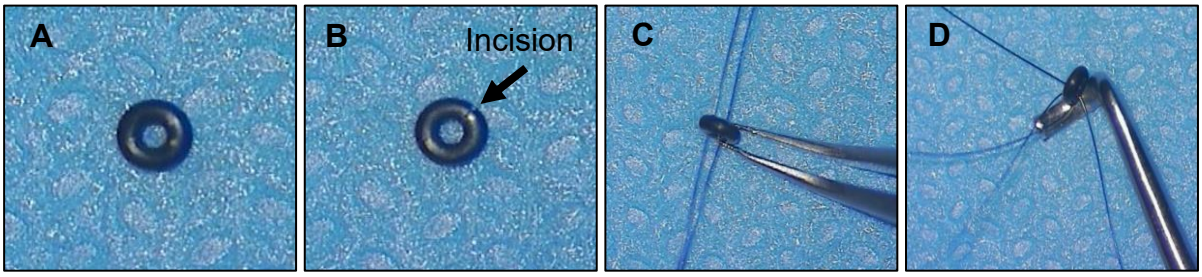

Figure 12. ORAB preparation for transverse aortic constriction.
A: O-ring before preparation. **B:** Incision made with a scalpel. **C:** Non-absorbable 7-0 ethicon suture at each end of the opening cut. **D:** Suture ends from the same side of O-ring passed through hole of spinal cord hook. ORAB: o-ring aortic banding; inner diameter of 0.5mm.

On the day of the surgery, a sterile area was prepared, and surgical tools were cleaned with 70% ethanol (EtOH). Buprenorphine was administrated subcutaneously 20 min prior to surgery (0.05 mg/kg). The mouse was anesthetized in an induction chamber with 5% isoflurane provided in 1L/min O_2 and quickly fixed in a supine position on the sterile field above a 37°C heating plate. For intubation of the animal, its head was pulled back by its upper incisor teeth, its tongue was pulled out and the mouth kept opened with an intubation spatula. The vocal cords were visualized by placing a light source above the throat. Once the tracheal opening was seen, the endotracheal tube (IV catheter 22G) was inserted (~5 mm), secured with a piece of tape and connected to the ventilator system (MiniVent ventilator) with 1.5-2% isoflurane provided in 1L/min O_2. The animal chest was shaved and disinfected with povidone-iodine (Braunol). A longitudinal 1.5 mm skin incision was made on the left side of the chest to have access to the intercostal muscles. The major and minor pectoral muscles were retracted using a mouse retractor set (Kent Scientific #13-005-180). The third intercostal muscle was pierced with extra fine Graefe forceps (FST #11151-10) and the incision was extended with sharp scissors. The transverse aorta was accessed by retracting thymus and costae. For better reproducibly, the fat surrounding the aorta was carefully cleaned using Dumont SS forceps (FST 11203-25). The suture ends from the same side of the o-ring were passed under the aorta between the brachiocephalic and left common

carotid arteries using a spinal cord hook (FST #10162-12) (**Figure 13A**). The o-ring was opened and placed around the aorta by grasping and pulling the suture ends on both sides of the aorta (**Figure 13B**). After closing the o-ring by tiding the lower and upper sutures with a double knot, the excess ends were cut (**Figure 13C**). The retraction system was removed and the thymus was placed back. The incision was closed with two single-sutures using 6-0 prolene (Ethicon #8889H) and covered by pectoral muscles. The skin was closed with continuous sutures using 6-0 prolene. Anesthesia and ventilation were stopped and the mouse was placed in a cage on a heating plate until it awaken. Post operative pain management was treated by buprenorphine (0.05mg/kg, s.c.) every 12h for 4 days. Supplementary food was provided by DietGel Recovery (Clear H_2O).

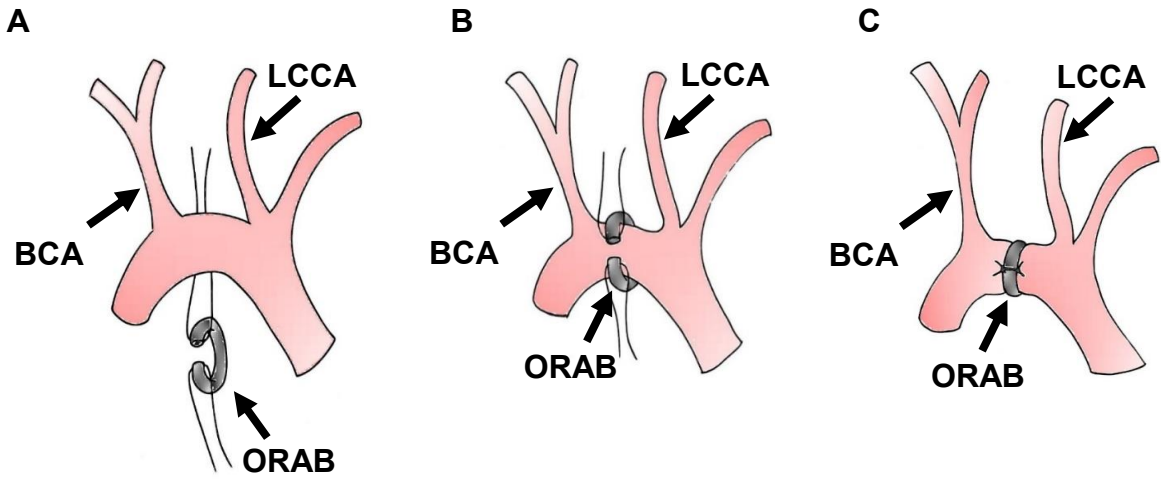

Figure 13. Schematic representation of transverse aortic constriction with ORAB.
A: Suture ends passed under the aorta between BCA and LCCA. **B:** Opening of ORAB to place it around the aorta. **C:** Closing of the ORAB leading to constriction of the aorta. BCA: brachiocephalic artery; LCCA: left common carotid artery; ORAB: o-ring aortic banding. Figure published in Lopez *et al.* (2022)[122].

One week post-surgery, animals were injected intraperitoneally (i.p.) with tamoxifen (333mg/kg) on three consecutive days to induce the knockout of POR in endothelial cells. Hypertrophy of the LV was assessed by echocardiography at days 7, 14, 21, 28, 35, 42, 49, 56 and 61 post-surgery. At day 61, animals were weighted and subsequently sacrificed by isoflurane overdose. After transcardiac perfusion by gravity flow with Hank's buffer, hearts and lungs were collected. The organs were weighted for the ratio to body weight and lungs were snap frozen in liquid nitrogen. For fibrosis detection, the hearts were cut in short axis plane, transferred into a 2mL Eppendorf tubes filled with 4% PFA for 1h, then placed overnight in a 2mL tubes with 30%

sucrose. The next day, cardiac biopsies were embedded in OCT™ compound for Sirius red staining. Planning of TAC experiments is depicted in **Figure 14**.

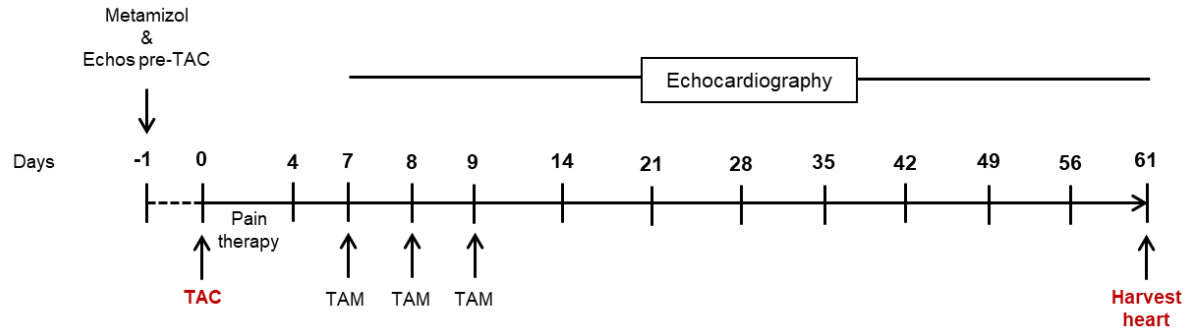

Figure 14. Workflow of transverse aortic constriction in ecPOR mice.
One week post-TAC, the knockout of POR was induced with tamoxifen injected intraperitoneally for 3 consecutive days. Echocardiography was performed one day before TAC surgery, followed by once a week until the mice were sacrificed after 61 days. TAC: transverse aortic constriction; Echos: echocardiography; TAM: tamoxifen; Pain theray: metamizol (2 mg/mL) and buprenorphine (0.05 mg/kg).

4.2 Molecular biology methods

4.2.1 Reductase activity in aortic rings

Nitro blue tetrazolium (NBT) is a chemical compound with 2 tetrazole rings that can be reduced by POR using NADPH as electron donors[123–125]. Such reducing capacity of POR in aortic SMCs was visualized by conversion of yellow NBT salt to the insoluble blue formazan in smcPOR$^{-/-}$ and control littermates.

Aortas from smcPOR$^{-/-}$ and CTL mice were freshly isolated and cleaned of fat tissue. Endothelium was removed by incubating the aortas for 15 sec with Krebs-Henseleit buffer supplemented with 1% CHAPS and 5% glucose. After 3 washes of 15 sec with Krebs-Henseleit, aortas were embedded in OCT™ (Tissue-Tek®) and frozen on dry ice. Tissues sections of 10 µm were incubated with 0.02% NBT and 100 µM NADPH in Hepes Tyrode (HT) buffer for 30 min at 37°C. After washing with HT buffer, the tissue sections were embedded in Dako Fluorescence Mounting medium and cover slipped. Formation of formazan crystals were studied under a light microscope.

4.2.2 Isometric tension recordings

Organ chamber experiments for isometric tension recordings are a classical pharmacological tool which allows the rapid evaluation of concentration-response relationship of contractile tissues *ex vivo*[126]. In this context, the relaxation of aortic rings of smcPOR$^{-/-}$ animals in response to NO donor drugs was studied.

Aortas from smcPOR$^{-/-}$ and control animals were isolated on the day of the experiment. The surrounding fat was trimmed and aortas were cut into 1 mm rings. In selected experiments, the endothelium was removed by a brief treatment with the detergent CHAPS. For this, the rings were incubated in Krebs-Henseleit buffer supplemented with 1% CHAPS and 5% glucose, as described above. Before each experiment, standardized 1 g weights were used for calibrating the organ bath setup. To maintain the viability of the rings, the organ chambers were filled with a carbogen-aerated Krebs-Henseleit buffer (95% O_2, 5% CO_2, 37°C, pH 7.4). Aortic rings were mounted on a triangular setup, made of two triangular metals, which was then attached to a F30 force transducer (Hugo Sachs Elektronik Harvard Apparatus) (**Figure 15**).

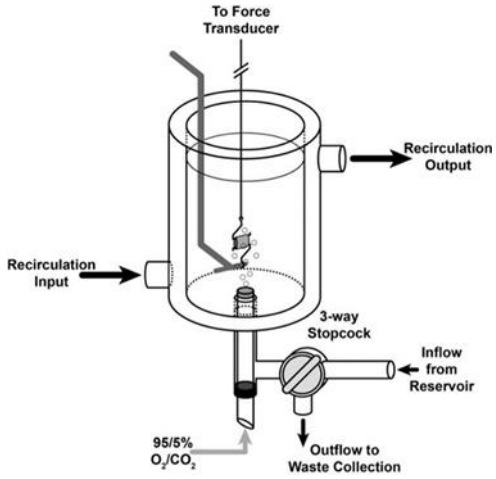

Figure 15. Schematic of an organ bath chamber with mounted aortic ring.
The aortic ring is fixed on a two-end triangular setup with one of the ends fixed to a force transducer and is always bathed in a Krebs-Henseleit buffer. The buffer is continuously aerated with carbogen (95% O_2 and 5% CO_2) and the buffer can with exchanged through an outflow valve. The circulation of water in the inner of the double-wall glass allows the temperature of the chamber to be kept at 37°C. Figure from Jespersen *et al.* (2015)[126].

After pre-conditioning the vessels to a starting force of 1 g, their maximum vascular contraction was reached by exchanging the buffer to a KCl-enriched buffer (80 mM). The vessels were relaxed by using the initial KCl-free buffer and contracted once again using the KCl-enriched buffer (80 mM). This second contraction was referred as the maximum contractile response for each individual ring.

After three washing steps with KCl-free Krebs-Henseleit buffer, 80% of the initial KCl constriction was reached by cumulatively increasing phenylephrine concentration (range of 10^{-10} M to 10^{-6} M). Subsequently, vessels relaxation was achieved with cumulative doses of acetylcholine (ACh), NTG or PETN (10^{-10} M to 10^{-5} M). Additionally, vessel relaxation by spontaneous NO-release of DETA-NONOate was

used as a positive control. Finally, in selected experiments, aortic vessels were pre-exposed to the ADLH2 inhibitor benomyl (100 µM, 5 min) in organ bath chamber prior to addition of phenylephrine, ACh, NTG or PETN. The dilation dose-response curves were analyzed using the software LabChart8 and represented relative to the constrictor response to phenylephrine.

4.2.3 Immunofluorescence

Aortas from smcPOR$^{-/-}$ and control mice were freshly isolated and embedded in OCT™ (Tissue-Tek®) compound and frozen on dry ice. Frozen tissues were cut to a thickness of 10 µm over Superfrost® plus slides. Aortic rings were first fixed with 4% paraformaldehyde (PFA) for 10 min at RT and then permeabilized with 0.3% Tween (in PBS) for three times 5 min. After 30 min incubation with 3% bovine serum albumin (BSA), the tissue sections were stained overnight with an antibody against caldesmon-1 (diluted 1:200) or α-smooth muscle actin (Cy3 conjugate, diluted 1:300). After three washing steps, the sections stained for caldesmon-1 were incubated for 30 min with an anti-rabbit Alexa Fluor 546 (diluted 1:500). Finally, nuclei were counter-stained with 4',6-Diamidino-2-phenylindol (DAPI, diluted 1:200) and after three washing steps, the sections were embedded in Dako Fluorescence Mounting Medium. Pictures were taken using a Zeiss LSM 800 confocal microscope and analyzed using ImageJ software.

4.2.4 Hematoxylin & Eosin staining

Hematoxylin and Eosin (H&E) staining is a histological staining used for a broad overview of the cellular structures of both frozen and paraffin embedded tissues. While hematoxylin stains for the nuclei in a blue-purple color, the cytoplasma and other structures like extracellular matrix are stained in pink with eosin[127].

Frozen tissues were cut over Superfrost® plus microscope slides and fixed with 4% PFA for 10 minutes at RT. Nuclei were stained with Mayer's hematoxylin for 6 minutes and after three washing steps, the cytoplasm was stained with eosin (2% in ddH_2O) for 1.5 minute. Tissue sections were dehydrated as followed: 70% EtOH, 100% EtOH, 100% isopropanol, and xylen. The slides were embedded in entellan and the vascular structure were studied under a light microscope (Microscope Axiovert 40 ETL).

4.2.5 Wheat Germ Agglutinin staining

Wheat germ agglutinin (WGA), a lectin, is widely used in cell biology. Combined to Alexa Fluor dyes, WGAs are probes used for the detection of N-acetyl-D-glucosamine and sialic acid on cell membranes[128]. Based on those characteristics, cross sectional area of cardiac sarcolemma was determined with WGA. Staining and analysis were performed by our collaborator Dr. Deepak Prabhu Ramanujam (Technische Universität München, Munich, Germany).

Hearts of ecPOR$^{-/-}$ and control littermates were freshly isolated and transverse sections of heart samples was fixed with 4% PFA for 1 hour and transferred in a 2 mL Eppis with 30% sucrose overnight. The next day, samples were embedded in OCT™ (Tissue-Tek®) and frozen on dry ice. Frozen tissues were cut to a thickness of 8 µm over Superfrost® plus slides. The antigen retrieval sodium-citrate buffer was added on top of the tissue sections and heated up for 4 min in the microwave. Tissue sections were incubated with WGA (1:100 in PBS) for 1.5 hour at RT and nuclei were stained with Sytox Green (10 min, 1:1000 in PBS). After three washing steps, slides were embedded in Aquatex and stored at 4°C until analysis. Images were taken using a confocal microscope (Leica TCS SP5 II) and the average cross-sectional area of cardiomyocytes was determined using Metamorph software[129].

4.2.6 RNA isolation, reverse transcription and quantitative real-time PCR

Isolation of total RNA was performed using RNeasy fibrous tissue mini kit (Qiagen). A stainless steel bead and 300 µL RLT buffer were added to 25 mg heart tissue and samples were homogenized for 5 min 50Hz by a tissue lyser. The lysates were transferred into a new 2 mL tube with 590 µL RNase-free water and 10 µL proteinase K. Samples were incubated for 10 min at 55°C and centrifuged at RT for 3 min at 10,000x*g*. Supernatant was mixed with 450 µL absolute ethanol, transferred to the Rneasy mini column (provided by the kit) and centrifuged for 15 sec at 10,000x*g*. RW1 buffer (350 µL) was added to the RNA-bound column followed by centrifugation for 15 sec at 10,000x*g*. DNase I mix was directly added to the column membrane. After 15 min incubation at RT, 350 µL RW1 buffer was added and samples were centrifuged for 15 sec at 10,000x*g*. The column was washed twice with RPE buffer (500 µL): 15 sec at 10,000x*g* and 2 min at 10,000x*g*. Column was dried by centrifugation for 1 min at full speed. Purified RNA was eluted with 50 µL RNase-free water. RNA

concentration was determined by measuring the absorption spectra difference between 260 nm and 280 nm using a Nanodrop 2000 spectrophotometer.

A specific amount of purified RNA (500 ng) was reversely transcribed into complementary DNA (cDNA) according to manufacturers' protocol of SuperScript III:

Table 15. Master mix cDNA synthesis I

Chemicals	Volume [µL]
RNA 500 ng	X
Random Primer (50 µg/mL)	1
dNTPs (10 mM)	1
Oligonucleotides (70 µM)	0.7
RNase-free water	12.05 – x

In order to facilitate the binding of the random primers to the RNA, the master mix I was first incubated at 65°C for 5 min and cooled down to 4°C. Afterwards, the master mix II was added:

Table 16. Master mix cDNA synthesis II

Chemicals	Volume [µL]
5-fold buffer	4
DDT (0.1 M)	1
SuperScript III (2000 U/µL)	0.25

The following program was run to complete the reverse transcription:

Table 17. Temperature for reverse transcription

Temperature [C°]	Time [min]
25	5
50	60
70	15
4	∞

Expression levels of mRNA transcripts were determined using the quantitative real-time polymerase chain reaction (PCR) method. Amplification of cDNA with specific oligonucleotides was quantified by fluorescence measurements of the fluorophore SYBR Green. As the latter intercalates into double stranded cDNA, which massively increases its fluorescence, the resulting fluorescence was proportional to the initial

concentration of cDNA of a specific gene and measured as the so-called cycle threshold (C_T). For real time PCR, diluted cDNA (1:1) was added to the following reaction:

Table 18. Master mix for qRT-PCR

Chemicals	Volume [µL]
2-fold SYBR Green	10
cDNA	1
DNase free water	8
Forward Primer (10 µM)	0.5
Reverse Primer (10 µM)	0.5

Each reaction was performed in technical duplicates and the binding specificity of the oligonucleotides was ensured by looking at the melting curves at the end of the reaction. The following program was used for the qRT-PCR:

Table 19. Program for qRT-PCR

Reaction	Time [s]	Temperature [C°]	Cycles
Activation	195	95	1
Denaturation	15	95	
Annealing	20	60	45
Elongation	20	72	
	30	95	
Melting curve	30	55	1
	30	95	

The relative expression of each gene of interest was normalized to β-actin, used as a reference gene, and then analyzed by the $2^{-\Delta\Delta C_T}$ method with the Agilent Aria 1.5 Software.

4.2.7 Isolation of cardiac endothelial cells for RNA sequencing

Cardiac endothelial cells were isolated from left ventricle (LV) of ecPOR$^{-/-}$ and CTL mice while the remaining cardiac tissue was used as cardiac fraction. Two LV per genotype were pooled in 1 mL HBSS and minced into small pieces with dissecting scissors. Mince tissues were then transferred to a 50 mL Falcon containing an enzyme mix (dispase: 1.2 U/mL; collagenase II: 2 mg/mL; elastase: 0.03 mg/mL) for 20 min

digestion at 37°C. Digestion was stopped with stopping solution (DMEM + 10% FBS) followed by filtration with 100µm strainer. Samples were centrifuged (10 min, 500 xg, 4°C), the pellet was re-suspended in 10 mL RBC lysis buffer and the samples were centrifuged (5 min, 500 xg, 4°C). The pellet was re-suspended in 6.2 mL cold DPBS, transferred to a 15 mL Falcon, 1.8 mL Debris Removal Solution (Miltenyi Biotec) was added and overlayed very gently with 4 mL cold DPBS. After centrifugation (10 min, 3000xg, 4°C), the two top phases were aspirate, filled up to 15 mL with cold DPBS, and samples were centrifuged (10 min, 3000 xg, 4°C). The pellet was re-suspended in 200 µL DMEM + 10% FCS containing the antibody (Lectin FITC conjugate). After 20 min incubation, 500 µL DMEM + 10% FCS were added and samples were centrifuge (5 min, 300 xg, 4°C). Cells were re-suspended in 200 µL FACS buffer 1 (DPBS, 0.5% BSA and 2 mM EDTA) containing DRAQ5 (BioLegend). FACS-sorting was performed by Praveen Mathoor (Institute of Biochemistry I, Frankfurt, Germany). Cells positive for both DRAQ5 and Lectin were selected and FACS-sorted into 300 µL FACS buffer 2 (DPBS, 10% FCS, 3 mM EDTA and 25 mM HEPES). After sorting, cells were centrifuged (5 min, 500 xg, 4°C) and total RNA was isolated using the RNeasy micro kit (Qiagen, Hilden, Germany) combined with on-column DNase digestion (DNase-Free DNase set, Qiagen) to avoid contamination by genomic DNA. Total RNA from LV (cardiac fraction) of ecPOR$^{-/-}$ and CTL animals was isolated using the RNeasy fibrous tissue mini kit (Qiagen) combined with on-column DNase digestion (DNase-Free DNase set, Qiagen).

4.2.8 RNA sequencing

RNA and library integrity checks were performed by Dr. Stefan Günther (Max Planck Institute for Heart and Lung, Bad Nauheim, Germany) and verified with LabChip Gx Touch 24 (Perkin Elmer). For cardiac samples 4 µg of total RNA was used as input for VAHTS Stranded mRNA-seq Library preparation following manufacture's protocol (Vazyme). For EC samples 9.5 µl total RNA was used for SMART-Seq® v4 Ultra® Low Input RNA Kit (Takara Bio). Sequencing was performed on NextSeq2000 instrument (Illumina) with 1 x 72 bp single end setup. The resulting raw reads were assessed for quality, adapter content and duplication rates with FastQC[130].

4.3 Protein biochemical methods

4.3.1 Protein isolation and Bradford assay

Protein isolation of tissue: freshly isolated organs were homogenized in Triton x-100 lysis buffer with a TissueLyser LT (Qiagen) at 50 Hertz, for 1 or 5 min depending on the tissue. The lysate was centrifuged (10 min, 16000 x*g*, 4°C) and the supernatant was collected for further analysis. In selected experiments, freshly isolated thoracic aorta and liver were weighted and grinded with TissueLyser in an adapted volume to get 10 µg/µL of proteins.

Protein isolation of cardiac endothelial cells: cells were isolated as described in section 4.2.8 (RNA sequencing) with the following modifications. After centrifugation (5 min, 500 x*g*, 4°C), the pellet was re-suspended in 1 mL washing buffer. Samples were centrifuged (10 min, 300 x*g*, 4°C) and a CD144-coupled beads mix was added to the cell pellet and rotated for 40 min at RT. After three washing steps with DMEM + 10% FCS, the beads were eluted from the cells by adding Triton x-100 lysis buffer. The lysates were centrifuged and the supernatant was harvested for further analysis.

Protein concentration of the supernatant was determined by the Bradford assay. After adding 2.5-fold Bradford solution (ROTI®-Quant) to 1:100 diluted samples, the absorbance was measured at 595 nm by a Tecan 2000 plate reader. A bovine serum albumin (BSA) protein standard curve with known concentrations (water, 2.5 µg/mL, 5 µg/mL, 10 µg/mL, 20 µg/mL, 30 µg/mL, 40 µg/mL and 50 µg/mL) was used to calculate the protein sample concentrations. In order to reduce and break the bisulfide bonds, a DTT-containing sample buffer (Laemmli-buffer) was added to the lysate. Afterwards, samples were boiled at 95°C for 5 min.

4.3.2 SDS-PAGE and Western blotting

Proteins were fractionated by sodium dodecyl sulfate polyacrylamide gel electrophoresis (SDS-PAGE). 10 to 300 µg of total protein were loaded on a Tris/HCl polyacrylamide buffered stacking gel (5% polyacrylamide, pH 6.8) at 60 V. Next, proteins were separated in a Tris/HCl polyacrylamide separating gel (10%, pH 8.8) at 120 V. The samples were run together with a size standard (Precision Plus Protein All Blue Standard) in order to define the size of the proteins of interest. Afterwards, the gels were blotted onto a methanol activated nitrocellulose membrane at 250 mA for 90 min. To overcome any unspecific binding, membranes were first blocked for 30 min

with ROTI® block and then incubated overnight at 4°C with primary antibody. After three washing steps, membranes were incubated with infrared-fluorescent-dye-conjugated secondary antibody. Depending on the fluorescence of the conjugated antibody used, the proteins of interest were detected at 680 or 800 nm with an infrared imaging detection system (LI-COR).

4.4 Metabolomics

Mice were sacrificed and perfused with Hanks buffer. Untargeted global metabolomics from cardiac tissue (50 mg left ventricle) was performed by Metabolon Inc. (Morrisville, NC, USA) using a Waters ACQUITY ultra-performance liquid chromatography (UPLC) and a Thermo Scientific Q-Exactive high resolution/accurate mass spectrometer interfaced with a heated electrospray ionization (HESI-II) source and Orbitrap mass analyzer operating at 35,000 mass resolution as previously described[131–133]. Samples were extracted with methanol to remove the protein fraction. The extract was divided into five fractions: two for analysis by two separate reverse phase (RP)/UPLC-MS/MS methods with positive ion mode electrospray ionization (ESI), one for analysis by RP/UPLC-MS/MS with negative ion mode ESI, one for analysis by hydrophilic interaction chromatography (HILIC)/UPLC-MS/MS with negative ion mode ESI, and one sample as a backup.

4.5 Statistics for wet lab

Unless otherwise indicated, data are shown as mean ± standard error of the mean (SEM). Calculation were performed with GraphPad Prism 8.3.0. In case of multiple testing, Bonferroni or Tukey correction was applied. For multiple group comparisons, ANOVA was performed followed by post hoc testing. For repeated measurements, ANOVA followed by Geisser-Greenhouse correction was applied. Individual statistics of unpaired samples was performed by t-test and if not normally distributed by Mann-Whitney *U* test. P values of <0.05 were considered as significant. *n* indicates the number of individual experiments or animals.

4.6 Computational methods

4.6.1 RNA-sequencing data analysis

The analysis of the RNAseq of both cardiac ECs and heart was carried out using R studio. The sequencing reads for all samples were aligned against the hg38 transcriptome, obtained from Ensembl using Salmon (v1.5.2)[134,135]. Reads not aligned

to the transcriptome were discarded at this point. Differential gene expression analysis was performed using DESeq2 (v1.32.0) in R (v4.1.1)[136,137]. Raw transcript counts were summed per gene and used in the standard DESeq2 differential gene expression analysis workflow, using a negative binomial test over gene counts in each of the combinations of conditions. Batch information was also included in the contrast formula, and genes with more than 4 zero counts across samples were removed from the analysis. The normalized gene counts, p-values and log2fold-change values were combined in an excel table. Differentially expressed genes were used for calculation of GO terms in Enrichr (online tool)[138–140]. The R package ggplot2 was used to create heatmaps in RStudio.

4.6.2 Metabolomics analysis

Raw data were extracted, peak-identified, and quality control-processed by Metabolon. Compounds were identified by comparison to library entries with over 3300 commercially available purified standard compounds[132]. A batch correction was performed by Metabolon[141]. Following log transformation and imputation of missing values, if any, with the minimum observed value for each compound, Mixed Model Contrasts were used to identify biochemicals that differed significantly between experimental groups. Missing values were imputed, and statistically analyzed using log transformed data. P values of <0.05 were considered significant. Visualizations and plots of metabolomics data were generated using the R package ggplot2 (v3.3.5) in R (v4.1.1).

5 Results

5.1 Part 1: Cytochrome P450 monooxygenases and vascular biotransformation of organic nitrates

The first part of this study focuses on the vascular biotransformation of organic nitrates. The capacity of recombinant CYP450 microsomes in biotransforming nitrovasodilators was determined by nitrite measurements. To study whether the POR/CYP450 system is part of the vascular biotransformation of organic nitrates, organ chamber experiments were performed using a smooth muscle cell-specific, tamoxifen inducible knockout of POR.

5.1.1 Recombinant CYP microsomes can biotransform nitrovasodilators

Previous studies showed that the hepatic POR/CYP450 system can bio-transforme NO prodrugs[80,142]. However, the vascular involvement of this system is still unclear. To further investigate their involvement, the CYP450 isoforms were selected based on their expression in the murine and human aorta as reported in published sequencing data[11,23,143]. Criteria were set to select for CYPs enzymes typically expressed in the aorta and commercially available in the form of recombinant Supersome^{TM}. Therefore, experiments were conducted with CYP2C8, 2C9, 3A4 and 1B1.

Nitrite release from NTG, PETN, ISDN, ISMN and molsidomine was measured as a nitric oxide (NO) footprint when incubated individually with each POR/CYP450 combination (**Figure 16**). As the negative control POR+Cytb$_5$ showed no signal when incubated with any NO donors, it confirmed the requirement of the catalytic CYP unit for the reaction. Interestingly, the nitrite production differed for NO donors, with NTG giving the highest signal. Moreover, the nitrite production was CYP-specific with CYP2C8 and CYP2C9 being more effective in releasing NO from NTG and PETN (**Figure 16A** and **Figure 16B**) than CYP3A4 and CYP1B1. In comparison, CYP2C9 and CYP1B1 were the only CYP oxidases able to generate nitrite from ISDN and molsidomine respectively (**Figure 16C** and **Figure 16E**). At equimolar concentrations, none of the POR/CYP450 combinations could generate nitrite from ISMN (**Figure 16D**). As expected, the positive control NONOate spontaneously released NO by a zero-order kinetic when incubated with POR+Cytb$_5$ (**Figure 16E**).

Together, these results indicate that recombinant microsomes can release nitrite from NO prodrugs in a CYP and dose-dependent manner. For further experiments, we

selected NTG, which is the most common organic nitrate, and PETN which does not lead to nitrate tolerance[61].

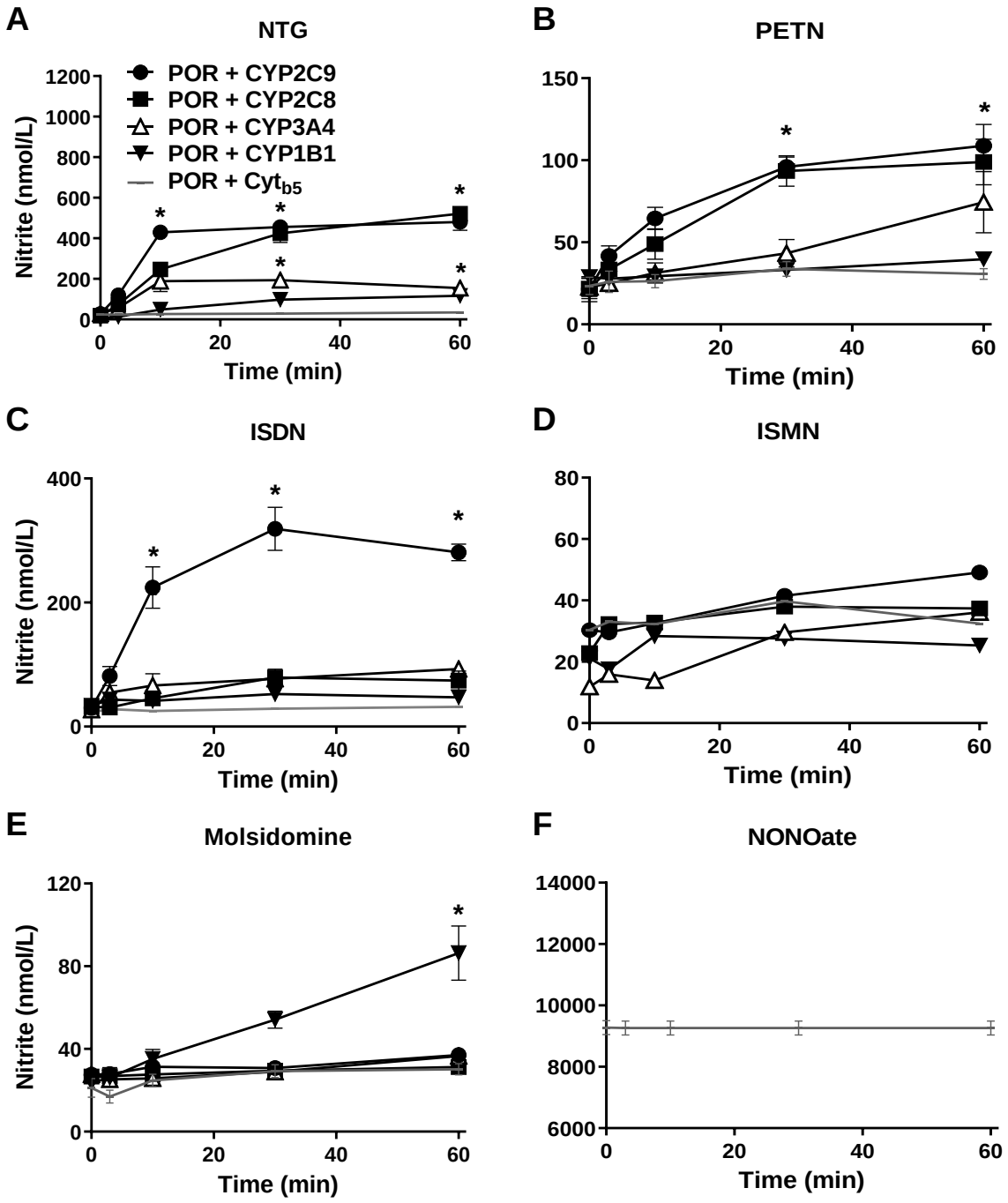

Figure 16. Nitrite (NO_2^-) production from nitrovisadilators by CYP-containing microsomes.

A-E: Nitrite production from microsomes (10 µg) when incubated either with NTG, PETN, ISDN, ISMN and molsidomine (100 µM) at 3, 10, 30 and 60 minutes. NADPH (100 µM) was supplemented to the samples. F: Nitrite production from the positive control NONOate which spontaneously release NO in contact with water. *p<0.05 compared to POR+Cytb5. n=5 independent experiments. Figure published in Lopez *et al.* (2021)[53].

5.1.2 A non-selective CYP suicide inhibitor inhibits nitrite release in recombinant POR/CYP microsomes

Next, we tested the catalytic capacity of the POR/CYP450 system in the biotransformation of NTG and PETN using isolated microsomes expressing the recombinant form of these enzymes. As CYP2C8 and CYP2C9 being the most effective enzymes, microsomes expressing those were pre-incubated for 5 minutes with a non-selective suicide CYP450 inhibitor, SKF525[144], before adding the prodrugs (**Figure 17**).

When blocking the catalytic subunit of CYP2C8 and CYP2C9 with SKF525, the nitrite production from NTG was abolished (**Figure 17A**). As expected, the nitrite production from PETN was blocked when incubated with SKF525 (**Figure 17B**).

Together, these results highlight the capacity of the recombinant POR/CYP450 system in the biotransformation of prodrugs as NTG and PETN.

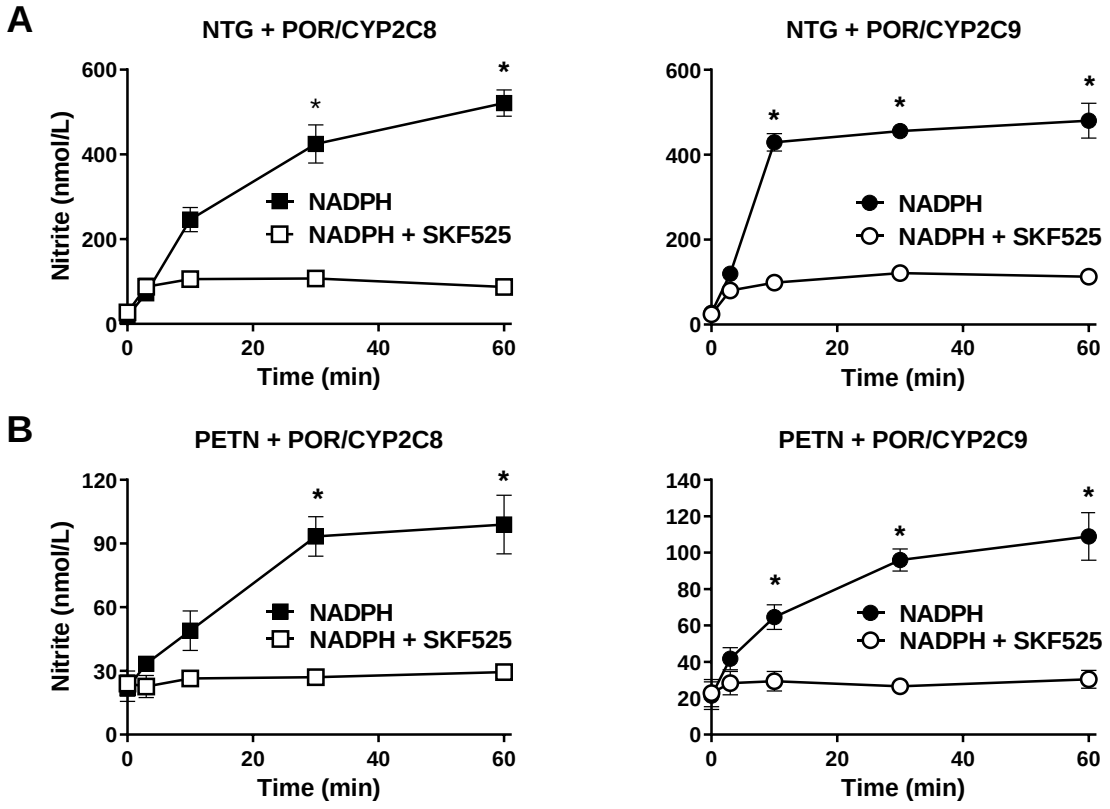

Figure 17. Nitrite production from nitrovisadilators by CYP-containing microsomes is blocked by a non-selective suicide CYP inhibitor.
A: Nitrite production from microsomes (10 µg) in presence of NTG (100 µM) when pre-incubated for 5 min with or without SKF525 (100 µM) at 3, 10, 30 and 60 min. **B:** Nitrite production from microsomes (10 µg) in presence of PETN (100 µM) when pre-incubated for 5 min with or without SKF525 (100 µM) at 3, 10, 30 and 60 min. NADPH (100 µM) was supplemented to the samples. *p<0.05 compared to NADPH. n=5 independent experiments. Figure published in Lopez *et al.* (2021)[53].

5.1.3 Deletion of POR in SMC does not lead to a cardiovascular phenotype

POR is broadly expressed in the vascular system and the constitutive knockout of POR is embryonically lethal[26,27]. Thus the first approach was to generate a global, tamoxifen-inducible knockout mouse of POR ($POR^{-/-}$). Surprisingly, global deletion of POR led to an early onset fatty liver (**Figure 18A**). Additionally, the knockout efficiency of POR differed between tissues, with a high variability and inefficiency in aorta (**Figure 18B**). This could be explained by the insufficient conversion of tamoxifen to its active form 4-hydroxytamoxifen by hepatic CYP450 enzymes[145]. As the progression of POR deletion in the liver potentially lowered hydroxy-tamoxifen levels, so that a sufficient knockout of POR in vessels could not be reached.

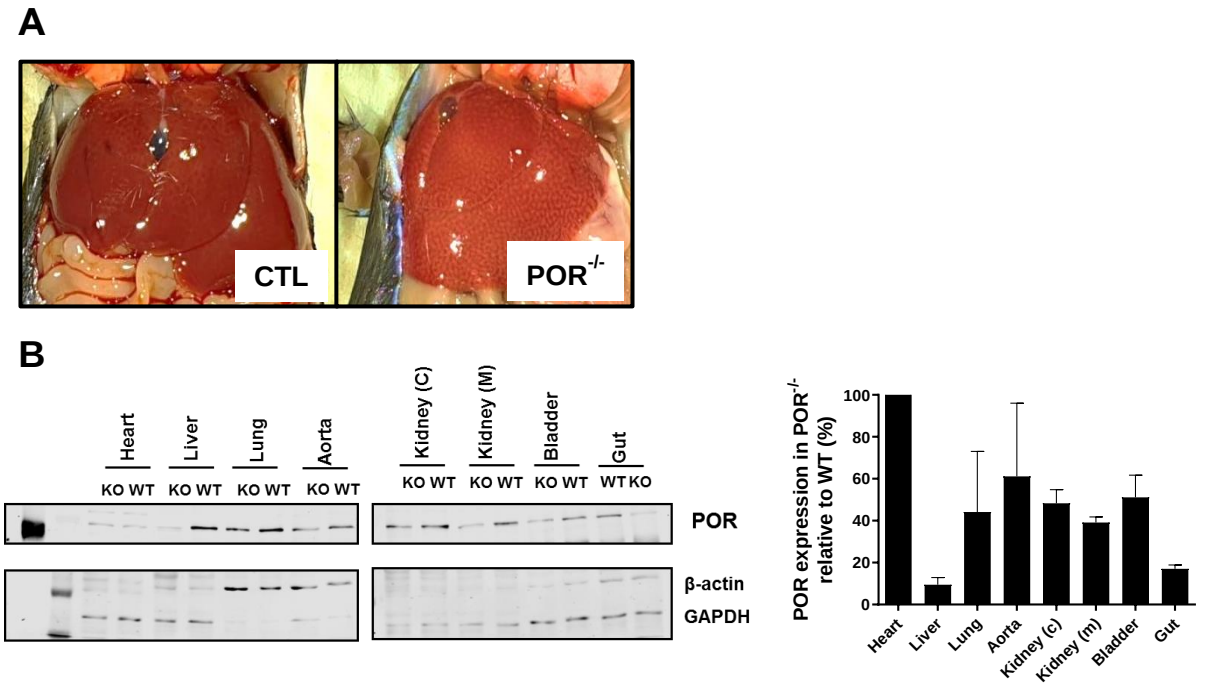

Figure 18. Knockout efficiency of global POR mouse model ($POR^{-/-}$).
A: Representative images of the fatty liver reported in $POR^{-/-}$ mice. **B:** Western blot analysis showing POR expression in different tissues after tamoxifen treatment. n=2 animals. Figure published in Lopez *et al.* (2021)[53].

Smooth muscle cells are not only the predominant vascular cell type but also the effectors of vascular relaxation[146]. Based on this, a smooth muscle-specific, tamoxifen inducible mouse knockout model was generated. First, the knockout efficiency of the $smcPOR^{-/-}$ mouse model was accessed (**Figure 19**) by Western blot. Analysis of aorta lysates showed a reduction of POR expression of about 70% in $smcPOR^{-/-}$ mice (**Figure 19A**). A complete deletion of POR could not be reached as other cells such endothelial cells or fibroblasts also express POR[23]. In order to confirm a complete ablation of POR activity in SMCs, NADPH-dependent reduction capacity of POR in

aortic SMCs was visualized by conversion of yellow NBT salt to the insoluble blue formazan in smcPOR$^{-/-}$ and CTL animals. Deletion of POR in SMCs resulted in a decrease in the reductase activity in vessels (**Figure 19B left panel**) as shown by a reduction in the conversion of NBT to formazan crystals. POR and other sources of NBT reducing enzymes, like eNOS (endothelial nitric oxide synthase) are still expressed in the endothelium. Thus removal of the endothelial layer led to a more pronounced difference between smcPOR$^{-/-}$ and control animals (**Figure 19B right pannel**).

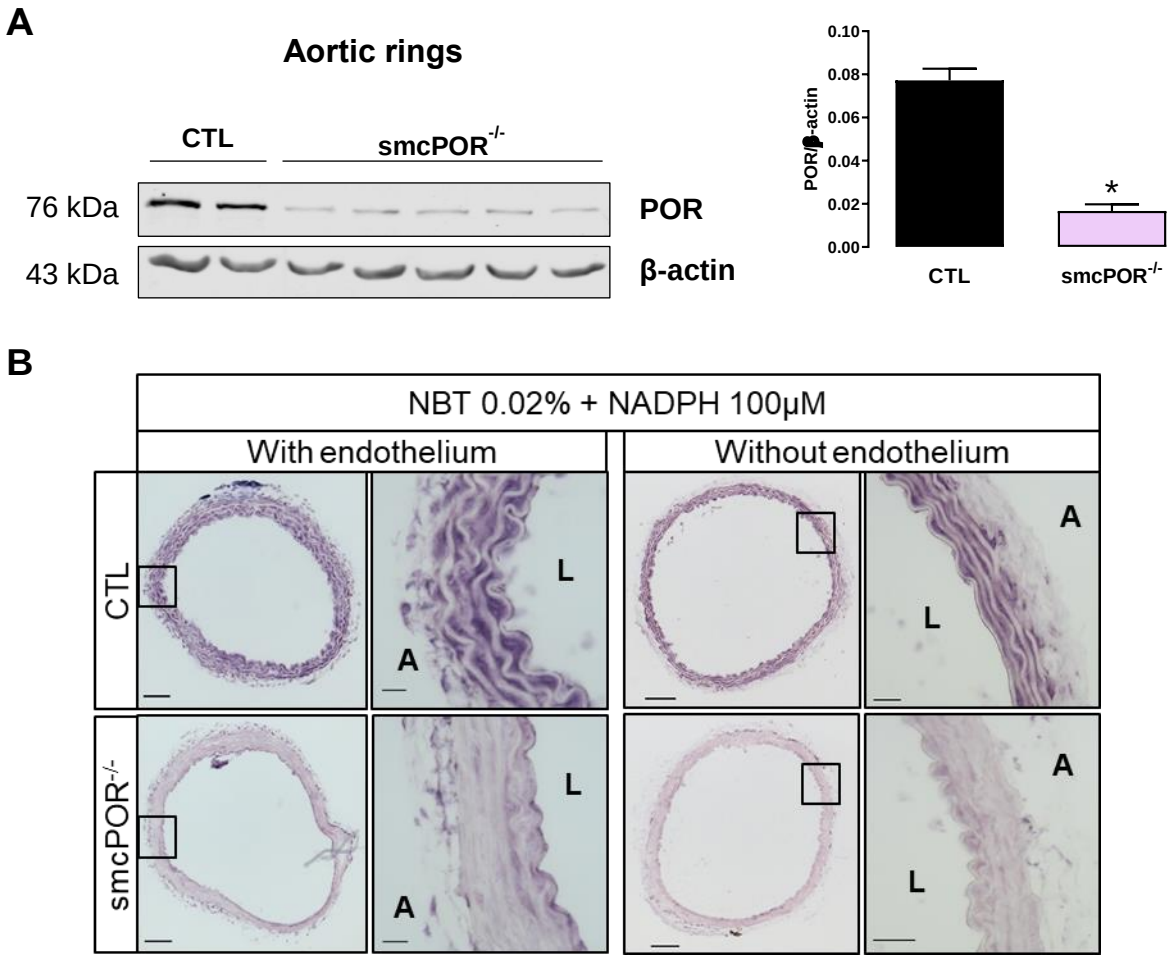

Figure 19. Knockout efficiency of smooth muscle cell-specific POR (smcPOR$^{-/-}$) mouse model. **A:** Western blot analysis showing POR expression in smooth muscle cells of aortic rings after tamoxifen treatment. *p<0.05 compared to CTL. n≥6 animals. **B:** Visualization of NADPH-dependent reduction capacity of POR in aortic SMC by conversion of yellow NBT salt to insoluble blue formazan. Left panels: scale bars 100 µm and 5x magnification; right panels: scale bars 20 µm and 40x magnification. L: lumen; A: adventitial face. n=5 animals. Figure published in Lopez *et al.* (2021)[53].

As SMCs are the predominant vascular cell type, histological staining was performed in order to determine whether deletion of POR in SMCs altered the vessel morphology (**Figure 20**). Visualization of vascular SCMs markers expression as α-smooth muscle

actin (ACTA2) and caldesmon-1 by immunofluorescence showed no evidence of alteration in the vessel morphology of smcPOR$^{-/-}$ mice compared to controls (**Figure 20A, Figure 20B**). Similarly, H&E staining of vessels indicated no morphological difference between smcPOR$^{-/-}$ and CTL animals (**Figure 20C**).

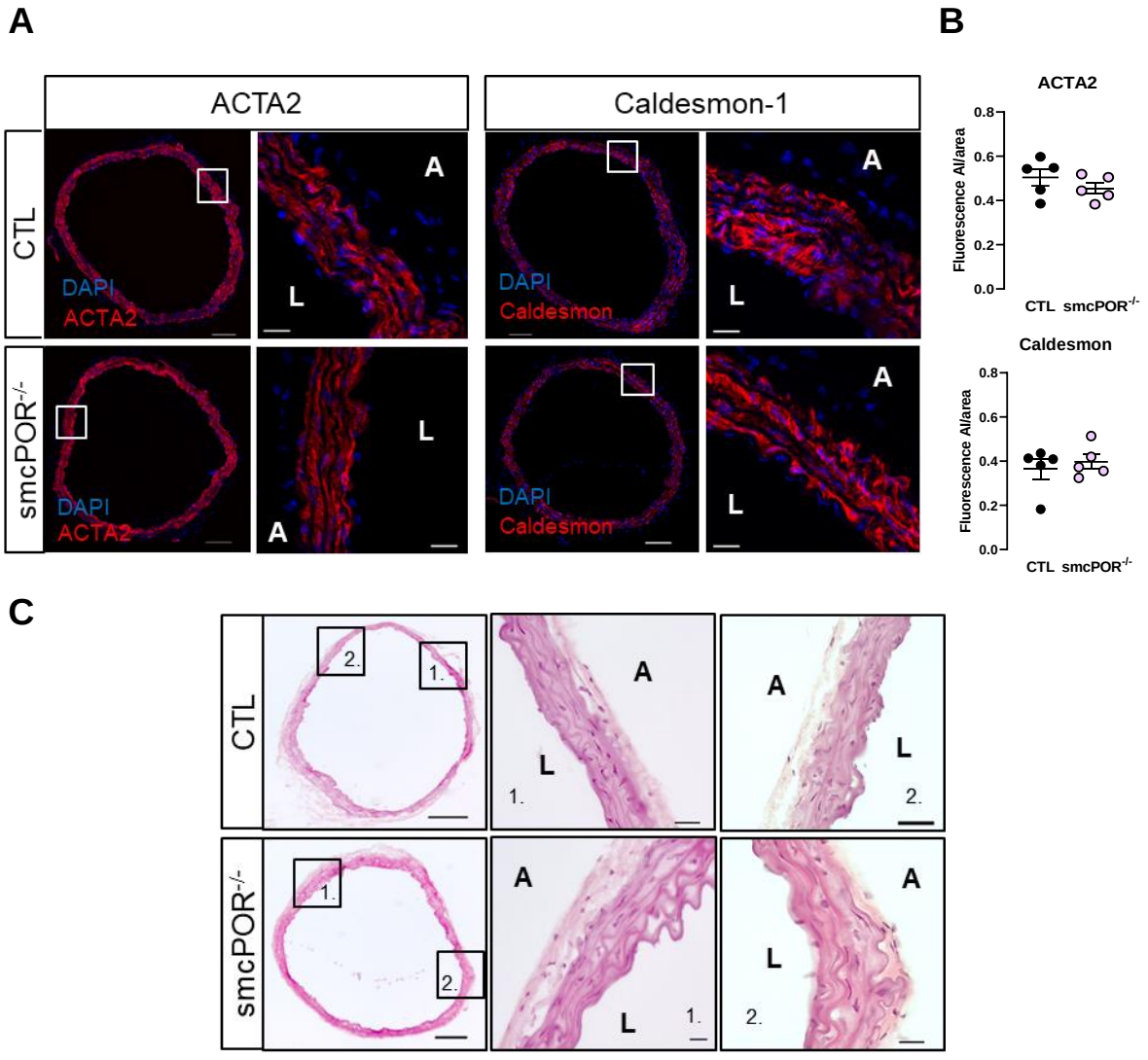

Figure 20. Vessel morphology is not altered in smcPOR$^{-/-}$ mice.
A: Visualization of VSMCs markers, α-smooth muscle actin (ACTA2) and caldesmon-1, in CTL and smcPOR$^{-/-}$ mice as analyzed by immunofluorescence. Whole aortic ring: scale bars 100 µm and 20x magnification; zoom: scale bars 20 µm and 40x oil magnification. **B:** Quantification of ACTA2 and caldesmon-1 in CTL and smcPOR$^{-/-}$ mice. **C:** Visualization of vessel morphology by Hematoxylin and Eosin (H&E) staining in CTL and smcPOR$^{-/-}$ mice. Whole aortic ring: scale bars 500 µm and 5x magnification; zoomed: scale bars 20 µm and 40 magnification. CTL: CPR$^{flox/flox}$SMMHC-CreERT2$^{+/y}$ without tamoxifen; smcPOR$^{-/-}$: CPR$^{flox/flox}$SMMHC-CreERT2$^{+/y}$ after tamoxifen. L: lumen, A: adventitial face. n=5 animals. Figure published in Lopez *et al.* (2021)[53].

As SMCs are effectors of relaxation, the cardiovascular phenotype of smcPOR$^{-/-}$ mice was investigated (**Figure 21**). However, no difference was observed in the endothelium-dependent relaxation of aortic arteries between CTL and smcPOR$^{-/-}$ mice

(**Figure 21A**). When looking at the heart weight to body weight ratio, smcPOR$^{-/-}$ showed no signs of cardiac hypertrophy (**Figure 21B**) and plasma nitrite levels were similar between both groups (**Figure 21C**).

Thus, we succeeded in abolishing the smooth muscle CYP activity by knocking out POR. Moreover, the deletion of POR specifically in SMCs did not interfer with the structural and functional properties of the vessels.

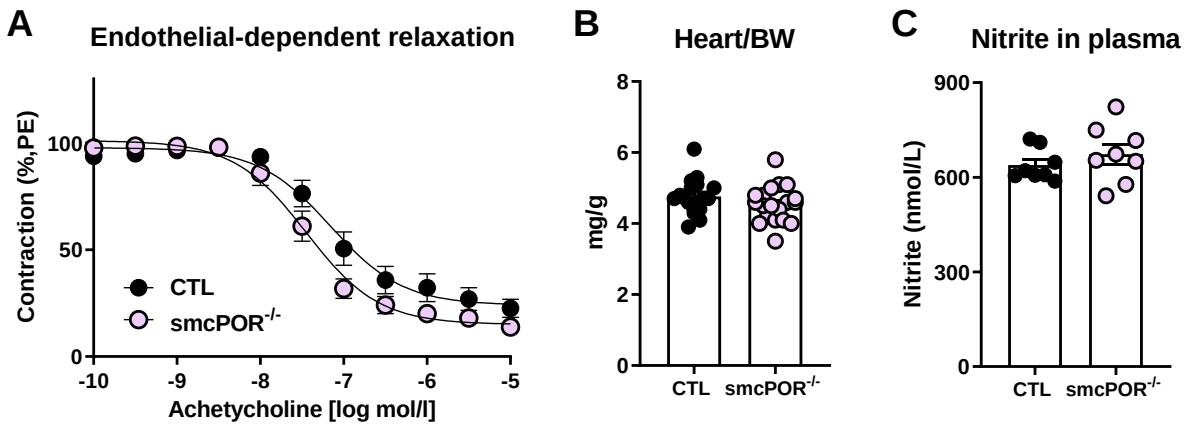

Figure 21. The smcPOR$^{-/-}$ mice showed no cardiovascular phenotype.
A: Organ bath experiments of aortic rings in reponse to acetylcholine. n≥9 animals. **B:** Heart weight to body weight ratio in smcPOR$^{-/-}$ and CTL animals. n≥17 animals. Body weight CTL: 26.8±1.79; Body weight smcPOR$^{-/-}$: 27.0±2.29. **C:** Plasma nitrite levels in smcPOR$^{-/-}$ and CTL animals. n=8 animals. *p<0.05 compared to CTL. CTL= CPR$^{flox/flox}$SMMHC-CreERT2$^{+/y}$ without tamoxifen; smcPOR$^{-/-}$= CPR$^{flox/flox}$SMMHC-CreERT2$^{+/y}$ after tamoxifen. Figure published in Lopez *et al.* (2021)[53].

5.1.4 Deletion of POR in SMC does not alter relaxation of aortic arteries in response to nitrovasodilators

Given that recombinant microsomes are able to release nitrite from NO prodrugs in a CYP and dose-related manner, we tested whether the POR/CYP system in SMCs was involved in the dilator response induced by organic nitrates. For that purpose, the relaxation of aortic rings isolated from CTL and smcPOR$^{-/-}$ in response to organic nitrates was studied in presence or absence of endothelium.

Relaxation in response to cumulative concentrations of NTG or PETN was first studied in intact endothelium vessels (**Figure 22**). As shown in **Figure 22A**, the response to NTG was identical between aortic rings of CTL and smcPOR$^{-/-}$ mice. Likewise, the dilator-curves of PETN was identical between both genotypes (**Figure 22B**). Moreover, deletion of POR in SMCs did not affect the vasodilation in response to cumulative concentrations of the spontaneous NO donor, DETA NONOate (**Figure 22C**).

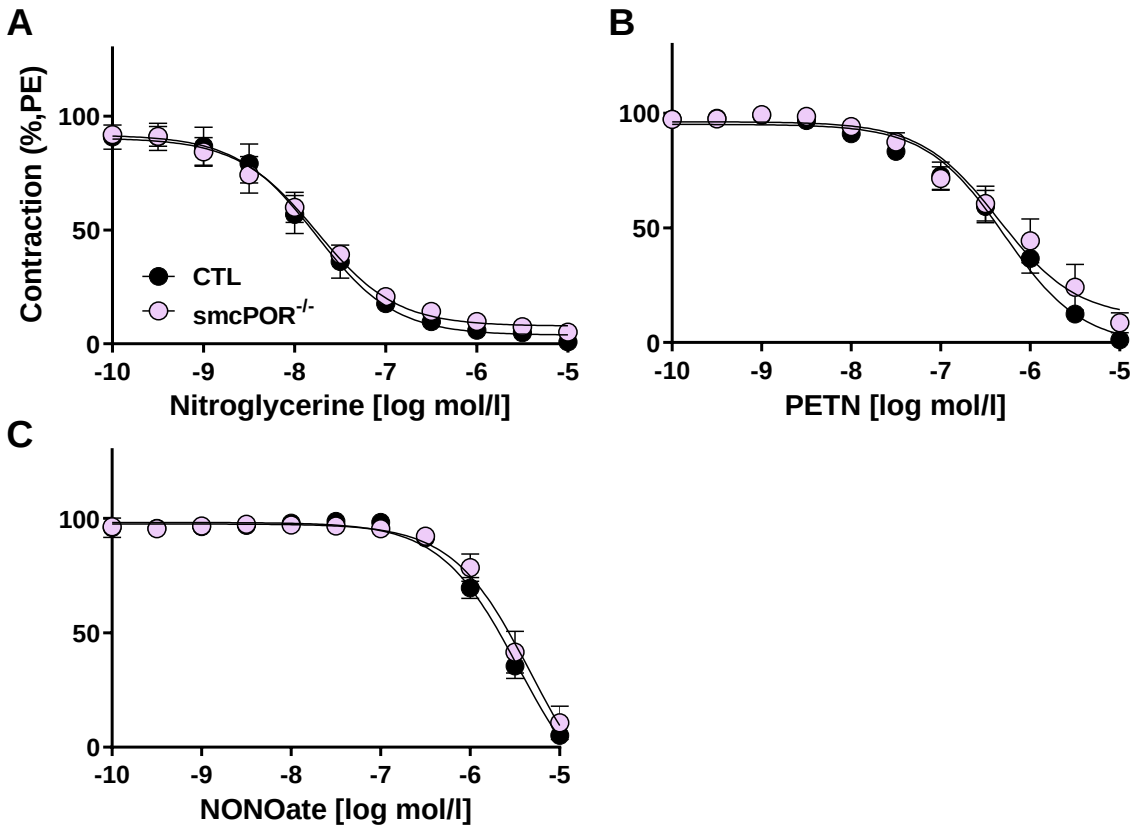

Figure 22. Aortic dilator responses to organic nitrates in CTL and smcPOR$^{-/-}$ mice.

Endothelium intact aortic rings from CTL and smcPOR$^{-/-}$ mice were pre-constricted with phenylephrine (PE). **A-C**: Dilator curves in response to increasing concentration of the indicated NO prodrugs. n≥9 animals. CTL= CPR$^{flox/flox}$SMMHC-CreERT2$^{+/y}$ without tamoxifen; smcPOR$^{-/-}$= CPR$^{flox/flox}$SMMHC-CreERT2$^{+/y}$ after tamoxifen. Figure published in Lopez *et al.* (2021)[53].

Binding of acetylcholine to muscarinic receptors on endothelial cell membrane triggers the release of stored intracellular calcium[147,148]. Increased concentration of intracellular calcium dislodges the inhibitor caveolin from calmodulin resulting in the activation of eNOS, which in turn converts L-arginine into L-citrulline and NO. The latter diffuses to VSMCs inducing relaxation through stimulation of sGC, hence production of cGMP[148]. As we were interested in the dilator response of SMCs to NTG and PETN, we decided to block the endogenous production of NO. For that purpose, the endothelial layer of both CTL and smcPOR$^{-/-}$ aortas was removed by incubating the rings in Krebs-Henseleit buffer containing the detergent CHAPS (1%) glucose (**Figure 23**).

To ensure the successful endothelium removal, aortic rings of CLT and smcPOR$^{-/-}$ animals were subjected to cumulative doses of acetylcholine. As expected, an acetylcholine-dependent relaxation could not be achieved in absence of the endothelium in both genotypes (**Figure 23A**). The sensitivity to NTG in aortic rings of smcPOR$^{-/-}$ mice was increased as illustrated with a change in the EC_{50} values: 8.2 nM without endothelium vs 17.6 nM with endothelium. However, the NTG-induced relaxation was not different between endothelium-denuded aortic rings of CTL and smcPOR$^{-/-}$ mice (**Figure 23B**). Removal of the endothelium increased the sensitivity to PETN as well with an EC_{50} of 49.1 nM without endothelium vs 0.4 µM with endothelium. Despite this change in sensitivity to PETN, relaxation-curves were identical between CTL and smcPOR$^{-/-}$ mice (**Figure 23C**). Finally, vessels of CTL and smcPOR$^{-/-}$ mice were similarly more sensitive to the spontaneous release of NO from NONOate after endothelium removal (**Figure 23D**).

Altogether, these results show that although the POR/CYP system in the form of recombinant microsomes can bio-transform NO prodrugs into nitrite, inactivation of vascular POR/CYP in SMCs has no impact on the dilator response to NTG and PETN.

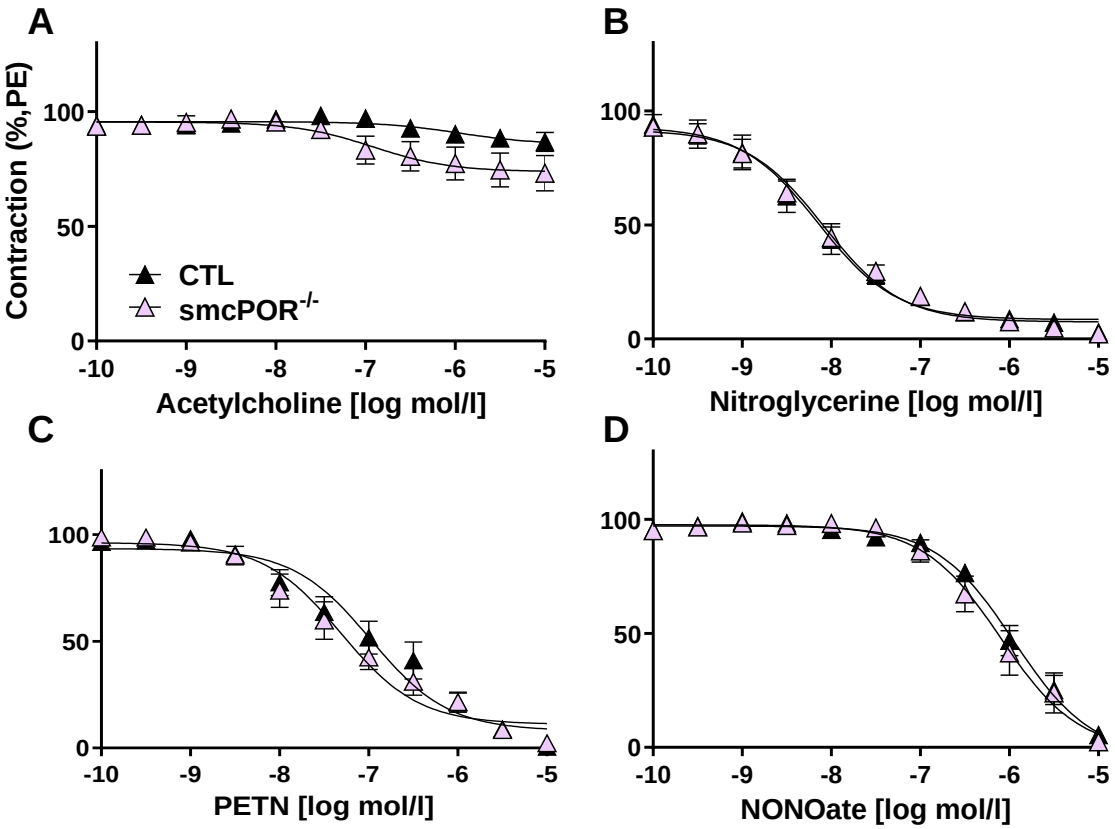

Figure 23. Dilator response of endothelium denuded aortic rings to organic nitrates in CTL and smcPOR$^{-/-}$ mice.

Endothelium denuded aortic rings from CTL and smcPOR$^{-/-}$ mice were pre-constricted with phenylephrine (PE). **A-C:** Dilator curves in response to increasing concentration of acetylcholine and the indicated NO prodrugs. n=9 animals. CTL= CPR$^{flox/flox}$SMMHC-CreERT2$^{+/y}$ without tamoxifen; smcPOR$^{-/-}$= CPR$^{flox/flox}$SMMHC-CreERT2$^{+/y}$ after tamoxifen. Figure published in Lopez *et al.* (2021)[53].

5.1.5 ALDH2 inhibition attenuates aortic nitrite production from nitrovasodilators

Whereas hepatic CYPs can contribute to the activation of NTG and PETN at suprapharmacological concentration[52,61], the mitochondrial aldehyde dehydrogenase (ALDH2) was shown to activate NTG and PETN at clinical concentration[61,73,74]. Therefore, we decided to compare the nitrite production in response to organic nitrates between CTL and smcPOR$^{-/-}$ aortic rings in the presence of benomyl, an ALDH2 inhibitor (**Figure 24**).

In absence of benomyl, the aortic production of nitrite from NTG was increased by 5-6 fold, whereas inhibition of ALDH2 with benomyl reduced the nitrite production by 2-3 fold (**Figure 24A**). However, deletion of POR in SMCs had no impact on the nitrite production from NTG. As for recombinant POR/CYP, the aortic nitrite production in presence of PETN was lower than in comparison to NTG (**Figure 24B**). Additionally, the nitrite production from PETN was identical between CTL and smcPOR$^{-/-}$ mice. Surprisingly, inhibition of ALDH2 with benomyl had no effect on the nitrite production by PETN as compared to NTG. As neither the deletion of POR in SMCs nor inhibition of ALDH2 could reduce the nitrite production from PETN, this suggests that an unknown third enzyme contributes to the activation of PETN.

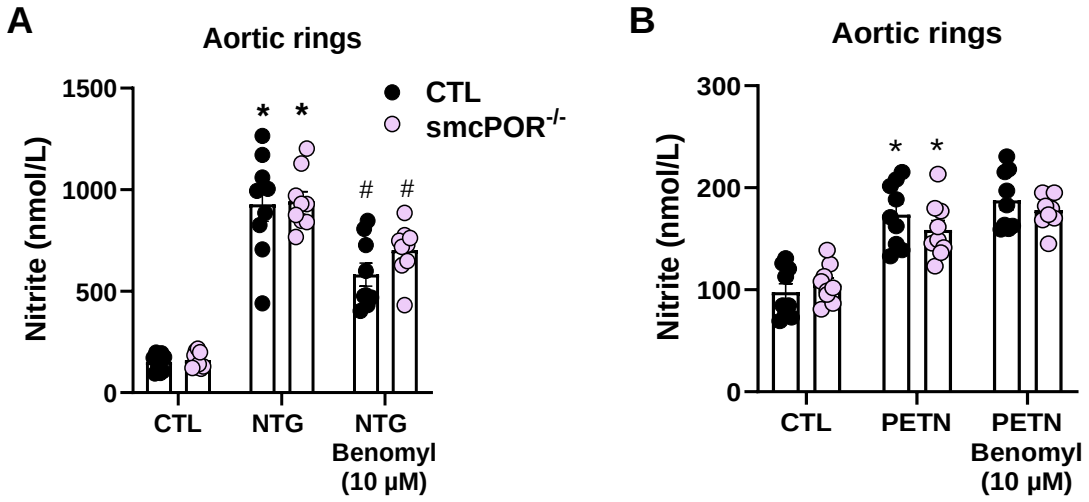

Figure 24. Nitrite production from nitrovasodilators by aortic rings.
A: Nitrite production from aortic rings of CTL and smcPOR$^{-/-}$ mice in presence of NTG (100 µM) when pre-incubated for 5 min with or without benomyl, an inhibitor of ALDH2, at 30 min. **B:** Nitrite production from aortic rings of CTL and smcPOR$^{-/-}$ mice in presence of PETN (100 µM) when pre-incubated with or without benomyl. *p<0.05 compared to CTL. #p<0.05 compared to NTG. n=9 animals. CTL= CPR$^{flox/flox}$SMMHC-CreERT2$^{+/y}$ without tamoxifen; smcPOR$^{-/-}$= CPR$^{flox/flox}$SMMHC-CreERT2$^{+/y}$ after tamoxifen. Figure published in Lopez *et al.* (2021)[53].

5.1.6 ALDH2 inhibition does not reveal a role of POR/CYP in SMCs for nitrovasodilator activation

We previously demonstrated that by blocking ALDH2, the aortic nitrite production was similarly reduced in CTL and smcPOR$^{-/-}$ animals and given its important role in the biotransformation of NTG and PETN[61,73,74], we next tested whether its inhibition by benomyl could reveal a potential role of the POR/CYP system in in endothelium-intact vessels (**Figure 25**).

Aortic rings from CTL and smcPOR$^{-/-}$ mice were pre-incubated for 5 min with benomyl (10 µM), followed by constriction with cumulative concentration of phenylephrine. As expected, the dilator response to the spontaneous NO-donor DETA-NONOate was unaffected by benomyl (**Figure 25A**). Likewise, benomyl had no effect on the acetylcholine-dependent relaxation in both CTL and smcPOR$^{-/-}$ mice (**Figure 25B**). When incubated with benomyl, the sensitivity to NTG was shifted to the right with an EC_{50} value of 0.4 µM with benomyl vs 21.3 nM without benomyl (**Figure 25C**). However, the NTG-induced relaxation was not different between aortic rings of CTL and smcPOR$^{-/-}$ mice. Inhibition of ALDH2 with benomyl had a small, yet significant, effect on PETN-induced relaxation as shown with an EC_{50} value of 1.40 µM with benomyl vs 0.29 µM without benomyl (**Figure 25D**). Despite the blocking of ALDH2 activity, the relaxation-curves in response to PETN were identical between genotypes.

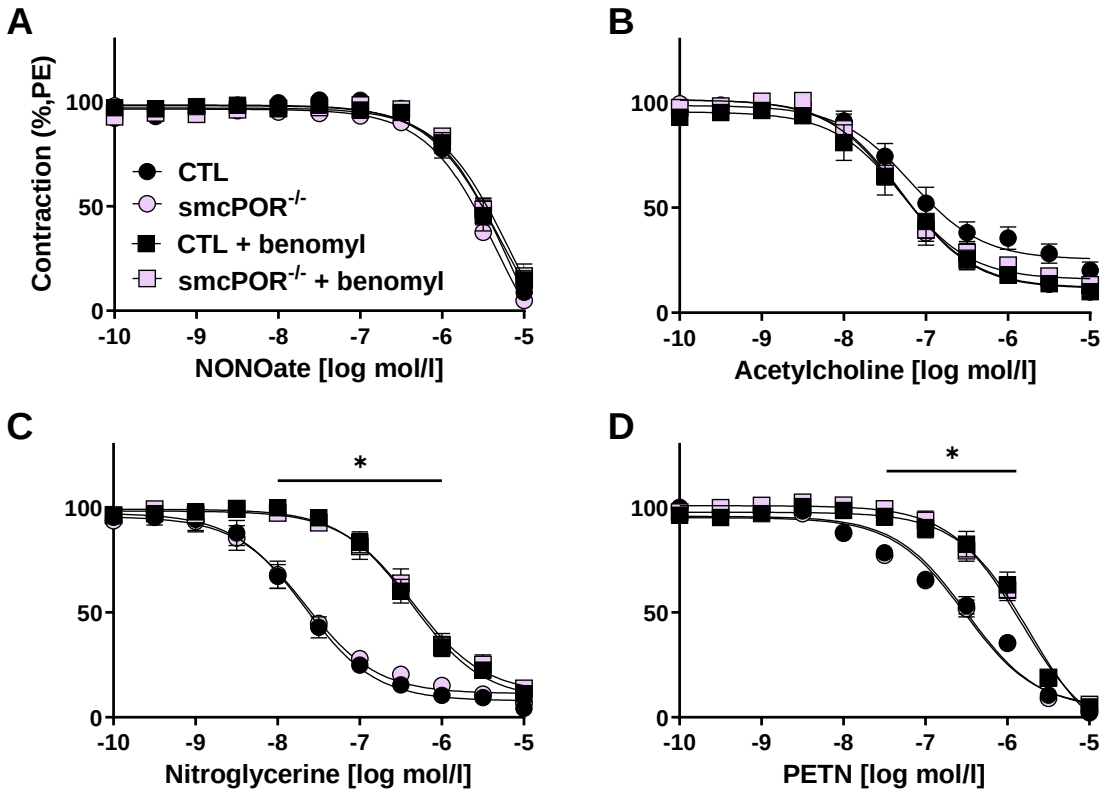

Figure 25. Effect of ALDH2 inhibition on the dilator response of aortic rings to organic nitrates in CTL and smcPOR$^{-/-}$ mice.

Aortic rings from CTL and smcPOR$^{-/-}$ mice incubated with or without benomyl (10 µM) for 5 min were pre-constricted with phenylephrine (PE). **A-D:** Dilator curves in reponse to acetylcholine and the indicated NO-prodrugs. *p<0.05 compared to CTL and smcPOR$^{-/-}$ without benomyl. n=10 animals. CTL= CPR$^{flox/flox}$SMMHC-CreERT2$^{+/y}$ without tamoxifen; smcPOR$^{-/-}$= CPR$^{flox/flox}$SMMHC-CreERT2$^{+/y}$ after tamoxifen. Figure published in Lopez *et al.* (2021)[53].

Inhibition of ALDH2 with benomyl did not unmask a contribution of POR to the dilator response to nitrovasodilators. However, endothelial cells still express POR and produce endogenous NO therefore potentially mask the effect of POR on the bioactivation of NTG and PETN. Thus, we decided to not only block the ADLH2 activity but to abolish the endogenous production of NO. For that purpose, endothelium-free aortic rings were pre-incubated with benomyl for 5 min followed by pre-constriction with phenylephrine (**Figure 26**).

Despite an increase in the sensitivity to DETA-NONOate after endothelium removal, benomyl had similarly no effect on the relaxation curves of CTL and smcPOR$^{-/-}$ mice in response to the spontaneous release of NO from DETA-NONOate (**Figure 26A**). To ensure the successful endothelium removal, aortic rings of CLT and smcPOR$^{-/-}$ animals pre-incubated with benomyl were subjected to cumulative doses of acetylcholine. As expected, an acetylcholine-dependent relaxation could not be

achieved in absence of the endothelium in both genotypes (**Figure 26B**). Despite inhibition of endogenous NO production and ALDH2 activity, the NTG-induced relaxation was not different between CTL and smcPOR$^{-/-}$ mice (**Figure 26C**). Finally, removal of the endothelium combined with benomyl administration also showed no difference in vessel relaxation between CTL and smcPOR$^{-/-}$ animals in response to PETN (**Figure 26D**).

To summarize these results, both blocking ALDH2 activity and abolishing the endogenous NO production did not unmask a contribution of vascular POR to the dilator response of NTG and PETN.

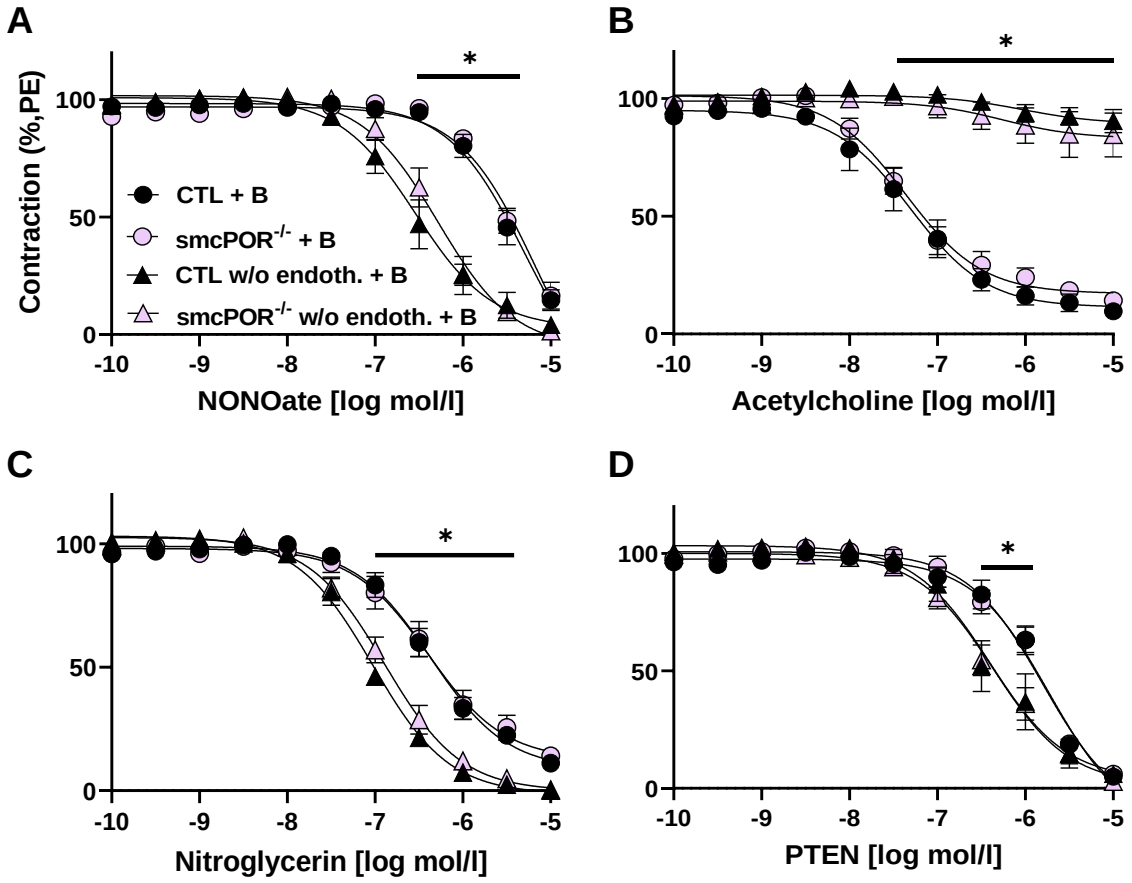

Figure 26. Effect of ALDH2 inhibition on the dilator response of endothelium-denuded aortic rings to organic nitrates in CTL and smcPOR$^{-/-}$ mice.
Endothelium-intact and endothelium-free aortic rings from CTL and smcPOR$^{-/-}$ mice incubated with or without benomyl (10 µM) were pre-constricted with phenylephrine (PE). **A-D:** Dilator curves in response to acetylcholine and the indicated NO-prodrugs. *p<0.05 with endothelium as compared to without endothelium. n≥8 animals. CTL= CPR$^{flox/flox}$SMMHC-CreERT2$^{+/y}$ without tamoxifen; smcPOR$^{-/-}$= CPR$^{flox/flox}$SMMHC-CreERT2$^{+/y}$ after tamoxifen. Figure published in Lopez *et al.* (2021)[53].

5.1.7 The vascular POR/CYP expression is lower than the hepatic POR/CYP expression

By the mean of nitrite production measurements, we demonstrated that CYP450 enzymes typically expressed in the aorta and commercially available in the form of recombinant Supersome^{TM} can contribute to the bioactivation of NTG and PETN. According to the literature, vascular CYP450 can contribute to the activation of NTG and PETN[52,61], however, we could not reproduce these results when using a smooth muscle-specific tamoxifen inducible knockout model approach (smcPOR$^{-/-}$ mice).

Therefore, we decided to have study the expression of the POR/CYP450 system in aorta as compared to the hepatic expression. CYP51 isoenzyme was selected for this as it is expressed in both liver and aorta. Moreover, it is one of the few CYPs for which an effective antibody is available for western blot application (**Figure 27**). The expression of both POR and CYP51 was already detectable when loading 10 µg of hepatic tissue (**Figure 27A**). The higher the amount of tissue, the higher the expression of POR and CYP51 in the liver was as compared to the aorta (**Figure 27A**). This observation was even stronger after quantification as illustrated in **Figure 27B**.

As POR and CYP51 are expressed differently in both tissues, it is tempting to speculate that this difference in expression may applied to CYP450 enzymes at large. Thus, these results suggest that the low expression of POR/CYP450 enzymes in the vessels might explain why vascular POR/CYP450 do not bio-activate NTG and PETN.

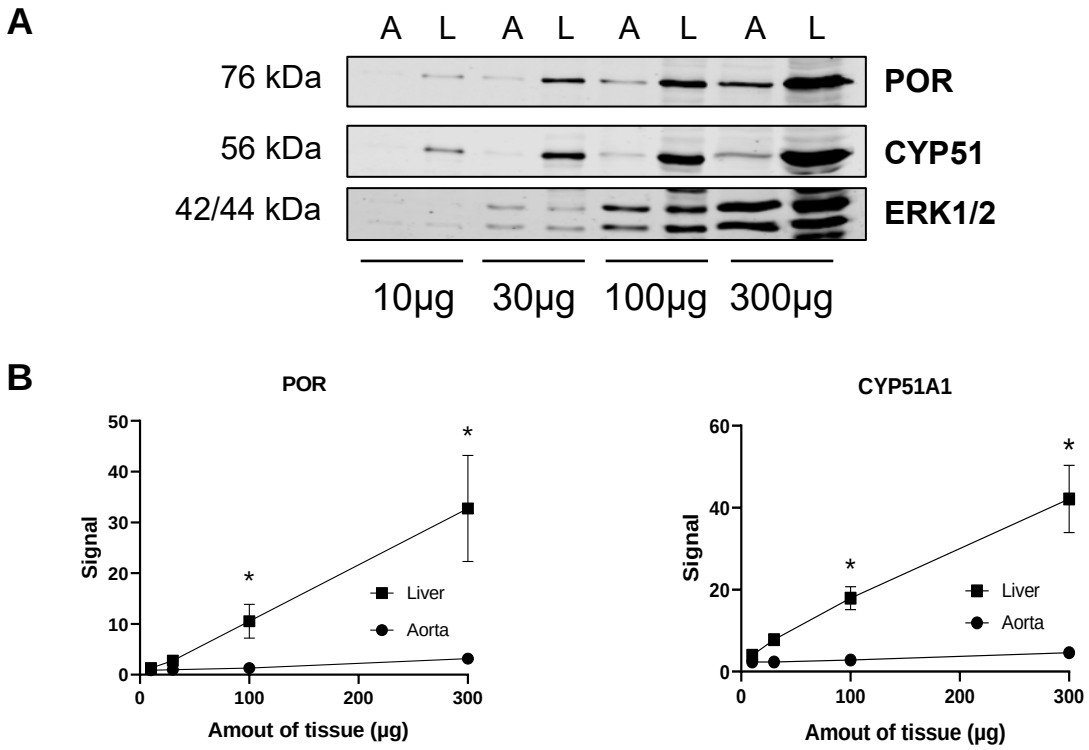

Figure 27. Comparison of hepatic and vascular expression of POR and CYP51 in C57BL6J mice. **A:** Representative image of POR and CYP51 expression in aorta and liver with different amounts of tissues: 10, 30, 100 and 300 µg. **B:** Quantification of POR and CYP51 expression in aorta and liver. *p<0.05 compared to aorta. n=5 animals. A: aorta; L: liver. Figure published in Lopez *et al.* (2021)[53].

5.2 Part 2: Cytochrome P450 reductase and cardiac remodelling

The second part of this thesis deals with the cardiac function of the POR/CYP450 system in endothelial cells. The phyiological relevance of POR was demonstrated using an endothelial cell-specific, tamoxifen-inducible knockout of POR (ecPOR$^{-/-}$). Transverse aortic constriction (TAC) was employed as a pressure-overload model to further evaluate whether or not endothelial deletion of POR had any functional consequences.

5.2.1 The cytochrome P450 reductase and the CYP450 cardiac repertoire

Previous studies showed that not only the heart expresses several CYP450 enzymes but also that the expression differs between the right and left ventricles[12]. However, the cardiac cell-specific pattern is not very well studied. Therefore, to provide a mechanistic basis for a cell type-specific CYP450 function in the heart, we looked at the expression of murine CYP450 isoenzymes in different cardiac cell types by RNA-sequencing from publicly available studies[149,150].

Interestingly, the expression pattern of CYP450 was cell-specific (**Figure 28**). Cardiac endothelial cells (ECs) exhibited an enrichment in the expression of Cyp1a1 as well as Cyp4b1, Cyp4f13, Cyp4f16 and Cyp4f17 of the Cyp4 family which is known to catalyse the ω-hydroxylation of saturated, branched and unsaturated fatty acids[151]. Additionally, Cyp2j6 and Cyp2j9 of the Cyp2j subfamily, known for producing EETs, were enriched in both ECs and cardiac fibroblasts (CFs). Cardiomyocytes (CMs) showed an enriched expression for CYP450-related lipids metabolism such as Cyp51 (cholesterol metabolism)[152] and Cyp2u1 (ω-hydroxylation of AA)[153].

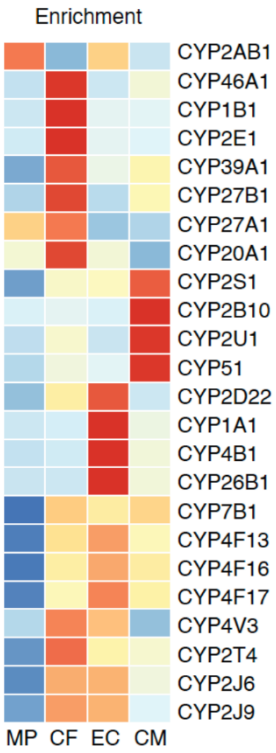

Figure 28. The cytochrome P450 reductase and the cardiac CYP450 repertoire.
Heatmap of CYP450 genes in different cardiac cell types isolated from the normal mouse heart (RNA-sequencing). MP: macrophages; CF: cardiac fibloblasts; EC: endothelial cells; CM: cardiomyocytes. Figure published in Lopez *et al.* (2022)[122].

Next, we searched for the corresponding human genes of the cardiac CYP450 isoenzymes identified in **Figure 28**. As mutations in human CYP genes can lead to functional alterations resulting in diseases[154,155], a potential genotype-phenotype association was determined PhenoScanner, an online tool[31,32] (**Table 20**). Genetic variants associated with diseases and traits related to cholesterol, fatty acid metabolism, congestive heart failure and cardiomyopathy were observed in CYP450 enriched in ECs and part of the CYP4 family. We further looked for other CYP450 isoenzymes known to be expressed in ECs. Among them, CYP2C8 and CYP2C9, which are important for the production of EETs, exhibited genetic variants related to peripheral vascular disease and/or dilated cardiomyopathy. Finally, genetic variants in POR were related to peripheral resistance disease and congestive heart failure.

To summarize, these results revealed an expression pattern of CYP450 isoenzymes to be cell type-specific, with endothelial CYP450 exhibiting genetic variants associated to cardiovascular diseases and lipid metabolism.

Gene (Human)	Gene (Mouse)	rsID	Position	Base	Base	Trait	Type	P-value
CYP1A1	Cyp1a1	rs17861084	chr15:75012019	T	G	Total cholesterol	Diseases and traits	6.14E-10
		rs17861084	chr15:75012019	T	G	Triglycerides	Diseases and traits	1.21E-07
CYP4B1	Cyp4b1	rs45468297	chr1:47282626	A	G	Cause of death: congestive heart failure	Diseases and traits	7.36E-13
CYP4F2	Cyp4f13	rs3093111	chr19:16007770	A	G	LDL cholesterol	Diseases and traits	9.45E-09
		rs3093193	chr19:15991914	C	G	Coronary artery disease	Diseases and traits	2.11E-06
CYP4F11	Cyp4f16	rs144570608	chr19:16045076	A	T	Cause of death: congestive heart failure	Diseases and traits	2.82E-16
CYP4F12	Cyp4f17	rs538943818	chr19:15794653	T	C	Cause of death: dilated cardiomyopathy	Diseases and traits	4.38E-15
		rs550467038	chr19:15802300	T	C	Cause of death: hypertensive heart disease with heart failure	Diseases and traits	1.33E-08
CYP4V2	Cyp4v3	rs532291947	chr4:187134385	T	C	Cause of death: ischaemic cardiomyopathy	Diseases and traits	1.59E-12
CYP2J2	-	rs11572277	chr1:60374467	A	G	Cause of death: heart failure, unspecified	Diseases and traits	1.05E-07
		rs41287722	chr1:60359036	A	T	Cause of death: ischaemic cardiomyopathy	Diseases and traits	1.48E-07
CYP2C8	Cyp2c8	rs565537760	chr10:96802435	A	G	Cause of death: peripheral vascular disease, unspecified	Diseases and traits	1.57E-18
		rs188011311	chr10:96825092	T	C	Cause of death: dilated cardiomyopathy	Diseases and traits	6.45E-18
CYP2C9	Cyp2c9	rs553150888	chr10:96734381	A	G	Cause of death: peripheral vascular disease, unspecified	Diseases and traits	9.95E-30
POR	Por	rs181538359	chr7:75566011	T	G	Cause of death: peripheral vascular disease, unspecified	Diseases and traits	6.59E-25
		rs113454523	chr7:75555973	A	G	Cause of death: congestive heart failure	Diseases and traits	1.32E-06

Table 20. Genotype-phenotype association of CYP450 isoenzymes determined with PhennoScanner (http://www.phenoscanner.medschl.cam.ac.uk/).
Table published in Lopez *et al.* (2022)[122].

5.2.2 Endothelial deletion of POR leads to cardiac remodelling

Cardiac ECs form the endocardium as well as capillaries and are the most abundant cell type of the heart[84]. As we were interested in the cardiac relevance of endothelial CYP450 isoenzymes, an endothelial cell-specific, tamoxifen-inducible knockout of POR (ecPOR$^{-/-}$) was generated.

First, we assessed the knockout efficiency of POR in different tissues (**Figure 29**). There was no difference at the hepatic level of POR expression between CTL and ecPOR$^{-/-}$ mice. A reduction in POR in ecPOR$^{-/-}$ mice was observed in whole aorta as well as in lung endothelial cells (LECs). Collectively, these results demonstrate that deletion of POR using Cdh5 as a driver was successful in the endothelium and did not alter hepatic POR expression.

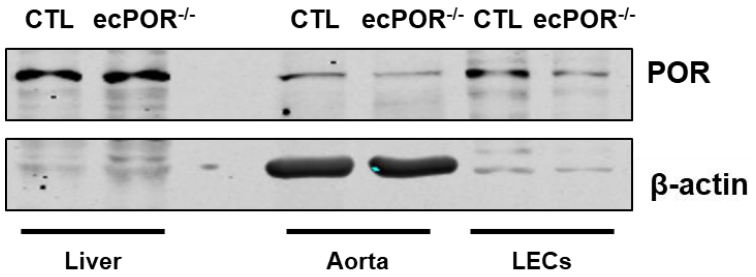

Figure 29. Knockout efficiency of POR in different tissues.
Western blot analysis showing POR expression in liver, aorta and lung endothelial cells (LECs) from CTL and ecPOR$^{-/-}$ mice after tamoxifen treatment. Figure published in Lopez *et al.* (2022)[122].

Next, we focused on the knockout efficiency of POR in cardiac ECs and characterized the mouse model (**Figure 30**). To validate the knockout efficiency by Western blot analysis, cardiac ECs were first enriched from ecPOR$^{-/-}$ and CTL mice as depicted by eNOS expression compared to the remaining cell fraction (**Figure 30A**). Specific deletion of POR in ECs was successfully reached as shown by an almost complete loss of POR signal in ECs as compared to the remaining cell fraction.

Next, we decided to get a first impression on the effect of ecPOR deletion on the heart. Heart to body weight is a well implemented method to analyse the cardiovascular phenotype in mice[156]. Thus, the heart weight to body weight ratio was determined 30 days after tamoxifen treatment (**Figure 30B**). A higher heart weight to body weight ratio was observed in ecPOR$^{-/-}$ mice as compared to CTL mice. This finding may suggest that cardiac remodelling occurs in response to endothelial deletion of POR resulting potentially in cardiac hypertrophy. Staining of cardiac sections with WGA

(wheat germ agglutinin, a lectin), showed an increase in cardiomyocyte area in ecPOR$^{-/-}$ mice compared to control mice (**Figure 30C**). Likewise, H&E staining of cardiac sections exhibited an increase in the diameter of cardiomyocytes in ecPOR$^{-/-}$ mice, in contrast to CTL mice (data not shown).

Although the phenotype observed under without additional stress models (i.e. 30 days after inducing the knockout by tamoxifen feeding) is mild, yet significant, our results suggest that endothelial deletion of POR leads to cardiac remodelling.

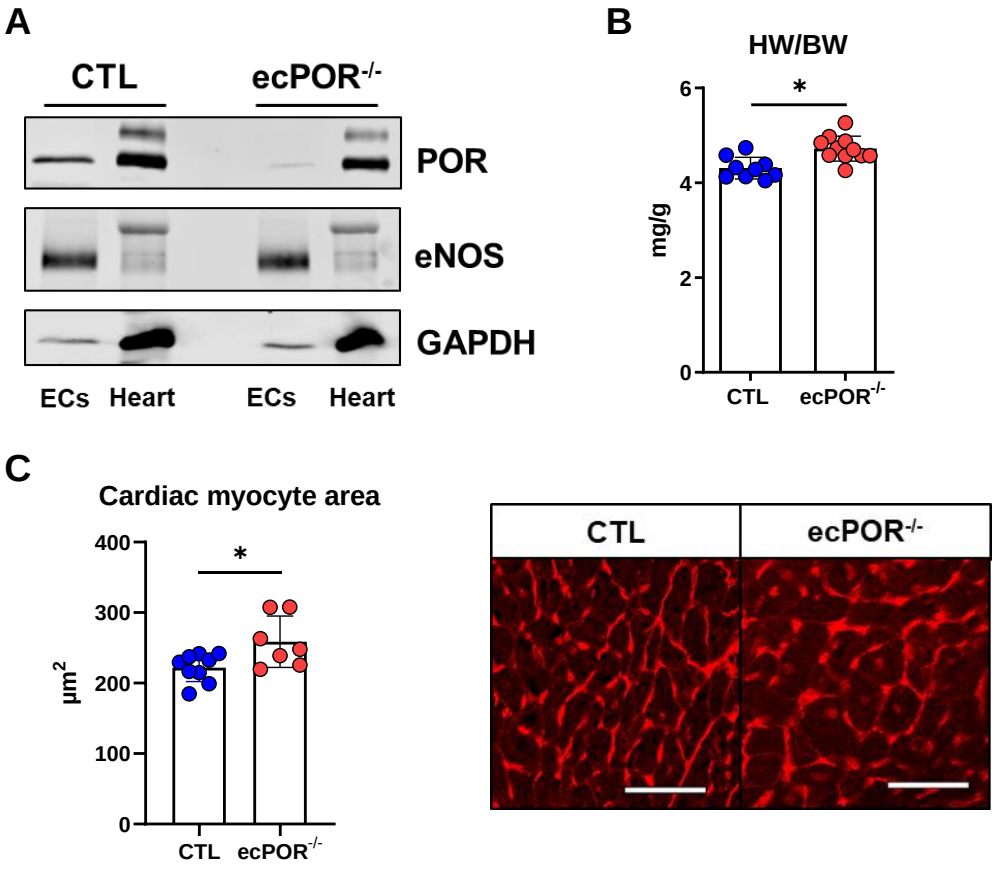

Figure 30. Knockout efficiency and characterization of ecPOR$^{-/-}$ mice.
A: Western blot analysis showing POR expression in cardiac endothelial cells (ECs) and left ventricle (LV) from CTL and ecPOR$^{-/-}$ mice after tamoxifen treatment. **B:** Ratio heart weight to body weight. n≥11 animals. Body weight CTL: 35.94 ± 2.56g; Body weight ecPOR$^{-/-}$: 36.33 ± 2.92g. **C:** Determination of cardiomyocytes area by Wheat Germ Agglutinin (WGA) staining. Scale bar: 50 µm. n≥7 animals. $p<0.05$ ecPOR$^{-/-}$ as compared to CTL mice. Figure published in Lopez *et al.* (2022)[122].

5.2.3 Deletion of POR in endothelial cells is associated with the expression of genes linked to protein synthesis and altered mitochondrial function

So far, our results suggest that cardiac remodelling occurs as a result of endothelial deletion of POR. As cardiac remodelling is complex and responds to oxidative stress, metabolic reprogramming, inflammation, and an increase in the production of extracellular matrix[157], we decided to study the underlying cause in our knockout mouse model through gene expression analysis by an unbiased method. Hence, RNA-sequencing was performed from cardiac ECs and the remaining cardiac tissue (LV) from ecPOR$^{-/-}$ and CTL mice.

As compared to control mice, POR was detected among the top50 most significantly downregulated genes in cardiac ECs of ecPOR$^{-/-}$ mice (**Figure 31A**). Based on Gene Ontology analysis (GO Biological Process 2021), processes like SRP (signal recognition particle)-dependent co-translational protein targeting to membrane or protein targeting to reticulum endoplasmic (ER), and protein synthesis were up-regulated upon deletion of POR (**Figure 31B**). Genes associated to those processes were Yipf7, known to be involved in vesicle-mediated transport between ER and Golgi[158] as well as Rpl and Rps, important for the synthesis of ribosomal large and small units, thus for protein synthesis[159] (**Table 22**). Several studies demonstrated that an increase in protein synthesis results in the activation of the ER stress machinery[160]. However, genes such as Hspa8, Hspa5 or Dnajb2 which are associated to the response to unfolded protein or ER stress-induced intrinsic apoptotic signaling pathway were down-regulated in ecPOR$^{-/-}$ mice (**Figure 31B**, **Table 23**).

In contrast to CTL mice, genes related to cardiac contractility such as Myl4, Myl7 and Sln[161] were among the top50 most significantly up-regulated genes in the cardiomyocyte fraction of ecPOR$^{-/-}$ mouse heart (**Figure 31C**). An up-regulation in genes related to cardiac development, circulatory system development and atrioventricular valve morphogenesis was observed in ecPOR$^{-/-}$ mice in comparison to CTL mice (**Figure 31D**, **Table 24**). Upon endothelial deletion of POR, the heart of ecPOR$^{-/-}$ mice showed a gene signature for altered mitochondrial function with a reduction in genes expression like Nduf (complex I), Sdhd (complex II), Coq10b (coenzyme Q), Uqcr (complex III) or Cox (cytochrome c oxidase) (**Figure 31D**, **Table 25**).

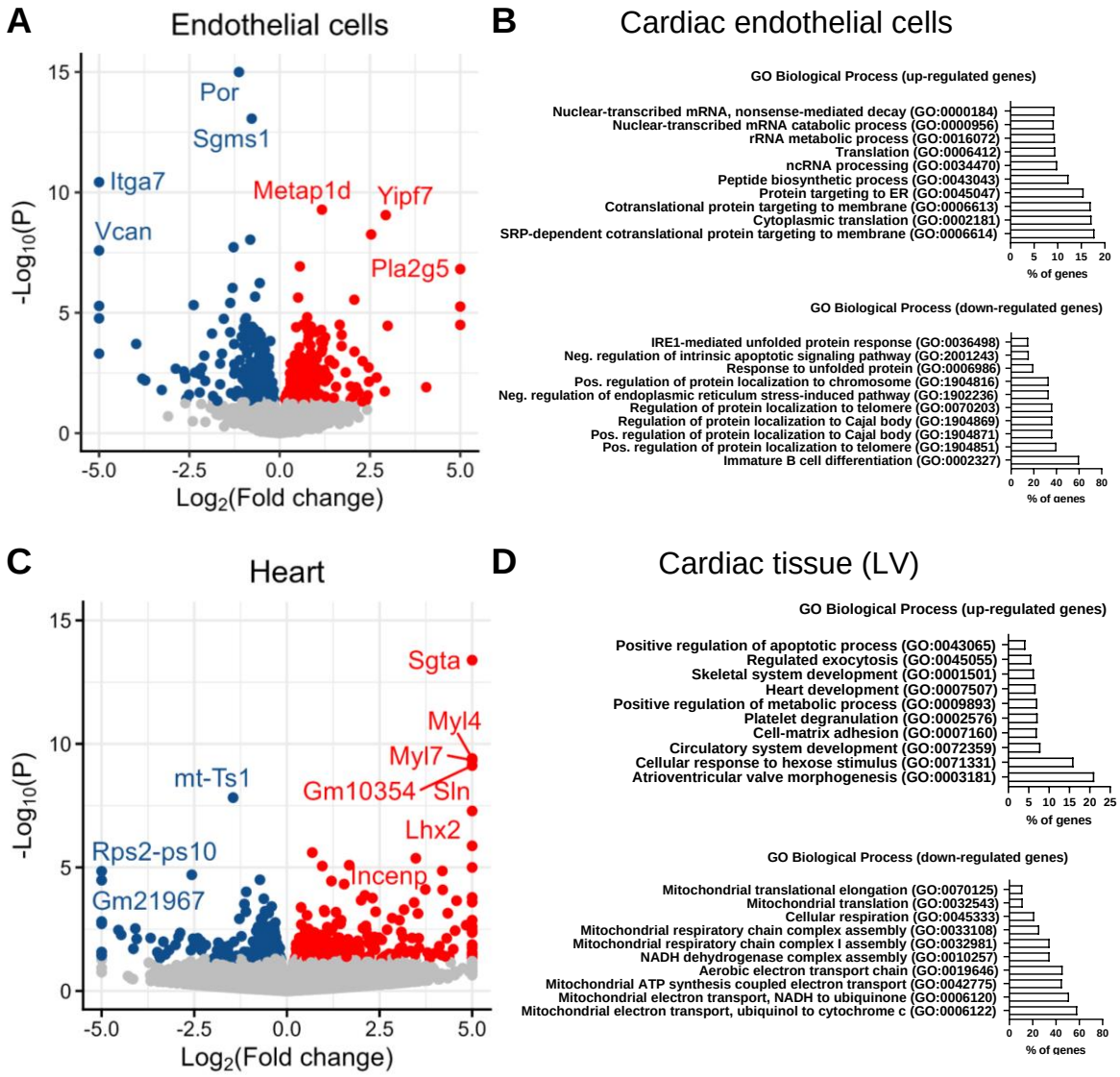

Figure 31. RNA-sequencing of isolated cardiac endothelial cells (ECs) and cardiac tissue (left ventricle; LV) of CTL and ecPOR$^{-/-}$ mice.
A: Volcano plot summarizing the significantly up- and down-regulated genes in cardiac ECs. n=3 (pool of 2 different animals). **B:** Ontology analysis (GO Biological Process 2021) for the top 500 up- and down-regulated genes in cardiac ECs. Bars represent the percentage of overlapping genes from the top ten analyzed ontologies. **C:** Volcano plot summarizing the significantly up- and down-regulated genes in the heart. n=3. **D:** Ontology analysis (GO Biological Process 2021) for the top 200 up- and down-regulated genes in the LV. Bars represent the percentage of overlapping genes from the top ten analyzed ontologies. Genes were plotted according to p-value ≤ 0.05. Figure published in Lopez *et al.* (2022)[122].

During the electron transfers from POR to the CYP450 heme subunit, oxygen is activated and subsequently hydroxylates the substrate (R-OH). As a consequence, reactive oxygen species (ROS) can be released as a side product of the one-electron-reduced ternary complex decay[17], making the POR/CYP450 a potential source of ROS, i.e. oxidative stress[162]. Therefore, we decided to study genes associated with

the term “response to oxidative stress” (GO:0006979) as oxidative stress is linked to cardiac remodeling (**Figure 32**).

The expression of enzymes which are sources of ROS like NADPH oxidases was not increased in neither ECs nor CMs. In fact, genes that are activated in response to oxidative stress like Bnip3 (Bcl-2/E1B-19K-interacting protein 3)[163] or induce oxidative stress like Aif1 (allograf inflammatory factor-1)[164] were down-regulated in ECs (**Figure 32A**, **Table 26**). Likewise, genes incuced in response to oxidative stress like Prdx2 (peroxiredoxin-2) and Sod2 (superoxide dismutase)[165] were mildly, yet significantly, down-regulated in CMs (**Figure 32B**, **Table 27**).

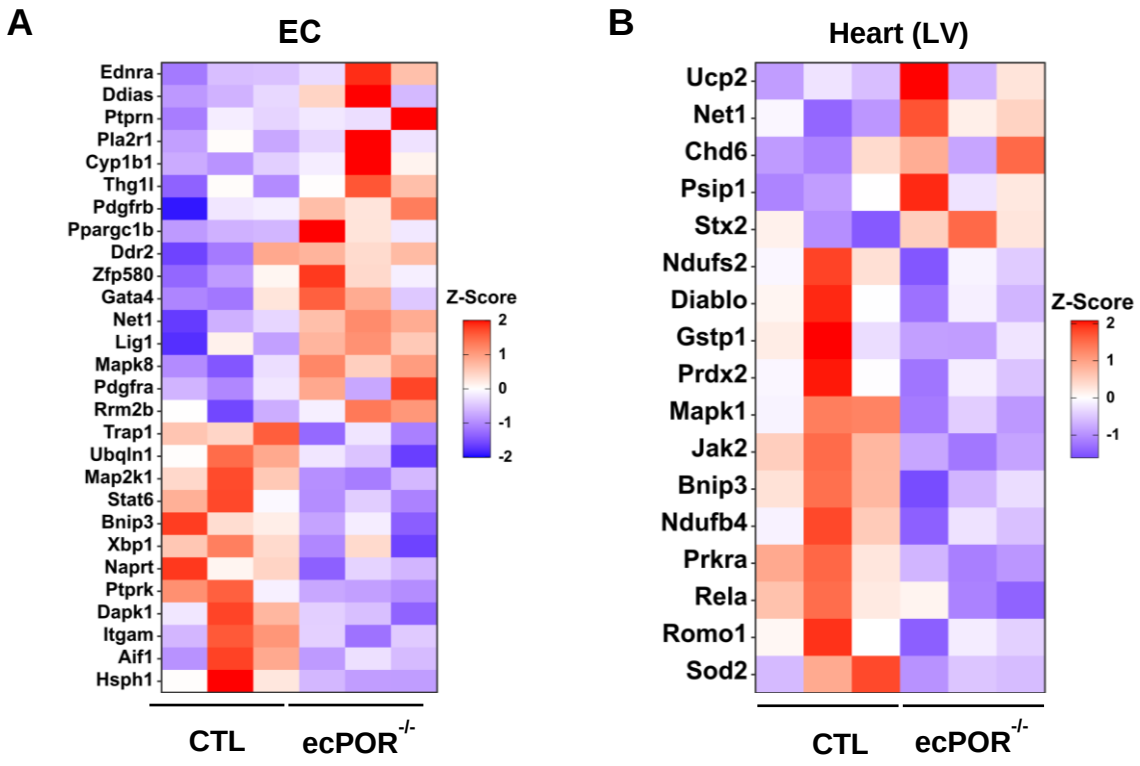

Figure 32. Expression of genes associated to oxidative stress (GO:0006979) in cardiac endothelial cells (ECs) and heart (LV) from CTL and ecPOR$^{-/-}$ mice.
A: Heatmap summarizing the significantly altered genes associated to oxidative stress in ECs. n=3 (pool of 2 different animals). **B:** Heatmap summarizing the significantly altered genes associated to oxidative stress in the heart. n=3. *p<0.05. Figure published in Lopez *et al.* (2022)[122].

Together these data suggest that oxidative stress is unlikely to occur in response to endothelial deletion of POR as genes responding or leading to oxidative stress were down-regulated in response to knockout. In fact, the RNA-sequencing data rather suggest that deletion of POR in endothelial cells potentially lead to ribosomal biogenesis and protein synthesis alterations without inducing stress respose, which might affect the cardiac contractility in ecPOR$^{-/-}$ mice.

5.2.4 Endothelial deletion of POR does not lead to changes in the cardiac metabolic function

In addition to the cardiac remodelling phenotype previously observed in ecPOR$^{-/-}$ mice, gene ontology analysis suggested changes in the mitochondrial function. Those observations gave rise to two hypotheses: i. plasma fatty acids, which have to trans-pass the endothelial barrier[166,167], could be oxidized via ω-hydroxylation by the endothelial POR/CYP450 system before serving as a source of energy for cardiomyocytes via β-oxidation; ii. the loss of the cardioprotective effects[110,168] and vascular tone control of endothelial EETs[36] might explain the cardiac alterations in ecPOR$^{-/-}$ mice. In fact, we previously described that a lack of EETs in ecPOR$^{-/-}$ animals resulted in increased vascular stiffness[117] which potentially alter the cardiac contractility as a compensatory mechanism.

To determine whether the first hypothesis would explain the cardiac alterations in ecPOR$^{-/-}$ animals, we decided to study the cardiac metabolic function using untargeted metabolomics of whole hearts. Moreover, we are the first one to explore with such untargeted analysis the metabolism of fatty acids, lipids of the eicosanoid class as well as other metabolic pathways in the context of the cardiac POR/CYP450 system. Pathway enrichment analysis revealed that mostly purine and glycerophospholipd metabolisms were impacted by the endothelial deletion of POR (**Figure 33A**), with only 12 of the 863 metabolites identified as significantly changed in ecPOR$^{-/-}$ cardiac tissue as compared to CTL (**Figure 33B**, **Table 28**). Among those metabolites, one was chemically unnamed: X-17146. However, those changes cannot be linked to the direct enzymatic function of POR.

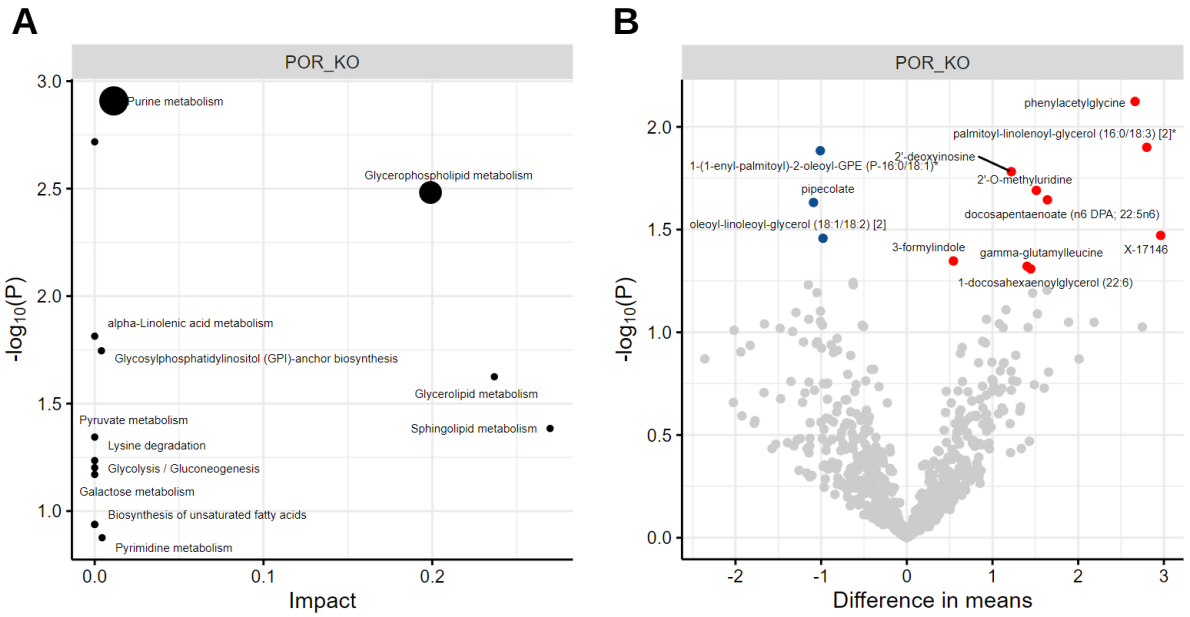

Figure 33. Metabolomics of cardiac tissue from control and ecPOR$^{-/-}$ animals.
A: Pathway enrichment of significantly altered metabolism in cardiac tissue of ecPOR$^{-/-}$ mice as compared to CTL. **B:** Volcano plot of significantly altered metabolites in cardiac tissue of ecPOR$^{-/-}$ as compared to CTL. Metabolites are represented as differential mean. In red are represented the metabolites reduced and in blue the metabolites increased in ecPOR$^{-/-}$ mice. n=7 animals. Figure published in Lopez *et al.* (2022)[122].

A common response of the heart to metabolic stress is the reactivation of the fetal gene program as a compensatory mechanism[169]. In mice, an isoform switch in the sarcomeric proteins occurs from the predominant adult isoform MHC-α (Myh6) to the foetal isoform MHC-β (Myh7). Additional features include a switch from fatty acids to carbohydrates as a source of energy, as well as the expression of atrial natriuretic factor (ANF)[169,170]. Therefore, we decided to look at the expression of typical genes linked to metabolic reprogramming in the heart (**Figure 34**). However, none of the genes we selected showed changes in their expression in ecPOR$^{-/-}$ animals as compared to CTL.

Collectively, these results show that the endothelial POR/CYP450 system is unlikely to have a metabolic function in the heart.

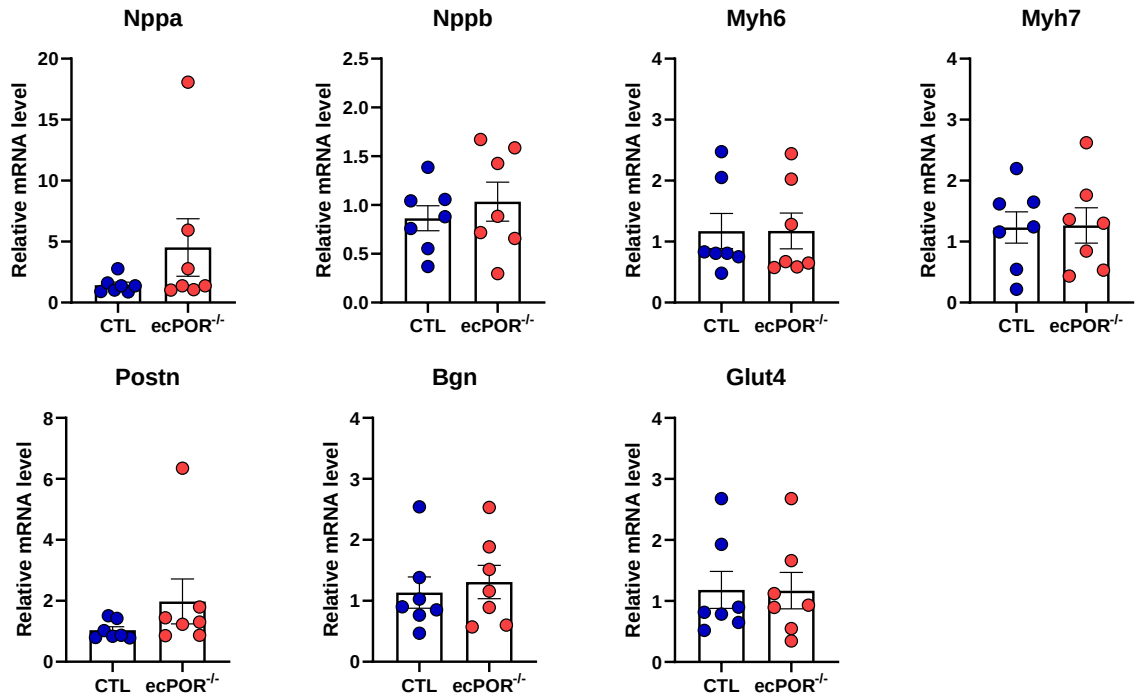

Figure 34. Expression of genes linked to metabolic reprogramming in the heart.
mRNA expression of metabolic reprogramming genes (Nppa, Nppb, Myh6, Myh7, Postn, Bgn and Glut4) as determined by qRT-PCR in hearts of CTL and ecPOR$^{-/-}$ animals. n=7 animals. Figure modified from Lopez *et al.* (2022)[122].

5.2.5 Combination of transverse aortic constriction and endothelial deletion of POR accelerates the development of heart failure

Under unstress conditions, i.e. 30 days after inducing the knockout, ecPOR$^{-/-}$ mice exhibited cardiac remodelling with an increase in heart weight to body weight and cardiomyocytes area, as well as re-expression of atrial contractile genes (Myl4, Myl7) in the left ventricle. Transverse aortic constriction (TAC) was first described by Rockmann et al. and is the most widely used pressure-overload model[119]. Therefore, to further evaluate whether or not the cardiac remodelling observed in ecPOR$^{-/-}$ mice had any functional consequences, mice were subjected to transverse aortic constriction (TAC). The constriction was achieved using O-rings (**Figure 12**, **Figure 13**) with an inner diameter of 0.50 mm[121] and endothelial deletion of POR was induced by *i.p.* injection of tamoxifen one week post surgery. Left ventricle structure and function were assessed by echocardiography before the surgery and at days 7, 14, 21, 28, 35, 42, 49, 56 and 61 post surgery (**Figure 35**).

The ejection fraction was reduced from ~64% (day 0) to 43% at day 7 post-TAC in both CTL and ecPOR$^{-/-}$ mice (**Figure 35A**). Over time, the ejection fraction further declined until reaching 30%. However, no differences was observed in the response to TAC between CTL and ecPOR$^{-/-}$ animals. In response to TAC, the left ventricle mass, cardiac systolic and diastolic volumes increased over time but without significant difference between genotypes (**Figure 35B-D**). In contrast, the cardiac output was significantly reduced upon endothelial deletion of POR (**Figure 35E**). As a consequence, ecPOR$^{-/-}$ animals showed a significant reduction in the stroke volume as compared to CTL animals (**Figure 35F**). Ratios of heart to body weight and lung weight to body weight were similar between the two genotypes (**Figure 35G**).

Together, these results suggest efficiency of TAC as a pressure-overload model and excludes that endothelial deletion of POR impacts on the development of heart failure in this model.

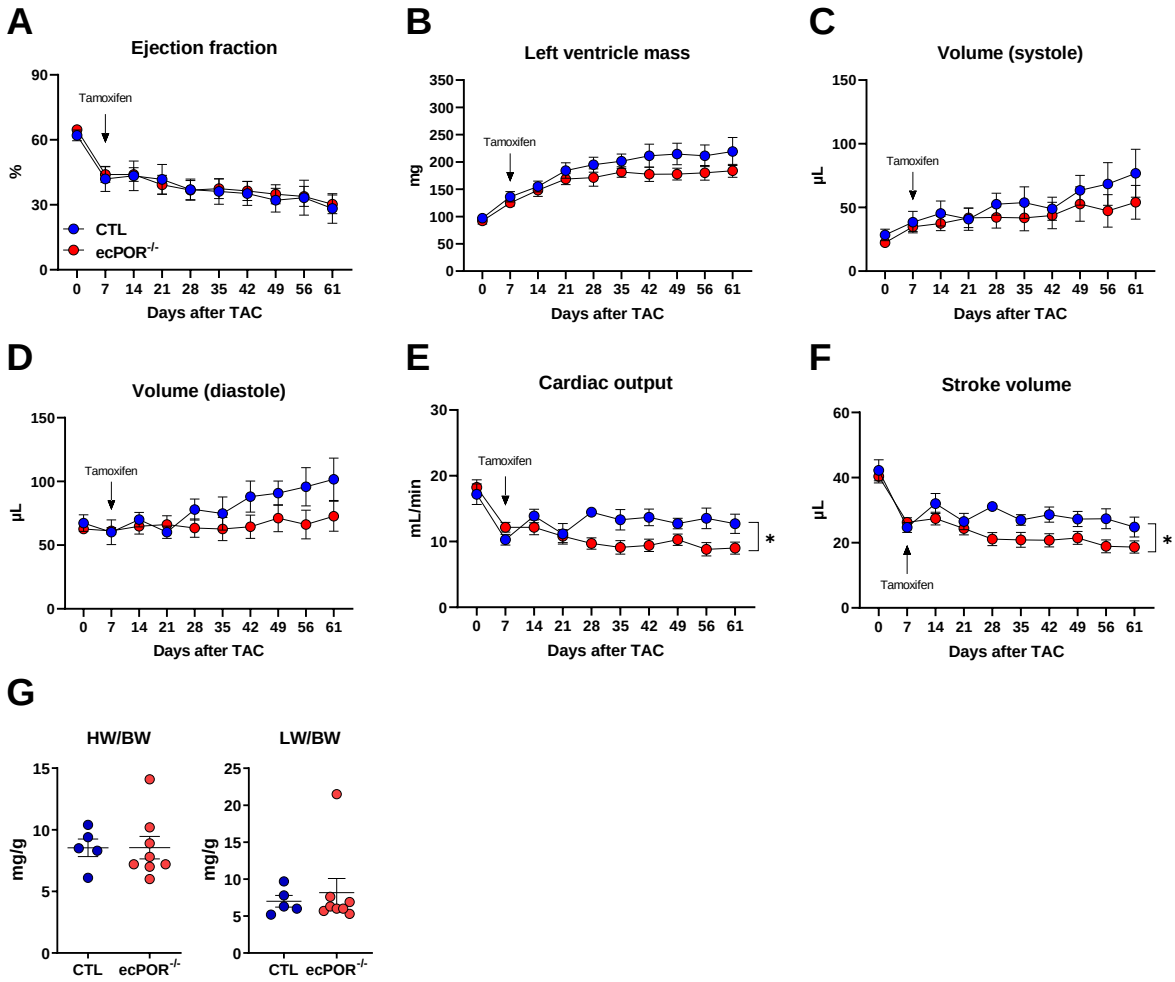

Figure 35. Combination of transverse aortic constriction with endothelial deletion of POR accelerates the development of heart failure.

A-F: Cardiac parameters measured by echocardiography at baseline (0), 7, 14, 21, 28, 35, 42, 49, 56 and 61 days post TAC surgery. Two-Way ANOVA for repeated measurements. *p<0.05. **G:** Ratio of heart weight (HW) and lung weight (LW) to body weight. n≥5 animals. Figure published in Lopez *et al.* (2022)[122].

6 Discussion

6.1 Cytochrome P450 monooxygenases and organic nitrates

In the first part of this work, the role of cytochrome P450 monooxygenases on the biotransformation of organic nitrates was investigated. Previous studies showed that the hepatic POR/CYP450 system contributes to the bioactivation of organic nitrates[80,142]. Recombinant microsomes released nitrite from nitrovasodilators in a CYP450 and dose-dependent manner. However, smooth muscle cell-specific deletion of POR, i.e. indirectly switching off the function of all CYPs in SMCs, revealed that the vascular POR/CYP450 system had no impact on the dilator response of NTG and PETN. In line with previous publications, blockage of ALDH2, known as the main enzyme responsible for the activation of NTG and PETN, and/or abolishment of the endogenous NO production did not unmask a contribution of the POR/CYP450 system to the dilator response of NTG and PETN[73,74]. We showed that POR and CYP51 are differently expressed in liver and aorta suggesting that the insufficient vascular expression of CYP450 enzymes reflects the physiological unimportance of the enzymatic activity of the POR/CYP450 system for the bioactivation of NTG and PETN. Further experiments could be performed to determine whether the tolerance to NTG is POR dependent[171,172].

6.1.1 Microsomes containing recombinant POR/CYP450 are involved in the biotransformation of organic nitrates

The capacity of the POR/CYP450 system in the biotransformation of NTG was first studied using hepatic microsomes isolated from rat, where denitration of NTG was shown to be CYP450-dependent and inhibited after pre-treatment with SKF525 and carbon monoxide (CO)[78,80]. The formation of nitric oxide during denitration of NTG was shown to be catalyzed by the POR/CYP450 system using visible spectroscopy[80].

In the present study, the amount of nitrite produced from organic nitrates was measured in the presence of POR/CYP450-containing microsomes typically expressed in vessels. The release of NO from NTG and PETN was more effective in presence of CYP2C8 and CYP2C9. These results are in line with previous studies, where the formation of NO from the biotransformation of NTG has been reported in bovine pulmonary and coronary arteries as well as cultured porcine aortic smooth muscle cells[173,174]. The reduction of nitrite production from NTG and PETN after pre-treatment with SKF525 corresponds with previous findings in regard to the requirement of the catalytic CYP unit in the biotransformation of organic nitrates[77,175]. Bennett et al. described reduced NADPH-dependent biotransformation of NTG by rat aortic microsomes in presence of SKF525 and CO[175]. Although the microsomal preparation differed in the present study, the biotransformation of organic nitrates was comparably NADPH dependent and inhibited by SKF525.

Albeit indirect, our results reinforce the concept that vascular POR/CYP450 system might be involved in the biotransformation of organic nitrates. However, the validation of these observations using an *in vivo* model is still missing. In order to investigate whether the vascular POR/CYP450 can locally bioactivate organic nitrates, a smooth muscle cell, tamoxifen inducible knockout of POR was generated and utilized in the present study.

6.1.2 The vascular response to organic nitrates is not mediated by the POR/CYP450 system in SMCs

There is a current paradigm that at least two pathways are involved in the bioactivation of highly potent organic nitrates in vessels: vascular ALDH2 releases NO from NTG and PETN at low concentrations (<1 µM) while the vascular POR/CYP450 system could potentially bio-transform NTG and PETN at high concentration (>1 µM)[55,61,75]. Deletion of POR in SMCs had no impact on the biotransformation of organic nitrates. Indeed, neither relaxation nor nitrite production of aortic rings in response to NTG and PETN were affected by deletion of POR in SMCs, even if the endothelium was removed. These results suggest that smooth muscle and endothelial CYP450s are physiologically not important in the biotransformation of organic nitrates. Indeed, since the report of the Stamler group, ALDH2 is considered as the main enzymes responsible for the bioactivation of highly potent organic nitrates in vessels[73,74]. They demonstrated that both inhibition and deletion of ALDH2 in animals resulted in a reduced relaxation in response to NTG and a lack of sGC stimulation by NTG. Subsequent studies supported these findings with NO being release from NTG by ALDH2 in humans[76] and animals[176,177]. In the present work, our results could confirm the importance of vascular ALDH2 for the response to NTG. Pre-treatment of aortic rings with benomyl (ALDH2 inhibitor) resulted in a rightward shift of the NTG concentration-response curve, but did not lead to a total loss of vasorelaxation in response to NTG. Interestingly, the effect of benomyl on the PETN-induced relaxation was not as strong as shown by previous studies[55], and PETN-induced nitrite formation was not affected by benomyl. Given that daidzin (ALDH2 inhibitor) and genetic deletion of ALDH2 were shown to attenuate the dilator response to PETN in both rat aorta and mouse aorta, these results are unexpected[55,75,178]. This may suggest that specifics of the interaction of PETN with benomyl but not ALDH2 are responsible for this observation. In conclusion, our findings are in line with the concept that ALDH2 locally releases nitrite from NTG and PETN in vessels at low concentrations, whereas the vascular POR/CYP450 is physiologically irrelevant in the bioactivation of organic nitrates. Nevertheless, the maximal relaxation was not altered by inhibition of ALDH2 with benomyl. In line with previous research, our results suggest that other enzymatic systems might be involved in the bioactivation of highly potent organic nitrates in SMCs.

6.1.3 The vascular POR/CYP expression is low compared to the hepatic POR/CYP expression

The fact that POR/CYP-containing microsomes generate nitrites from highly potent organic nitrates, i.e. NTG and PETN, but that vascular POR/CYP450 does not contribute to the dilator response to NTG and PETN gives rise to two hypotheses: i. the biotransformation of highly potent organic nitrates by the POR/CYP450 system does not contribute in the generation of an active reactive nitrogen intermediate; ii. the POR/CYP450 activity is physiologically unimportant in vessels due to its low expression. The first hypothesis is rather unlikely as it is not supported by the current literature. In fact either inhibition of CYP450 enzymes by SKF525 and CO, or inhibition of the reductase by DPI (diphenyleneiodonium chloride; a POR inhibitor) results in reduced biotransformation of NTG[56,78–80,179]. Therefore, the second hypothesis most likely explains the results observed in this study. Indeed our data suggest that the POR/CYP450 system can bio-transform NTG and PETN in the form of recombinant microsomes but its vascular expression is insufficient for the biotransformation of organic nitrates. Based on immunoblot analysis, the vascular expression of POR and CYP51 appears to be 10- to 40-fold less than the hepatic expression, which supports our second hypothesis.

The concept of NO being released from organic nitrates is well established for vessels[57,61,73,74], however, controversy remains whether organic nitrates, in particular NTG, can release NO in extravascular tissues[180]. Although studies reported the formation of NO from NTG in hepatic microsomes[80], there are studies suggesting that NTG is metabolized in the liver to nitrite, 1,2-glyceryl dinitrate and 1,3-glyceryl dinitrate when administrated orally (doses of 46 µM)[180]. Interestingly, nitrite was long perceived as measurable oxidative end product of NO until it was shown that nitrite acts as a NO pool which can be reduced back to NO[181,182]. Several studies demonstrated a nitrite reductase activity of deoxyhemoglobin, implying the involvement of erythrocytes in the conversion of nitrite to NO under hypoxic conditions, making nitrite a promising therapeutic agent[180,181,183]. In addition, Dejam et al. reported that erythrocytes may also serve as a reservoir for intravascular nitrite[184]. Furthermore, they found an artery-to-vein gradient for erythrocytes nitrite in humans where nitrite might be used as a source of NO in the microvasculature bed which is consistent with the idea that nitrite might act as a NO donor for hypoxic visodilation[183,184]. In conclusion, our data suggest

that the liver, which is rich in POR/CYP450, is possibly the predominant extravascular site of biotransformation of organic nitrates *in vivo*. Therefore, it is tempting to speculate that the hepatic POR/CYP450 system is responsible for the generation of nitrite from NTG (i.e. taken by the oral route), which is then stored in erythrocytes to be transported to distant vessels.

6.1.4 Concluding remarks and outlook

This study supports the importance of ALDH2 in the local biotransformation of NTG in vessels, whereas the vascular POR/CYP450 system has no local contribution in the biotransformation of highly potent organic nitrates as illustrated in **Figure 36**. Furthermore, numerous studies pointed out the enzymatic metabolism of organic nitrates being concentration dependent with ALDH2 responsible for the bioactivation at low concentration while the POR/CYP450 system metabolizes organic nitrates at high concentration[52,61,180]. Our data showed that vascular ALDH2 could metabolize NTG and PETN at low concentrations, resulting in vessels relaxation, which was altered in presence of benomyl, an ALDH2 inhibitor. These results match with the common way of nitroglycerin administration, which is sublingually. This allows a quick drug entry into bloodstream, thus systemic circulation in order to stop an angina attack[185,186].

In addition, nitroglycerin can be administrated orally to prevent angina, resulting in the first-pass metabolism which takes place in the liver[186–190]. As our results showed that the hepatic POR/CYP450 system could generate nitrite from NTG and PETN using high concentrations (100 µM), the hepatic POR/CYP450 system is most likely responsible for the bioactivation of NTG when taken by the oral route. In conclusion, this study confirms the current studies with vascular ALDH2 and hepatic POR/CYP450 system bio-activating NTG and PETN in a concentration and potentially drug intake manner.

Of importance, continuous or frequent daily use of organic nitrates leads to nitrate tolerance leading to an attenuation or complete loss of therapeutic efficacy[52,112]. Numerous hypotheses were raised in an attempt to explain the loss of efficacy. Studies showed that chronic use of organic nitrates resulted in sGC desensitization[52,191,192], which in turn lead to a reduction in cGMP activity and an alteration in cGMP turnover[112,193] resulting to an attenuation in responsiveness towards organic nitrates NO-release. Furthermore, nitroglycerin metabolism is known to promote reactive oxygen species resulting in oxidation of thiol groups in the catalytic unit of ALDH2[52,55,194]. Thus, inhibition of ALDH2 leads to a reduction of NTG biotransformation, hence its efficacy[52]. It has been shown that CYP450 enzymes are reversibly inhibited by organic nitrates NO-released compound[195]. Indeed NO binds to the heme in competition with oxygen, forming a nitrosyl-heme, therefore inhibiting

CYP450 enzymes[182,195]. Additionally, it has been shown that organic nitrate tolerance affects the cytochrome P450 isoenzymes, as degradation of both vascular and hepatic CYP450 enzymes occurred in response to nitrate tolerance[171,172,196]. These observations were reversible after cessation of the NTG infusion. Furthermore, they observed an increase of NTG-induced NO formation in vessels of rats pre-treated with a CYP450 inducer (acetone)[171]. Although the results of the present study refute the importance of the vascular POR/CYP450 in the biotransformation of organic nitrates, the involvement of the POR/CYP450 system in nitrate tolerance should be investigated in further studies.

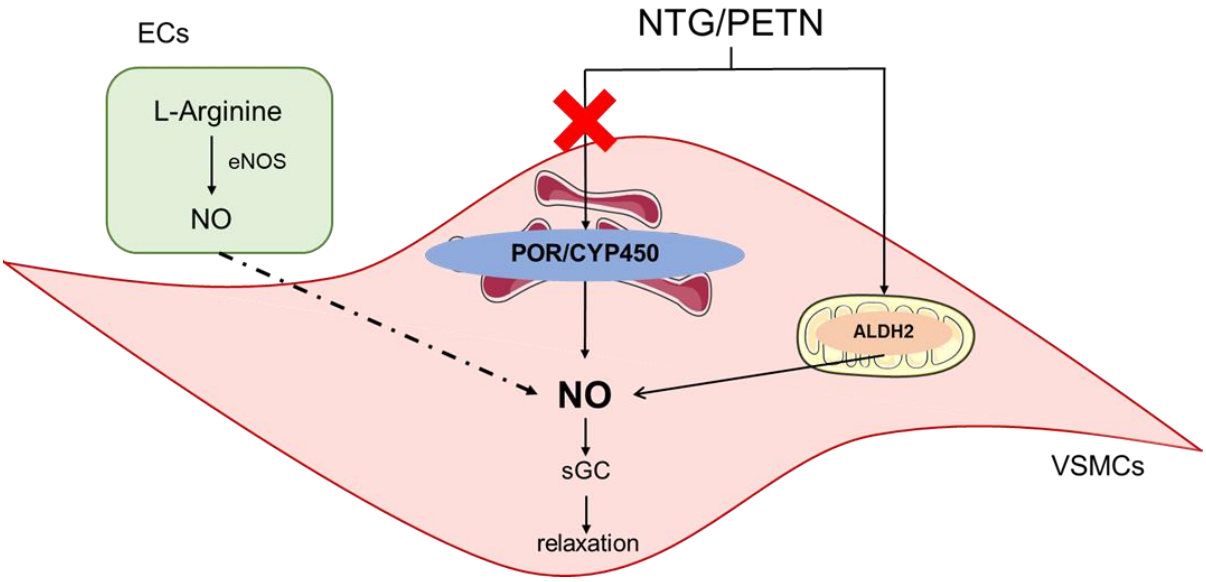

Figure 36. Biotransformation of organic nitrates in vascular smooth muscle cells.
Under basal condition, eNOS produces nitric oxide in endothelial cells. NO diffuses to the smooth muscle layer which results in relaxation through sGC stimulation, In case of angina, NTG or PETN are administrated. ALDH2 is responsible for the biotransformation of NTG and PETN, with the concomittent metabolite(s) stimulating sGC. Whereas the POR/CYP450 system is involved in the biotransformation of NTG and PETN in the liver, this system is physiologically unimportant in vessels. ECs: endothelial cells; VSMCs: vascular smooth muscle cells; NTG: nitroglycerin; PETN: pentaerythritol tetranitrate; POR: cytochrome P450 reductase: CYP450: cytochrome P450 enzymes; eNOS: endothelial nitric oxide synthase; ALDH2: mitochondrial aldehyde dehydrogenase; NO: nitric oxide; sGC: soluble guanylyl cyclase. Figure published in Lopez *et al.* (2021)[53].

6.2 Cytochrome P450 reductase and cardiac remodeling

The second part of this work focused on the role of endothelial cytochrome P450 reductase in the cardiac function. RNA-sequencing of the heart of a healthy mice revealed that the CYP450 expression is cell-specific with cardiac ECs exhibiting an enrichment in the expression of the Cyp4 family (known to be involved in the ω-oxidation of fatty acids) and of the Cyp2 family (known for production of EETs). Under non-stressed conditions (i.e. 30 days after inducing the knockout by tamoxifen feeding), endothelial deletion of POR lead to cardiac remodelling as observed with an increase in the ratio of heart weight to body weight and an increase in the cardiomyocytes area. Based on the RNA-sequencing data, it is unlikely that loss of POR in ECs results in oxidative stress. The sequencing data rather suggested that POR might alter the ribosomal biogenesis and protein synthesis, which could potentially affect the cardiac contractility in ecPOR$^{-/-}$ mice. Metabolomics from cardiac tissue of CTL and ecPOR$^{-/-}$ mice did not highlight a metabolic function of the endothelial POR/CYP450 system in the heart. Rather, the combination of TAC with endothelial deletion of POR accelerates the development of heart failure likely as a result of an increase in overall vascular stiffness.

6.2.1 High expression of CYP2 and CYP4 families in cardiac endothelial cells

In the present study, the expression of CYP450 enzymes in cardiac cells of murine healthy heart was shown to be cell-specific, with the CYP2 and CYP4 families showing the highest expression in endothelial cells. Interestingly, studying human genotype-phenotype association revealed that isoforms of CYP2 and CYP4 families are associated with cardiovascular diseases. These results are in line with previous studies which reported the expression of the CYP2 and CYP4 families in the heart[12,36,197–199].

Among the CYP2 family, Cyp2j6 and Cyp2j9 were enriched in ECs. The CYP2J subfamily is known to have an epoxygenase enzymatic activity, i.e. converting arachidonic acid to EETs[95]. In the vascular system, EETs are known as endothelium-derived hyperpolarizing factors (EDHFs) and important in the regulation of vascular tone[36,103], whereas they have a cardioprotector effect in the heart[104,200,201]. Overexpression of CYP2J2 in cardiomyocytes exhibited improved left ventricular postischemic recovery as a result of mitoK_{ATP} channels activation[106]. Reduction of the infarct size in rat hearts subjected to ischemia/reperfusion (I/R) was observed after exogenous administration of 11,12-EET and 14,15-EET[168]. Furthermore, a study demonstrated that increasing EETs bioavailability by inhibiting soluble epoxide hydrolase (sEH) prevented the development of cardiac hypertrophy in a TAC model[202]. Our results showed an enriched expression of the CYP2 family in endothelial cells, suggesting that loss of EETs in endothelial cells could affect the cardio-protective role of EETs. In addition to members of the CYP2 family, the expression of Cyp4f13, Cyp4f16 and Cyp4f17 was enriched in cardiac ECs. The CYP4 family has a ω-hydroxylase which converts arachidonic acid to 20-HETE, a vasoconstrictor agent[93]. In addition, the CYP4 family is involved in the metabolism of fatty acids through ω-oxidation[151] and fatty acid ω-oxidation has been suggested as a rescue pathway for fatty acid oxidation disorders[203].

In order to further investigate the cardiac function of the endothelial POR/CYP450 system, an endothelial-specific, tamoxifen-inducible knockout mouse of POR was utilized in the present study. By knocking out POR, all microsomal CYP450 enzymes are inactivated, thus overcoming the lack of specific inhibitors or compensatory expression among the isoenzymes[36].

6.2.2 The endothelial POR/CYP450 system is unlikely to affect fatty acid oxidation

Endothelial cells are more than an inner monolayer in vessels serving as a “plumbing” for the cardiovascular system[204], they serve as gatekeeper in fatty acid metabolism[166,204]. Indeed, the cardiac activity and its high energy demand depends on the fatty acids transfer across the endothelium[166,205]. Recently, the importance of CD36 in fatty acid uptake in ECs and fatty acid delivery to CMs has been demonstrated by deletion of CD36 in endothelial cells in mice[205]. Furthermore, there are evidences for fatty acid transport proteins (FATPs) to be involved in fatty acid uptake in tissues[166,206], as ECs express both FATB3 and FATB4 which are required for VEGFB-induced fatty acid uptake[207]. Interestingly, Ibrahim et al. showed that endothelial mitochondrial ATP plays a role in fatty acid uptake, where the ATP-dependent acyl-CoA synthase activity of FATP4 uses mitochondrial ATP to promote the endothelial fatty acid uptake[206].

In the present study, inactivation of the endothelial POR/CYP450 lead to an increase in the ratio of heart to body weight, in addition to an increase in the area of cardiomyocytes. These results suggest that loss of endothelial POR/CYP450 leads to cardiac remodeling. In addition, deletion of POR in endothelial cells resulted in a mitochondrial signature in cardiomyocytes. Indeed, gene ontology analysis suggested changes in the mitochondrial function of heart of ecPOR$^{-/-}$ mice. The heart is known to be highly demanding in energy, therefore mitochondrial dysfunction results in myocardial metabolic disturbance concomitant with left ventricular dysfuction[208]. The cardiac phenotype and the enriched expression of CYP4 family may suggest that plasma fatty acids, which have to trans-pass the endothelial barrier[166,167], could be oxidized via ω-hydroxylation by the endothelial POR/CYP450 system before serving as a source of energy for cardiomyocytes via β-oxidation. For that purpose, metabolomics of cardiac tissue, a screening and unbiased approach, was performed. Unfortunately, these results did not support a metabolic role of the POR/CYP450 system in terms of fatty acid oxidation[151]. In fact, there was no alteration in fatty acid metabolism and RNA-sequencing of cardiac endothelial cells and cardiac tissue did not show a change in genes involved in fatty acid uptake, i.e. CD36 or FATP4 for example. Therefore, a role of the endothelial POR/CYP450 system in fatty acid metabolism seems rather unlikely.

6.2.3 Endothelial deletion of POR leads to cardiac remodeling

Cardiac remodeling refers to a change in the size, shape, structure and function of the heart, in response to physiological, i.e. exercising, or pathological conditions[83,209]. Furthermore, cardiac remodelling is complex and responds to oxidative stress, metabolic reprogramming, inflammation, and an increase in the production of extracellular matrix[157].

The endoplasmic reticulum (ER) plays an important role in the synthesis of secreted and integral membrane proteins as well as ER-bound ribosomes[210]. Based on gene ontology, endothelial deletion of POR disturbed the expression of genes related to vesicle trafficking and assembly of large and small ribosomal subunits. Moreover, POR is localized in the ER[211], suggesting a role of POR in the regulation of membrane protein synthesis and secretion. Interestingly, CYP450 enzymes are synthesized on membrane-bound ribosomes[212]. Although only a few CYP450 genes were up-regulated, the increase in ribosomal genes could be an attempt of increasing the synthesis of CYP450 enzymes as a compensatory mechanism due to the loss of CYP450 activity. Perturbation of the ER protein synthesis, folding and secretion creates a cellular state called ER stress, which activates the unfolded protein response (UPR) to restore the ER homeostasis[213]. However, the ER folding capacity does not seem to be exceeded as genes such as Hspa5[213–215] and Xbp1[213,216,217] were downregulated, which could be the result of a compensatory mechanism. However, how a potential increase in protein synthesis in endothelial cells affects the cardiac function remains unclear.

Although none of the classical fetal genes were changed (i.e. Myh6, Myh7, Glu4)[169], genes linked to cardiac contractility such as Myl4, Myl7 and Sln were up-regulated in the cardiomyocyte fraction of ecPOR$^{-/-}$ mouse heart. The atrial light chain-1 (ALC1, protein coded by Myl4) is expressed in the atria, but re-expression of ALC1 in the ventricle of patients with hypertrophic cardiomyopathy was reported by Schaub and collaborators[218]. Re-expression of ALC1 in ventricle is characterized by a higher Ca^{2+}-sensitivity of force generation, hence improved contractility which could be seen as an adaptive mechanism in response to hypertrophy[219,220]. The rate of muscle relaxation together with the sarcoplasmic reticulum (SR) Ca^{2+} load available for the next cycle of contraction depends on the SERCA pump which is regulated by phospholamban. However, sarcolipin (protein coded by Sln) has been reported as an important player

in the regulation of SERCA pump activity[221–223]. At the adult stage, sarcolipin is atrial restricted however its expression in adult hypertrophied ventricles was up-regulated in Nkx2-5 null mice[224], and SR calcium transport is decreased upon overexpression of SLN in cardiomyocytes, resulting in reduced cardiac contractility[221].

A reduction in cardiac output and stroke volume (both parameters classify for heart failure), was observed in ecPOR$^{-/-}$ mice subjected to transverse aortic constriction. We recently reported that eNOS activity is maintained by expression of POR in endothelial cells and its loss leads to vascular dysfunction[117]. Indeed, a reduction in vascular EETs together with a lower diameter in carotids were observed in ecPOR$^{-/-}$ mice as compared to controls[117]. Since vascular stiffness increases afterload (pressure the left ventricule has to work against at each contraction to eject blood) and can be influenced by endothelial dysfunction[225,226], our results suggest an overall increased vascular stiffness in ecPOR$^{-/-}$ mice.

Collectively, our results suggest that endothelial deletion of POR induces an increased vascular stiffness resulting in cardiac remodeling with increased expression of genes related to cardiac contractility. Further studies could determine whether this increase in SLN and ALC1 genes is observed at the protein level and whether it affects the cardiac function and/or contractility in the heart of ecPOR$^{-/-}$ mice.

6.2.4 Concluding remarks

In the present study, we conclude that deletion of the cytochrome P450 reductase in endothelial cells leads to cardiac remodeling in response to an increase in vascular stiffness. We previously demonstrated that vascular EETs are reduced in ecPOR$^{-/-}$ mice resulting in vasoconstriction as shown by a lower diameter in their carotids[117]. Our RNA-sequencing data suggest that deletion of POR in endothelial cells potentially lead to ribosomal biogenesis and protein synthesis alterations without inducing stress response, which might affect the cardiac contractility and mitochondrial function in ecPOR$^{-/-}$ mice. Metabolomics results did not point to a mitochondrial dysfunction (i.e. lower ATP production or increased ATP hydrolysis) that was observed at the gene level, i.e. reduction in genes related to electron transport. Moreover, the changes observed with metabolomics could not be linked to the direct enzymatic function of POR making it difficult to interpret these results. Overall, the cardiac remodeling observed upon deletion of POR in endothelial cells most likely responds to the reduction of vascular EETs, i.e. vascular stiffness.

7 Summary

Cytochrome P450 enzymes are a large superfamily of membrane-bound heme-containing monooxygenases. They are essential for the oxidative metabolism of endogenous substrates such as steroids and fatty acids, and biotransformation of xenobiotic substrates such as pollutants and drugs. Although the highest expression of CYPs is found in the liver, their cardiovascular expression is not negligible with CYP450 subfamilies being responsible for the production of vasoactive lipids. Of importance, the enzymatic activity of all microsomal CYP450 isoenzymes is dependent on the cytochrome P450 reductase (POR), an electron donor.

In the first part of this work, the role of cytochrome P450 monooxygenases on the biotransformation of organic nitrates was investigated. Recombinant Supersomes™ were selected and incubated with NTG and PETN, where nitrite release was measured as a nitric oxide (NO) footprint. The capacity of the recombinant POR/CYP450 system to release nitrite from NO prodrugs was shown to be CYP-specific and dose-dependent. To study the involvement of CYP450 enzymes in the vascular biotransformation of organic nitrates *in vivo*, a smooth muscle-cell specific, inducible knockout model of POR (smcPOR$^{-/-}$) was generated. Organ chamber experiments revealed that the vascular POR/CYP450 system had no impact on the dilator response of NTG and PETN. In line with previous publications, inhibition of ALDH2, known as the main enzyme responsible for the activation of NTG and PETN, and/or abolishment of the endogenous NO production did not reveal a contribution of the POR/CYP450 system to the dilator response of NTG and PETN. To better understand these results, we looked at the expression of the hepatic and vascular expression of the POR/CYP450 system where the hepatic was increased by 10- to 40-fold as shown by Western blot analysis. We concluded that due to insufficient vascular expression of CYP450 enzymes their contribution to the bioactivation of NTG and PETN is only minor.

The second part of this work focused on the cardiac relevance of endothelial isoenzymes. For that purpose, an endothelial cell-specific, tamoxifen-inducible knockout model of POR was generated and characterized in the present study. RNA-sequencing of the heart of healthy mice revealed that the CYP450 expression is cell-specific with cardiac endothelial cells (ECs) exhibiting an enrichment in the expression

of the Cyp4 family (ω-oxidation of fatty acids) and of the Cyp2 family (production of EETs). Under non-stredded conditions (i.e. 30 days after inducing the knockout by tamoxifen feeding), endothelial deletion of POR was associated with cardiac remodelling as observed by an increase in the ratio of heart weight to body weight and an increase in the cardiomyocyte area. RNA-sequencing of cardiac ECs suggested that loss of POR might alter ribosomal biogenesis and protein synthesis, which could potentially affect the cardiac contractility in ecPOR$^{-/-}$ mice. Metabolomics from cardiac tissue of CTL and ecPOR$^{-/-}$ mice were not indicative for an important metabolic function of the endothelial POR/CYP450 system in the heart. The combination of transverse aortic constriction (TAC) with endothelial deletion of POR accelerates the development of heart failure in mice as detected by a reduction in cardiac output and stroke volume. These effects were mediated most likely by a reduction in vascular EETs production, which increases vascular stiffness, resulting in cardiac remodeling.

8 Deutsche Zusammenfassung

Die Cytochrom-P450-Enzyme sind eine große Superfamilie von membrangebundenen Häm-Monooxygenasen. CYP450-Enzyme sind für den oxidativen Stoffwechsel endogener Substrate wie Steroide und Fettsäuren sowie für die Biotransformation xenobiotischer Substrate wie Schadstoffe und Arzneimittel von wesentlicher Bedeutung. Die Leber weißt dabei die höchste CYP450-Expression auf, von denen alleine 15 Isoenzyme an der Phase I des Arzneimittelstoffwechsels beteiligt sind. Die Expression der CYP450-Familie im kardiovaskulären System ist jedoch nicht zu vernachlässigen, da Epoxygenasen (CYP2C- und CYP2J-Sufamilien) und ω-Hydroxylasen (CYP4A- und CYP4F-Subfamilien) für die Produktion vasoaktiver Lipide (*epoxyeicosatrienoic acids*, EETs) und *hydroxyeicosarrienoic acids*, HETEs) verantwortlich sind. Wichtig ist dabei, dass die enzymatische Aktivität aller CYP450 Enzyme von der Cytochrom-P450-Reduktase (POR), abhängig ist, welche diese mit Elektronen versorgt.

Die vorliegenden Arbeit glieder sich in zwei Abschnitte. Der erste Teil fokussiert auf den Metabolismus organischer Nitrate, der zweite auf CYP450 im Herzen. Über ein Jahrhundert lang wurden Angina pectoris oder ischämische Herzerkrankungen mit Nitroglycerin (NTG) oder Pentaerythrittetranitrat (PETN) behandelt. Bei diesen Verbindungen handelt es sich um Produkte, die enzymatisch bioaktiviert werden, um ihre Nitrovasodilatoren freizusetzen: die Aldehyddehydrogenase (ALDH2) bei therapeutischen Konzentrationen oder CYP450-Enzyme bei suprapharmakologischen Konzentrationen. In zahlreichen Studien wurde ALDH2 als das für die Aktivierung organischer Nitrate in den Gefäßen hauptverantwortliche Enzym bezeichnet. Mehrere Studien zeigten, dass das hepatische POR/CYP450-System an der Bioaktivierung von organischen Nitraten beteiligt ist. Die Rolle des vaskulären POR/CYP450-Systems bei der Biotransformation von organischen Nitraten ist jedoch noch unklar.

Zu diesem Zweck wurden CYP450-Isoformen, die typischerweise in der Aorta exprimiert werden und im Handel in Form von rekombinanten Supersomen™ erhältlich sind, ausgewählt und mit NTG und PETN inkubiert, wobei die Nitritfreisetzung als Stickoxid (NO)-Fußabdruck gemessen wurde. Insgesamt zeigte

sich, dass die Fähigkeit des rekombinanten POR/CYP450-Systems, Nitrit aus NO-Prodrugs freizusetzen, CYP-spezifisch und dosisabhängig ist.

Um die Beteiligung von CYP450-Enzymen an der vaskulären Biotransformation von organischen Nitraten *in vivo* zu untersuchen, wurde eine glatte Muskelzell-spezifische, induzierbare Knockout-Maus von POR (smcPOR$^{-/-}$) erzeugt. In Folge des Verlustes der Expression von POR sollte es zu einem vollständigen Aktivtätitsverlust der abhängigen CYP450-Enzymekommen. Die Relaxation von Kontroll- und smcPOR$^{-/-}$-Aortenringen als Reaktion auf organische Nitrate wurde nachfolgenden mit und ohne Entfernung des Endothels untersucht. Obwohl das POR/CYP450-System in Form von rekombinanten Mikrosomen NO-Prodrugs biotransformieren kann, hatte die Inaktivierung von CYP450 im Gefäßsystem keinen Einfluss auf die Dilatation auf NTG und PETN. Nach Hemmung von ALDH2 mit Benomyl war die Nitritproduktion von Kontroll- und smcPOR$^{-/-}$-Aortenringen unter NTG reduziert. Im Gegensatz dazu führte die Deletion von POR in glatten Muskelzellen (*smooth muscle cells*, SMCs) zu keiner Reduktion der Nitritbildung aus NTG. Unerwartet werden die Effekte auf den NO-Donor PETN: Anders als beschrieben, hatte Hemmung von ALDH2 keinen Einfluss auf die Nitritproduktion durch PETN, was darauf hindeutet, dass ein weiteres Enzym neben ALDH oder POR die Fähigkeit hat, PETN zu bioaktivieren.

Um zu testen, ob die Hemmung von ALDH2 eine mögliche Rolle des POR/CYP450-Systems bei der Biotransformation von NTG und PETN in Gefäßen demaskieren könnte, wurde die Relaxation von Kontroll- und smcPOR$^{-/-}$-Ringen als Reaktion auf NTG und PETN nach Inkubation mit Benomyl untersucht. Die Hemmung der ALDH2-Aktivität konnte jedochen keinen Beitrag des vaskulären POR/CYP450-Systems an der Dilatationsreaktion auf NTG und PETN aufdecken. Der Literatur zufolge tragen vaskuläre CYP450-Enzyme zur Bioaktivierung von NTG und PETN in suprapharmakologischen Konzentrationen bei, jedoch konnten diese Beobachtungen in smcPOR$^{-/-}$ Mäusen nicht reproduziert werden. Um diese Ergebnisse besser zu verstehen, wurde die Expression des POR/CYP450-Systems in der Aorta mit seiner hepatischen Expression verglichen. Die hepatische Expression von POR und CYP51 war viel höher als die vaskuläre Expression. Es ist daher sehr wahrscheinlich, dass die unzureichende vaskuläre Expression von CYP450-Enzymen physiologisch gesehen die geringe enzymatische Aktivität von CYP450 bei der Bioaktivierung von NTG und PETN widerspiegelt.

Die kontinuierliche Verabreichung oder der häufige tägliche Gebrauch von Nitroglycerin führt zu einer Nitrat-Toleranz, bei der eine Abschwächung oder ein vollständiger Verlust der therapeutischen Wirksamkeit zu beobachten ist. Studien haben gezeigt, dass organische Nitrate, die NO freisetzen, das CYP450-Enzymsystem reversibel hemmen, wobei NO in Konkurrenz mit Sauerstoff an das Häm bindet und ein Nitrosyl-Häm bildet. Weitere Studien berichteten, dass die hepatische und vaskuläre Expression von CYP450-Enzymen bei nitrat-toleranten Tieren beeinträchtigt war. Obwohl die Ergebnisse der vorliegenden Arbeit die Bedeutung des vaskulären POR/CYP450-Systems für die Biotransformation organischer Nitrate widerlegen, sollte die Beteiligung des POR/CYP450-Systems an der Nitrattoleranz in weiteren Studien untersucht werden.

Der Schwerpunkt des zweiten Teils dieser Studie lag auf der Rolle der endothelialen Cytochrom-P450-Reduktase für die Herzfunktion. Das Herz ist ein komplexes multizelluläres Organ mit einem integrierten Netzwerk interzellulärer Kommunikation. Kardiale Endothelzellen (ECs) sind der häufigste Zelltyp des Herzens und bilden die kardialen Kapillaren und das Endothel. Zahlreiche Studien haben gezeigt, dass ECs Autacoide und Metaboliten produzieren und freisetzen, die die Funktion der Herzmuskelzellen (CMs) beeinflussen. Wie die Endothelzellen exprimieren auch Kardiomyozyten POR und CYP450-Isoenzyme wie Epoxygenasen (CYP2C- und CYP2J-Suffamilien) und ω-Hydroxylasen (CYP4A- und CYP4F-Subfamilien). Kardiale Epoxygenasen erzeugen EETs, und die kardioprotektive Wirkung dieser Metaboliten wurde in verschiedenen Studien nachgewiesen: Sie modulieren kardiale Ca^{2+}-Kanäle vom L-Typ und aktivieren K_{ATP}-Kanäle. Außerdem zeigte sich bei Mäusen mit kardialer Hypertrophie eine verbesserte Herzfunktion, nachdem sie mit EETs behandelt worden sind. Die mutmaßliche kardioprotektive Funktion kardialer endothelialen EETs bleibt jedoch unklar. Während die CYP4-Familie in SMCs 20-HETE erzeugt, können diese Enzyme auch langkettige Fettsäuren hydroxylieren, die dann zu Dicarbonsäuren umgewandelt werden, um die β-Oxidation in Kardiomyozyten zu unterstürtzen.

Um die kardiale Relevanz endothelialer CYP450 zu identifizieren, wurde in der vorliegenden Studie ein endothelzellspezifisches, Tamoxifen-induzierbares Knockout-Modell von POR ($ecPOR^{-/-}$) erzeugt und charakterisiert.

Um eine mechanistische Grundlage für eine zelltypspezifische CYP450-Funktion im Herzen zu schaffen, wurde die Expression von murinen CYP450-Isoenzymen in verschiedenen Herzzelltypen aus RNA-Sequenzierung öffentlich-verfügbarer Studien untersucht. Darüber hinaus wurde eine mögliche Genotyp-Phänotyp-Assoziation mittels PhenoScnaner, einem Online-Tool, ermittelt. Diese Ergebnisse zeigten, dass das Expressionsmuster der CYP450-Isoenzyme zelltypspezifisch ist, wobei das endotheliale CYP450 genetische Varianten aufweist, die mit kardiovaskulären Erkrankungen und dem Fettstoffwechsel in Verbindung gebracht werden.

Um einen ersten Eindruck von den Auswirkungen der endothelialen Deletion von POR auf das Herz zu erhalten, wurde 30 Tage nach der Tamoxifen-Behandlung das Verhältnis von Herzgewicht zu Körpergewicht bestimmt, wobei bei ecPOR$^{-/-}$ Mäusen ein höheres Verhältnis im Vergleich zu Kontrollmäusen beobachtet wurde. Die Färbung von Herzschnitten mit Wheat Germ Agglutining (WGA) zeigte eine Vergrößerung der Kardiomyozytenfläche bei ecPOR$^{-/-}$ Mäusen im Vergleich zu den Kontrollen. Diese Beobachtungen deuten darauf hin, dass die endotheliale Deletion von POR zu einer Restrukturierung des Herzens führt.

Um die zugrundeliegende Ursache im Knockout-Mausmodell besser zu verstehen, wurde eine RNA-Sequenzierung von kardialen ECs und dem restlichen Herzgewebe (linke Herzkammer) von ecPOR$^{-/-}$ und Kontrollmäusen durchgeführt. Nach der Deletion von POR wurde eine erhöhte Expression von Genen, die mit der Proteinsynthese assoziiert sind, wie z. B. Rpl und Rps, die für die Synthese der großen und kleinen ribosomalen Einheiten wichtig sind, in den kardialen ECs beobachtet. Trotz einer Hochregulierung von Genen, die mit der Proteinsynthese in Verbindung stehen, wurden Gene, die mit der Stressmaschinerie des Endoplasmatischen Retikulums in Verbindung stehen, in ecPOR$^{-/-}$ Mäusen herunterreguliert. Gene, die mit der kardialen Kontraktilität zusammenhängen, wie Myl4 (*myosin light chain 4*), Myl7 (*myosin light chain 7*) und Sln (*sarcolipin*), gehörten zu den 50 am stärksten hochregulierten Genen in der Kardiomyozytenfraktion des ecPOR$^{-/-}$ Mausherzens. Im ecPOR$^{-/-}$ Mausherz wurde eine Gensignatur für eine veränderte mitochondriale Funktion mit einer reduzierten Expression von Genen wie Nduf (*NADH:ubiquinone oxidoreductase subunits*), Sdhd (*succinate dehydrogenase complex subunit D*), Coq10b (*coenzyme Q*) und Cox (*cytochrome c oxidase*) beobachtet. Die RNA-Sequenzierungsdaten deuten darauf hin, dass die Deletion von POR in Endothelzellen

zu einer veränderten ribosomalen Biogenese und Proteinsynthese führen könnte, ohne eine Stressreaktion auszulösen, was die kardiale Kontraktilität in ecPOR$^{-/-}$ Mäusen beeinträchtigen könnte.

Um festzustellen, ob Plasmafettsäuren über ω-Hydroxylierung durch das endotheliale POR/CYP450-System oxidiert werden, bevor sie zur β-Oxidation in die Herzmuskelzellen gelangen, wurden die Metabolite des gesamten Herzgewebes auf Veränderungen hin untersucht. Nur 12 Metabolite waren in ecPOR$^{-/-}$ Herzgewebe im Vergleich zur Kontrolle signifikant verändert und diese Veränderungen konnten nicht mit der direkten enzymatischen Funktion von POR in Verbindung gebracht werden. Daher ist es unwahrscheinlich, dass das endotheliale POR/CYP450-System eine metabolische Funktion im Herzen hat.

Um festzustellen, ob das in ecPOR$^{-/-}$ Mäusen beobachtete kardiale Remodeling funktionelle Auswirkungen hat, wurden die Mäuse einer der aortalen Bändelung (*transverse aortic constriction*, TAC*)* unterzogen, was zu einer dramatischen Steigerung der Nachlast führt. Die Verengung wurde mit einem O-Ring mit einem Innendurchmesser von 0.50 mm vorgenommen, und die endotheliale Deletion von POR wurde durch intraperiotoneale Injektion von Tamoxifen induziert. An den Tagen 0 (vor TAC), 7, 14, 21, 28, 35, 42, 49, 56 und 61 nach der Operation durch die Herzfunktion mittels Echokardiographie bestimmt. Als Reaktion auf die TAC veränderten sich mehrere Parameter (verringerte Auswurffraktion, vergrößerte linke Herzkammer), wobei sich keine signifikante Unterschiede zwischen den Herzen der Kontroll- und ecPOR$^{-/-}$ Mäuse fanden. Im Gegensatz dazu waren das Herzzeitvolumen und das Schlagvolumen, Parameter für die Herzinsuffizienz, nach der endothelialen Deletion von POR signifikant reduziert. Die Kombination von TAC mit endothelialer Deletion von POR könnte somit einen beschleunigenden Effekt auf die Entwicklung der Herzinsuffizienz nach TAC haben.

Insgesamt deuten die Ergebnisse der vorliegenden Studie darauf hin, dass die endotheliale Deletion von POR zu einer erhöhten Gefäßsteifigkeit führt, die höchstwahrscheinlich auf eine Verringerung der vaskulären EETs in Verbindung mit einem geringeren Durchmesser der Karotiden in ecPOR$^{-/-}$ Mäusen zurückzuführen ist. Dies kann zu einem kardialen Remodeling mit erhöhter Expression von Genen führen, die mit der kardialen Kontraktilität zusammenhänge.

9 References

1. Degtyarenko KN, Archakov AI. Molecular evolution of P450 superfamily and P450-containing monooxygenase systems. *FEBS Letters*. 1993;332:1–8. doi: 10.1016/0014-5793(93)80470-f
2. Dorner ME, McMunn RD, Bartholow TG, Calhoon BE, Conlon MR, Dulli JM, Fehling SC, Fisher CR, Hodgson SW, Keenan SW, Kruger AN, Mabin JW, Mazula DL, Monte CA, Olthafer A, Sexton AE, Soderholm BR, Strom AM, Hati S. Comparison of intrinsic dynamics of cytochrome p450 proteins using normal mode analysis. *Protein Sci*. 2015;24:1495–1507. doi: 10.1002/pro.2737
3. Neve EPA, Ingelman-Sundberg M. Intracellular transport and localization of microsomal cytochrome P450. *Anal Bioanal Chem*. 2008;392:1075–1084. doi: 10.1007/s00216-008-2200-z
4. Danielson PB. The cytochrome P450 superfamily: biochemistry, evolution and drug metabolism in humans. *Curr Drug Metab*. 2002;3:561–597. doi: 10.2174/1389200023337054
5. Manikandan P, Nagini S. Cytochrome P450 Structure, Function and Clinical Significance: A Review. *Curr Drug Targets*. 2018;19:38–54. doi: 10.2174/1389450118666170125144557
6. Mansuy D. The great diversity of reactions catalyzed by cytochromes P450. *Comp Biochem Physiol C Pharmacol Toxicol Endocrinol*. 1998;121:5–14. doi: 10.1016/s0742-8413(98)10026-9
7. Sono M, Roach MP, Coulter ED, Dawson JH. Heme-Containing Oxygenases. *Chem Rev*. 1996;96:2841–2888. doi: 10.1021/cr9500500
8. Esteves F, Rueff J, Kranendonk M. The Central Role of Cytochrome P450 in Xenobiotic Metabolism-A Brief Review on a Fascinating Enzyme Family. *J Xenobiot*. 2021;11:94–114. doi: 10.3390/jox11030007
9. Zanger UM, Schwab M. Cytochrome P450 enzymes in drug metabolism: regulation of gene expression, enzyme activities, and impact of genetic variation. *Pharmacol Ther*. 2013;138:103–141. doi: 10.1016/j.pharmthera.2012.12.007
10. McDonnell AM, Dang CH. Basic review of the cytochrome p450 system. *J Adv Pract Oncol*. 2013;4:263–268. doi: 10.6004/jadpro.2013.4.4.7
11. Fleming I. Cytochrome p450 and vascular homeostasis. *Circ Res*. 2001;89:753–762. doi: 10.1161/hh2101.099268

12. Chaudhary KR, Batchu SN, Seubert JM. Cytochrome P450 enzymes and the heart. *IUBMB Life*. 2009;61:954–960. doi: 10.1002/iub.241
13. Wang B, Wu L, Chen J, Dong L, Chen C, Wen Z, Hu J, Fleming I, Wang DW. Metabolism pathways of arachidonic acids: mechanisms and potential therapeutic targets. *Signal Transduct Target Ther*. 2021;6:94. doi: 10.1038/s41392-020-00443-w
14. Hunter AL, Cruz RP, Cheyne BM, McManus BM, Granville DJ. Cytochrome p450 enzymes and cardiovascular disease. *Can J Physiol Pharmacol*. 2004;82:1053–1060. doi: 10.1139/y04-118
15. Nithipatikom K, Gross GJ. Review article: epoxyeicosatrienoic acids: novel mediators of cardioprotection. *J Cardiovasc Pharmacol Ther*. 2010;15:112–119. doi: 10.1177/1074248409358408
16. Peterson JA, Ebel RE, O'Keeffe DH, Matsubara T, Estabrook RW. Temperature dependence of cytochrome P-450 reduction. A model for NADPH-cytochrome P-450 reductase:cytochrome P-450 interaction. *Journal of Biological Chemistry*. 1976;251:4010–4016. doi: 10.1016/S0021-9258(17)33349-5
17. Pandey AV, Flück CE. NADPH P450 oxidoreductase: structure, function, and pathology of diseases. *Pharmacol Ther*. 2013;138:229–254. doi: 10.1016/j.pharmthera.2013.01.010
18. Wang M, Roberts DL, Paschke R, Shea TM, Masters BS, Kim JJ. Three-dimensional structure of NADPH-cytochrome P450 reductase: prototype for FMN- and FAD-containing enzymes. *Proc Natl Acad Sci U S A*. 1997;94:8411–8416. doi: 10.1073/pnas.94.16.8411
19. Mukherjee G, Nandekar PP, Wade RC. An electron transfer competent structural ensemble of membrane-bound cytochrome P450 1A1 and cytochrome P450 oxidoreductase. *Commun Biol*. 2021;4:55. doi: 10.1038/s42003-020-01568-y
20. Pandian BA, Sathishraj R, Djanaguiraman M, Prasad PVV, Jugulam M. Role of Cytochrome P450 Enzymes in Plant Stress Response. *Antioxidants (Basel)*. 2020;9. doi: 10.3390/antiox9050454
21. Hamdane D, Xia C, Im S-C, Zhang H, Kim J-JP, Waskell L. Structure and function of an NADPH-cytochrome P450 oxidoreductase in an open conformation capable of reducing cytochrome P450. *Journal of Biological Chemistry*. 2009;284:11374–11384. doi: 10.1074/jbc.M807868200

22. Gan L, Moltke LL von, Trepanier LA, Harmatz JS, Greenblatt DJ, Court MH. Role of NADPH-cytochrome P450 reductase and cytochrome-b5/NADH-b5 reductase in variability of CYP3A activity in human liver microsomes. *Drug Metab Dispos*. 2009;37:90–96. doi: 10.1124/dmd.108.023424
23. Kalluri AS, Vellarikkal SK, Edelman ER, Nguyen L, Subramanian A, Ellinor PT, Regev A, Kathiresan S, Gupta RM. Single-Cell Analysis of the Normal Mouse Aorta Reveals Functionally Distinct Endothelial Cell Populations. *Circulation*. 2019;140:147–163. doi: 10.1161/CIRCULATIONAHA.118.038362
24. Fang C, Gu J, Xie F, Behr M, Yang W, Abel ED, Ding X. Deletion of the NADPH-cytochrome P450 reductase gene in cardiomyocytes does not protect mice against doxorubicin-mediated acute cardiac toxicity. *Drug Metab Dispos*. 2008;36:1722–1728. doi: 10.1124/dmd.108.021881
25. Jabs EW, Lewanda AF. Craniosynostosis. In: *Craniosynostosis:* Elsevier, 2013:1–34
26. Otto DME, Henderson CJ, Carrie D, Davey M, Gundersen TE, Blomhoff R, Adams RH, Tickle C, Wolf CR. Identification of novel roles of the cytochrome p450 system in early embryogenesis: effects on vasculogenesis and retinoic Acid homeostasis. *Mol Cell Biol*. 2003;23:6103–6116. doi: 10.1128/MCB.23.17.6103-6116.2003
27. Shen AL, O'Leary KA, Kasper CB. Association of multiple developmental defects and embryonic lethality with loss of microsomal NADPH-cytochrome P450 oxidoreductase. *J Biol Chem*. 2002;277:6536–6541. doi: 10.1074/jbc.M111408200
28. Fukami M, Hasegawa T, Horikawa R, Ohashi T, Nishimura G, Homma K, Ogata T. Cytochrome P450 oxidoreductase deficiency in three patients initially regarded as having 21-hydroxylase deficiency and/or aromatase deficiency: diagnostic value of urine steroid hormone analysis. *Pediatr Res*. 2006;59:276–280. doi: 10.1203/01.pdr.0000195825.31504.28
29. Arlt W, Walker EA, Draper N, Ivison HE, Ride JP, Hammer F, Chalder SM, Borucka-Mankiewicz M, Hauffa BP, Malunowicz EM, Stewart PM, Shackleton CHL. Congenital adrenal hyperplasia caused by mutant P450 oxidoreductase and human androgen synthesis: analytical study. *Lancet*. 2004;363:2128–2135. doi: 10.1016/S0140-6736(04)16503-3
30. Huang N, Agrawal V, Giacomini KM, Miller WL. Genetics of P450 oxidoreductase: sequence variation in 842 individuals of four ethnicities and activities of 15

missense mutations. *Proc Natl Acad Sci U S A*. 2008;105:1733–1738. doi: 10.1073/pnas.0711621105

31. Kamat MA, Blackshaw JA, Young R, Surendran P, Burgess S, Danesh J, Butterworth AS, Staley JR. PhenoScanner V2: an expanded tool for searching human genotype-phenotype associations. *Bioinformatics*. 2019;35:4851–4853. doi: 10.1093/bioinformatics/btz469
32. Staley JR, Blackshaw J, Kamat MA, Ellis S, Surendran P, Sun BB, Paul DS, Freitag D, Burgess S, Danesh J, Young R, Butterworth AS. PhenoScanner: a database of human genotype-phenotype associations. *Bioinformatics*. 2016;32:3207–3209. doi: 10.1093/bioinformatics/btw373
33. Iyanagi T. Structure and function of NADPH-cytochrome P450 reductase and nitric oxide synthase reductase domain. *Biochem Biophys Res Commun*. 2005;338:520–528. doi: 10.1016/j.bbrc.2005.08.043
34. Nelson DR, Zeldin DC, Hoffman SMG, Maltais LJ, Wain HM, Nebert DW. Comparison of cytochrome P450 (CYP) genes from the mouse and human genomes, including nomenclature recommendations for genes, pseudogenes and alternative-splice variants. *Pharmacogenetics*. 2004;14:1–18. doi: 10.1097/00008571-200401000-00001
35. Gu J, Weng Y, Zhang Q-Y, Cui H, Behr M, Wu L, Yang W, Zhang L, Ding X. Liver-specific deletion of the NADPH-cytochrome P450 reductase gene: impact on plasma cholesterol homeostasis and the function and regulation of microsomal cytochrome P450 and heme oxygenase. *Journal of Biological Chemistry*. 2003;278:25895–25901. doi: 10.1074/jbc.M303125200
36. Fleming I. The pharmacology of the cytochrome P450 epoxygenase/soluble epoxide hydrolase axis in the vasculature and cardiovascular disease. *Pharmacol Rev*. 2014;66:1106–1140. doi: 10.1124/pr.113.007781
37. Riddick DS, Ding X, Wolf CR, Porter TD, Pandey AV, Zhang Q-Y, Gu J, Finn RD, Ronseaux S, McLaughlin LA, Henderson CJ, Zou L, Flück CE. NADPH-cytochrome P450 oxidoreductase: roles in physiology, pharmacology, and toxicology. *Drug Metab Dispos*. 2013;41:12–23. doi: 10.1124/dmd.112.048991
38. Albrecht EWJA, Stegeman CA, Heeringa P, Henning RH, van Goor H. Protective role of endothelial nitric oxide synthase. *J Pathol*. 2003;199:8–17. doi: 10.1002/path.1250

39. Goshi E, Zhou G, He Q. Nitric oxide detection methods in vitro and in vivo. *Med Gas Res*. 2019;9:192–207. doi: 10.4103/2045-9912.273957
40. Alderton WK, Cooper CE, Knowles RG. Nitric oxide synthases: structure, function and inhibition. *Biochem J*. 2001;357:593–615. doi: 10.1042/0264-6021:3570593
41. Huang PL. Endothelial nitric oxide synthase and endothelial dysfunction. *Curr Hypertens Rep*. 2003;5:473–480. doi: 10.1007/s11906-003-0055-4
42. Förstermann U, Münzel T. Endothelial nitric oxide synthase in vascular disease: from marvel to menace. *Circulation*. 2006;113:1708–1714. doi: 10.1161/CIRCULATIONAHA.105.602532
43. Förstermann U, Sessa WC. Nitric oxide synthases: regulation and function. *Eur Heart J*. 2012;33:829-37, 837a-837d. doi: 10.1093/eurheartj/ehr304
44. Fleming I, Busse R. Molecular mechanisms involved in the regulation of the endothelial nitric oxide synthase. *Am J Physiol Regul Integr Comp Physiol*. 2003;284:R1-12. doi: 10.1152/ajpregu.00323.2002
45. Govers R, Rabelink TJ. Cellular regulation of endothelial nitric oxide synthase. *Am J Physiol Renal Physiol*. 2001;280:F193-206. doi: 10.1152/ajprenal.2001.280.2.F193
46. Fleming I, Fisslthaler B, Dimmeler S, Kemp BE, Busse R. Phosphorylation of Thr(495) regulates Ca(2+)/calmodulin-dependent endothelial nitric oxide synthase activity. *Circ Res*. 2001;88:E68-75. doi: 10.1161/hh1101.092677
47. Siragusa M, Fleming I. The eNOS signalosome and its link to endothelial dysfunction. *Pflugers Arch*. 2016;468:1125–1137. doi: 10.1007/s00424-016-1839-0
48. Zhao Y, Vanhoutte PM, Leung SWS. Vascular nitric oxide: Beyond eNOS. *J Pharmacol Sci*. 2015;129:83–94. doi: 10.1016/j.jphs.2015.09.002
49. Harrison DG, Bates JN. The nitrovasodilators. New ideas about old drugs. *Circulation*. 1993;87:1461–1467. doi: 10.1161/01.CIR.87.5.1461
50. Fung HL, Chung SJ, Bauer JA, Chong S, Kowaluk EA. Biochemical mechanism of organic nitrate action. *Am J Cardiol*. 1992;70:4B-10B. doi: 10.1016/0002-9149(92)90588-P
51. Torfgård KE, Ahlner J. Mechanisms of action of nitrates. *Cardiovasc Drugs Ther*. 1994;8:701–717. doi: 10.1007/BF00877117

52. Divakaran S, Loscalzo J. The Role of Nitroglycerin and Other Nitrogen Oxides in Cardiovascular Therapeutics. *Journal of the American College of Cardiology*. 2017;70:2393–2410. doi: 10.1016/j.jacc.2017.09.1064
53. Lopez M, Malacarne PF, Gajos-Draus A, Ding X, Daiber A, Lundberg JO, Offermanns S, Brandes RP, Rezende F. Vascular biotransformation of organic nitrates is independent of cytochrome P450 monooxygenases. *Br J Pharmacol*. 2021;178:1495–1506. doi: 10.1111/bph.15362
54. van de Voorde J, Bogaert M. Basic Mechanisms of Action of Nitrovasodilators and Development of Tolerance to Organic Nitrates. In: Chang JB, ed. *Basic Mechanisms of Action of Nitrovasodilators and Development of Tolerance to Organic Nitrates.* New York, NY: Springer New York, 2000:122–131
55. Daiber A, Oelze M, Coldewey M, Bachschmid M, Wenzel P, Sydow K, Wendt M, Kleschyov AL, Stalleicken D, Ullrich V, Mülsch A, Münzel T. Oxidative stress and mitochondrial aldehyde dehydrogenase activity: a comparison of pentaerythritol tetranitrate with other organic nitrates. *Mol Pharmacol*. 2004;66:1372–1382. doi: 10.1124/mol.104.002600
56. Bennett BM, McDonald BJ, St James MJ. Hepatic cytochrome P-450-mediated activation of rat aortic guanylyl cyclase by glyceryl trinitrate. *J Pharmacol Exp Ther*. 1992;261:716–723
57. Mülsch A, Bara A, Mordvintcev P, Vanin A, Busse R. Specificity of different organic nitrates to elicit NO formation in rabbit vascular tissues and organs in vivo. *Br J Pharmacol*. 1995;116:2743–2749. doi: 10.1111/j.1476-5381.1995.tb17236.x
58. da Silva GM, da Silva MC, Nascimento DVG, Lima Silva EM, Gouvêa FFF, França Lopes LG de, Araújo AV, Ferraz Pereira KN, Queiroz TM de. Nitric Oxide as a Central Molecule in Hypertension: Focus on the Vasorelaxant Activity of New Nitric Oxide Donors. *Biology (Basel)*. 2021;10. doi: 10.3390/biology10101041
59. Morgado M, Cairrão E, Santos-Silva AJ, Verde I. Cyclic nucleotide-dependent relaxation pathways in vascular smooth muscle. *Cell Mol Life Sci*. 2012;69:247–266. doi: 10.1007/s00018-011-0815-2
60. Katzung BG, ed. *Basic & Clinical Pharmacology, 14e:* New York, NY: McGraw-Hill Education, 2017
61. Münzel T, Daiber A, Mülsch A. Explaining the phenomenon of nitrate tolerance. *Circ Res*. 2005;97:618–628. doi: 10.1161/01.RES.0000184694.03262.6d

62. Daiber A, Münzel T. Organic Nitrate Therapy, Nitrate Tolerance, and Nitrate-Induced Endothelial Dysfunction: Emphasis on Redox Biology and Oxidative Stress. *Antioxid Redox Signal*. 2015;23:899–942. doi: 10.1089/ars.2015.6376
63. Münzel T, Sayegh H, Freeman BA, Tarpey MM, Harrison DG. Evidence for enhanced vascular superoxide anion production in nitrate tolerance. A novel mechanism underlying tolerance and cross-tolerance. *J Clin Invest*. 1995;95:187–194. doi: 10.1172/JCI117637
64. Hink U, Oelze M, Kolb P, Bachschmid M, Zou M-H, Daiber A, Mollnau H, August M, Baldus S, Tsilimingas N, Walter U, Ullrich V, Münzel T. Role for peroxynitrite in the inhibition of prostacyclin synthase in nitrate tolerance. *Journal of the American College of Cardiology*. 2003;42:1826–1834. doi: 10.1016/j.jacc.2003.07.009
65. McVeigh GE, Hamilton P, Wilson M, Hanratty CG, Leahey WJ, Devine AB, Morgan DG, Dixon LJ, McGrath LT. Platelet nitric oxide and superoxide release during the development of nitrate tolerance: effect of supplemental ascorbate. *Circulation*. 2002;106:208–213. doi: 10.1161/01.cir.0000021600.84149.78
66. Sage PR, La Lande IS de, Stafford I, Bennett CL, Phillipov G, Stubberfield J, Horowitz JD. Nitroglycerin tolerance in human vessels: evidence for impaired nitroglycerin bioconversion. *Circulation*. 2000;102:2810–2815. doi: 10.1161/01.cir.102.23.2810
67. Sayed N, Baskaran P, Ma X, van den Akker F, Beuve A. Desensitization of soluble guanylyl cyclase, the NO receptor, by S-nitrosylation. *Proc Natl Acad Sci U S A*. 2007;104:12312–12317. doi: 10.1073/pnas.0703944104
68. Oelze M, Knorr M, Kröller-Schön S, Kossmann S, Gottschlich A, Rümmler R, Schuff A, Daub S, Doppler C, Kleinert H, Gori T, Daiber A, Münzel T. Chronic therapy with isosorbide-5-mononitrate causes endothelial dysfunction, oxidative stress, and a marked increase in vascular endothelin-1 expression. *Eur Heart J*. 2013;34:3206–3216. doi: 10.1093/eurheartj/ehs100
69. Gori T, Parker JD. Nitrate tolerance: a unifying hypothesis. *Circulation*. 2002;106:2510–2513. doi: 10.1161/01.cir.0000036743.07406.53
70. Sekiya M, Sato M, Funada J, Ohtani T, Akutsu H, Watanabe K. Effects of the long-term administration of nicorandil on vascular endothelial function and the progression of arteriosclerosis. *J Cardiovasc Pharmacol*. 2005;46:63–67. doi: 10.1097/01.fjc.0000162771.00174.a8

71. Thomas GR, DiFabio JM, Gori T, Parker JD. Once daily therapy with isosorbide-5-mononitrate causes endothelial dysfunction in humans: evidence of a free-radical-mediated mechanism. *Journal of the American College of Cardiology*. 2007;49:1289–1295. doi: 10.1016/j.jacc.2006.10.074
72. Daiber A, Wenzel P, Oelze M, Münzel T. New insights into bioactivation of organic nitrates, nitrate tolerance and cross-tolerance. *Clin Res Cardiol*. 2008;97:12–20. doi: 10.1007/s00392-007-0588-7
73. Chen Z, Zhang J, Stamler JS. Identification of the enzymatic mechanism of nitroglycerin bioactivation. *Proc Natl Acad Sci U S A*. 2002;99:8306–8311. doi: 10.1073/pnas.122225199
74. Chen Z, Foster MW, Zhang J, Mao L, Rockman HA, Kawamoto T, Kitagawa K, Nakayama KI, Hess DT, Stamler JS. An essential role for mitochondrial aldehyde dehydrogenase in nitroglycerin bioactivation. *Proc Natl Acad Sci U S A*. 2005;102:12159–12164. doi: 10.1073/pnas.0503723102
75. Wenzel P, Hink U, Oelze M, Seeling A, Isse T, Bruns K, Steinhoff L, Brandt M, Kleschyov AL, Schulz E, Lange K, Weiner H, Lehmann J, Lackner KJ, Kawamoto T, Münzel T, Daiber A. Number of nitrate groups determines reactivity and potency of organic nitrates: a proof of concept study in ALDH-2 −/− mice. *Br J Pharmacol*. 2007;150:526–533. doi: 10.1038/sj.bjp.0707116
76. Mackenzie IS, Maki-Petaja KM, McEniery CM, Bao YP, Wallace SM, Cheriyan J, Monteith S, Brown MJ, Wilkinson IB. Aldehyde dehydrogenase 2 plays a role in the bioactivation of nitroglycerin in humans. *Arterioscler Thromb Vasc Biol*. 2005;25:1891–1895. doi: 10.1161/01.ATV.0000179599.71086.89
77. Bennett BM, McDonald BJ, Nigam R, Craig Simon W. Biotransformation of organic nitrates and vascular smooth muscle cell function. *Trends in Pharmacological Sciences*. 1994;15:245–249. doi: 10.1016/0165-6147(94)90319-0
78. McDonald BJ, Bennett BM. Cytochrome P-450 mediated biotransformation of organic nitrates. *Can J Physiol Pharmacol*. 1990;68:1552–1557. doi: 10.1139/y90-236
79. Schröder H. Cytochrome P-450 mediates bioactivation of organic nitrates. *J Pharmacol Exp Ther*. 1992;262:298–302
80. Servent D, Delaforge M, Ducrocq C, Mansuy D, Lenfant M. Nitric oxide formation during microsomal hepatic denitration of glyceryl trinitrate: Involvement of

cytochrome P-450. *Biochem Biophys Res Commun*. 1989;163:1210–1216. doi: 10.1016/0006-291X(89)91106-6

81. Minamiyama Y, Takemura S, Akiyama T, Imaoka S, Inoue M, Funae Y, Okada S. Isoforms of cytochrome P450 on organic nitrate-derived nitric oxide release in human heart vessels. *FEBS Letters*. 1999;452:165–169. doi: 10.1016/S0014-5793(99)00612-2
82. Perbellini F, Watson SA, Bardi I, Terracciano CM. Heterocellularity and Cellular Cross-Talk in the Cardiovascular System. *Front Cardiovasc Med*. 2018;5:143. doi: 10.3389/fcvm.2018.00143
83. Talman V, Kivelä R. Cardiomyocyte-Endothelial Cell Interactions in Cardiac Remodeling and Regeneration. *Front Cardiovasc Med*. 2018;5:101. doi: 10.3389/fcvm.2018.00101
84. Kivelä R, Hemanthakumar KA, Vaparanta K, Robciuc M, Izumiya Y, Kidoya H, Takakura N, Peng X, Sawyer DB, Elenius K, Walsh K, Alitalo K. Endothelial Cells Regulate Physiological Cardiomyocyte Growth via VEGFR2-Mediated Paracrine Signaling. *Circulation*. 2019;139:2570–2584. doi: 10.1161/CIRCULATIONAHA.118.036099
85. Colliva A, Braga L, Giacca M, Zacchigna S. Endothelial cell-cardiomyocyte crosstalk in heart development and disease. *The Journal of Physiology*. 2020;598:2923–2939. doi: 10.1113/JP276758
86. Brindle NPJ, Saharinen P, Alitalo K. Signaling and functions of angiopoietin-1 in vascular protection. *Circ Res*. 2006;98:1014–1023. doi: 10.1161/01.RES.0000218275.54089.12
87. Arita Y, Nakaoka Y, Matsunaga T, Kidoya H, Yamamizu K, Arima Y, Kataoka-Hashimoto T, Ikeoka K, Yasui T, Masaki T, Yamamoto K, Higuchi K, Park J-S, Shirai M, Nishiyama K, Yamagishi H, Otsu K, Kurihara H, Minami T, Yamauchi-Takihara K, Koh GY, Mochizuki N, Takakura N, Sakata Y, Yamashita JK, Komuro I. Myocardium-derived angiopoietin-1 is essential for coronary vein formation in the developing heart. *Nat Commun*. 2014;5:4552. doi: 10.1038/ncomms5552
88. Wu Y-S, Zhu B, Luo A-L, Yang L, Yang C. The Role of Cardiokines in Heart Diseases: Beneficial or Detrimental? *Biomed Res Int*. 2018;2018:8207058. doi: 10.1155/2018/8207058

89. Hedhli N, Huang Q, Kalinowski A, Palmeri M, Hu X, Russell RR, Russell KS. Endothelium-derived neuregulin protects the heart against ischemic injury. *Circulation*. 2011;123:2254–2262. doi: 10.1161/CIRCULATIONAHA.110.991125
90. Tallima H, El Ridi R. Arachidonic acid: Physiological roles and potential health benefits - A review. *J Adv Res*. 2018;11:33–41. doi: 10.1016/j.jare.2017.11.004
91. Sonnweber T, Pizzini A, Nairz M, Weiss G, Tancevski I. Arachidonic Acid Metabolites in Cardiovascular and Metabolic Diseases. *Int J Mol Sci*. 2018;19. doi: 10.3390/ijms19113285
92. Hanna VS, Hafez EAA. Synopsis of arachidonic acid metabolism: A review. *J Adv Res*. 2018;11:23–32. doi: 10.1016/j.jare.2018.03.005
93. Hoopes SL, Garcia V, Edin ML, Schwartzman ML, Zeldin DC. Vascular actions of 20-HETE. *Prostaglandins Other Lipid Mediat*. 2015;120:9–16. doi: 10.1016/j.prostaglandins.2015.03.002
94. Campbell WB, Fleming I. Epoxyeicosatrienoic acids and endothelium-dependent responses. *Pflugers Arch*. 2010;459:881–895. doi: 10.1007/s00424-010-0804-6
95. Zeldin DC. Epoxygenase pathways of arachidonic acid metabolism. *Journal of Biological Chemistry*. 2001;276:36059–36062. doi: 10.1074/jbc.R100030200
96. Barbosa-Sicard E, Kaergel E, Muller DN, Honeck H, Luft FC, Schunck W-H. Cytochrome P450 Isoform Expression in Human Vascular Endothelial Cells. *Hypertension*. 2000;36:698. doi: 10.1161/hyp.36.suppl_1.698-a
97. Roman RJ. P-450 metabolites of arachidonic acid in the control of cardiovascular function. *Physiol Rev*. 2002;82:131–185. doi: 10.1152/physrev.00021.2001
98. Spector AA, Norris AW. Action of epoxyeicosatrienoic acids on cellular function. *Am J Physiol Cell Physiol*. 2007;292:C996-1012. doi: 10.1152/ajpcell.00402.2006
99. Sudhahar V, Shaw S, Imig JD. Epoxyeicosatrienoic acid analogs and vascular function. *Curr Med Chem*. 2010;17:1181–1190. doi: 10.2174/092986710790827843
100. Spector AA, Fang X, Snyder GD, Weintraub NL. Epoxyeicosatrienoic acids (EETs): metabolism and biochemical function. *Prog Lipid Res*. 2004;43:55–90. doi: 10.1016/S0163-7827(03)00049-3
101. Fleming I. The factor in EDHF: Cytochrome P450 derived lipid mediators and vascular signaling. *Vascul Pharmacol*. 2016;86:31–40. doi: 10.1016/j.vph.2016.03.001

102. Pfister SL, Gauthier KM, Campbell WB. Vascular pharmacology of epoxyeicosatrienoic acids. *Adv Pharmacol*. 2010;60:27–59. doi: 10.1016/B978-0-12-385061-4.00002-7

103. Yang L, Mäki-Petäjä K, Cheriyan J, McEniery C, Wilkinson IB. The role of epoxyeicosatrienoic acids in the cardiovascular system. *Br J Clin Pharmacol*. 2015;80:28–44. doi: 10.1111/bcp.12603

104. Xiao Y-F, Ke Q, Seubert JM, Bradbury JA, Graves J, Degraff LM, Falck JR, Krausz K, Gelboin HV, Morgan JP, Zeldin DC. Enhancement of cardiac L-type Ca2+ currents in transgenic mice with cardiac-specific overexpression of CYP2J2. *Mol Pharmacol*. 2004;66:1607–1616. doi: 10.1124/mol.104.004150

105. Lu T, Ye D, Wang X, Seubert JM, Graves JP, Bradbury JA, Zeldin DC, Lee H-C. Cardiac and vascular KATP channels in rats are activated by endogenous epoxyeicosatrienoic acids through different mechanisms. *The Journal of Physiology*. 2006;575:627–644. doi: 10.1113/jphysiol.2006.113985

106. Seubert J, Yang B, Bradbury JA, Graves J, Degraff LM, Gabel S, Gooch R, Foley J, Newman J, Mao L, Rockman HA, Hammock BD, Murphy E, Zeldin DC. Enhanced postischemic functional recovery in CYP2J2 transgenic hearts involves mitochondrial ATP-sensitive K+ channels and p42/p44 MAPK pathway. *Circ Res*. 2004;95:506–514. doi: 10.1161/01.RES.0000139436.89654.c8

107. Lai J, Chen C. The Role of Epoxyeicosatrienoic Acids in Cardiac Remodeling. *Front Physiol*. 2021;12:642470. doi: 10.3389/fphys.2021.642470

108. Qiu H, Li N, Liu J-Y, Harris TR, Hammock BD, Chiamvimonvat N. Soluble epoxide hydrolase inhibitors and heart failure. *Cardiovasc Ther*. 2011;29:99–111. doi: 10.1111/j.1755-5922.2010.00150.x

109. Edin ML, Wang Z, Bradbury JA, Graves JP, Lih FB, Degraff LM, Foley JF, Torphy R, Ronnekleiv OK, Tomer KB, Lee CR, Zeldin DC. Endothelial expression of human cytochrome P450 epoxygenase CYP2C8 increases susceptibility to ischemia-reperfusion injury in isolated mouse heart. *FASEB J*. 2011;25:3436–3447. doi: 10.1096/fj.11-188300

110. Oni-Orisan A, Alsaleh N, Lee CR, Seubert JM. Epoxyeicosatrienoic acids and cardioprotection: the road to translation. *J Mol Cell Cardiol*. 2014;74:199–208. doi: 10.1016/j.yjmcc.2014.05.016

111. Rocic P, Schwartzman ML. 20-HETE in the regulation of vascular and cardiac function. *Pharmacol Ther*. 2018;192:74–87. doi: 10.1016/j.pharmthera.2018.07.004

112. Thadani U. Challenges with nitrate therapy and nitrate tolerance: prevalence, prevention, and clinical relevance. *Am J Cardiovasc Drugs*. 2014;14:287–301. doi: 10.1007/s40256-014-0072-5

113. Hu J, Dziumbla S, Lin J, Bibli S-I, Zukunft S, Mos J de, Awwad K, Frömel T, Jungmann A, Devraj K, Cheng Z, Wang L, Fauser S, Eberhart CG, Sodhi A, Hammock BD, Liebner S, Müller OJ, Glaubitz C, Hammes H-P, Popp R, Fleming I. Inhibition of soluble epoxide hydrolase prevents diabetic retinopathy. *Nature*. 2017;552:248–252. doi: 10.1038/nature25013

114. Hu J, Geyer A, Dziumbla S, Awwad K, Zeldin DC, Schunck W-H, Popp R, Frömel T, Fleming I. Role of Müller cell cytochrome P450 2c44 in murine retinal angiogenesis. *Prostaglandins Other Lipid Mediat*. 2017;133:93–102. doi: 10.1016/j.prostaglandins.2017.04.002

115. Wu L, Gu J, Weng Y, Kluetzman K, Swiatek P, Behr M, Zhang Q-Y, Zhuo X, Xie Q, Ding X. Conditional knockout of the mouse NADPH-cytochrome p450 reductase gene. *Genesis*. 2003;36:177–181. doi: 10.1002/gene.10214

116. Wirth A, Benyó Z, Lukasova M, Leutgeb B, Wettschureck N, Gorbey S, Orsy P, Horváth B, Maser-Gluth C, Greiner E, Lemmer B, Schütz G, Gutkind JS, Offermanns S. G12-G13-LARG-mediated signaling in vascular smooth muscle is required for salt-induced hypertension. *Nat Med*. 2008;14:64–68. doi: 10.1038/nm1666

117. Malacarne PF, Ratiu C, Gajos-Draus A, Müller N, Lopez M, Pflüger-Müller B, Ding X, Warwick T, Oo J, Siragusa M, Angioni C, Günther S, Weigert A, Geißlinger G, Lütjohann D, Schunck W-H, Fleming I, Brandes RP, Rezende F. Loss of Endothelial Cytochrome P450 Reductase Induces Vascular Dysfunction in Mice. *Hypertension*. 2022;79:1216–1226. doi: 10.1161/HYPERTENSIONAHA.121.18752

118. Wang Y, Nakayama M, Pitulescu ME, Schmidt TS, Bochenek ML, Sakakibara A, Adams S, Davy A, Deutsch U, Lüthi U, Barberis A, Benjamin LE, Mäkinen T, Nobes CD, Adams RH. Ephrin-B2 controls VEGF-induced angiogenesis and lymphangiogenesis. *Nature*. 2010;465:483–486. doi: 10.1038/nature09002

119. Rockman HA, Ross RS, Harris AN, Knowlton KU, Steinhelper ME, Field LJ, Ross J, Chien KR. Segregation of atrial-specific and inducible expression of an atrial natriuretic factor transgene in an in vivo murine model of cardiac hypertrophy. *Proc Natl Acad Sci U S A*. 1991;88:8277–8281. doi: 10.1073/pnas.88.18.8277

120. deAlmeida AC, van Oort RJ, Wehrens XHT. Transverse aortic constriction in mice. *J Vis Exp*. 2010. doi: 10.3791/1729

121. Melleby AO, Romaine A, Aronsen JM, Veras I, Zhang L, Sjaastad I, Lunde IG, Christensen G. A novel method for high precision aortic constriction that allows for generation of specific cardiac phenotypes in mice. *Cardiovasc Res*. 2018;114:1680–1690. doi: 10.1093/cvr/cvy141

122. Lopez M, Malacarne PF, Ramanujam DP, Warwick T, Müller N, Hu J, Dewenter M, Weigert A, Günther S, Gilsbach R, Engelhardt S, Brandes RP, Rezende F. Endothelial deletion of the cytochrome P450 reductase leads to cardiac remodelling. *Front. Physiol.* 2022;13. doi: 10.3389/fphys.2022.1056369

123. Aitken RJ. Nitroblue tetrazolium (NBT) assay. *Reprod Biomed Online*. 2018;36:90–91. doi: 10.1016/j.rbmo.2017.09.005

124. Rezende F, Prior K-K, Löwe O, Wittig I, Strecker V, Moll F, Helfinger V, Schnütgen F, Kurrle N, Wempe F, Walter M, Zukunft S, Luck B, Fleming I, Weissmann N, Brandes RP, Schröder K. Cytochrome P450 enzymes but not NADPH oxidases are the source of the NADPH-dependent lucigenin chemiluminescence in membrane assays. *Free Radic Biol Med*. 2017;102:57–66. doi: 10.1016/j.freeradbiomed.2016.11.019

125. Auclair C, Torres M, Hakim J. Superoxide anion involvement in NBT reduction catalyzed by nadph-cytochrome P -450 reductase: A pitfall. *FEBS Letters*. 1978;89:26–28. doi: 10.1016/0014-5793(78)80514-6

126. Jespersen B, Tykocki NR, Watts SW, Cobbett PJ. Measurement of smooth muscle function in the isolated tissue bath-applications to pharmacology research. *J Vis Exp*. 2015:52324. doi: 10.3791/52324

127. Chan JKC. The wonderful colors of the hematoxylin-eosin stain in diagnostic surgical pathology. *Int J Surg Pathol*. 2014;22:12–32. doi: 10.1177/1066896913517939

128. Monsigny M, Roche AC, Sene C, Maget-Dana R, Delmotte F. Sugar-lectin interactions: how does wheat-germ agglutinin bind sialoglycoconjugates? *Eur J Biochem*. 1980;104:147–153. doi: 10.1111/j.1432-1033.1980.tb04410.x

129. Ramanujam D, Schön AP, Beck C, Vaccarello P, Felician G, Dueck A, Esfandyari D, Meister G, Meitinger T, Schulz C, Engelhardt S. MicroRNA-21-Dependent Macrophage-to-Fibroblast Signaling Determines the Cardiac Response to Pressure Overload. *Circulation*. 2021;143:1513–1525. doi: 10.1161/CIRCULATIONAHA.120.050682

130. Andrews Simon. FastQC: a quality control tool for high throughput sequence data. http://www.bioinformatics.babraham.ac.uk/projects/fastqc

131. Al-Khelaifi F, Diboun I, Donati F, Botrè F, Alsayrafi M, Georgakopoulos C, Suhre K, Yousri NA, Elrayess MA. A pilot study comparing the metabolic profiles of elite-level athletes from different sporting disciplines. *Sports Med Open*. 2018;4:2. doi: 10.1186/s40798-017-0114-z

132. Evans AM, DeHaven CD, Barrett T, Mitchell M, Milgram E. Integrated, nontargeted ultrahigh performance liquid chromatography/electrospray ionization tandem mass spectrometry platform for the identification and relative quantification of the small-molecule complement of biological systems. *Anal Chem*. 2009;81:6656–6667. doi: 10.1021/ac901536h

133. Bridgewater BR E am. High Resolution Mass Spectrometry Improves Data Quantity and Quality as Compared to Unit Mass Resolution Mass Spectrometry in High-Throughput Profiling Metabolomics. *Metabolomics*. 2014;04. doi: 10.4172/2153-0769.1000132

134. Howe KL, Contreras-Moreira B, Silva N de, Maslen G, Akanni W, Allen J, Alvarez-Jarreta J, Barba M, Bolser DM, Cambell L, Carbajo M, Chakiachvili M, Christensen M, Cummins C, Cuzick A, Davis P, Fexova S, Gall A, George N, Gil L, Gupta P, Hammond-Kosack KE, Haskell E, Hunt SE, Jaiswal P, Janacek SH, Kersey PJ, Langridge N, Maheswari U, Maurel T, McDowall MD, Moore B, Muffato M, Naamati G, Naithani S, Olson A, Papatheodorou I, Patricio M, Paulini M, Pedro H, Perry E, Preece J, Rosello M, Russell M, Sitnik V, Staines DM, Stein J, Tello-Ruiz MK, Trevanion SJ, Urban M, Wei S, Ware D, Williams G, Yates AD, Flicek P. Ensembl Genomes 2020-enabling non-vertebrate genomic research. *Nucleic Acids Res*. 2020;48:D689-D695. doi: 10.1093/nar/gkz890

135. Patro R, Duggal G, Love MI, Irizarry RA, Kingsford C. Salmon provides fast and bias-aware quantification of transcript expression. *Nat Methods*. 2017;14:417–419. doi: 10.1038/nmeth.4197

136. Love MI, Huber W, Anders S. Moderated estimation of fold change and dispersion for RNA-seq data with DESeq2. *Genome Biol*. 2014;15:550. doi: 10.1186/s13059-014-0550-8

137. R Core Team. R: A language and environment for statistical computing. R Foundation for Statistical Computing, Vienna, Austria

138. Chen EY, Tan CM, Kou Y, Duan Q, Wang Z, Meirelles GV, Clark NR, Ma'ayan A. Enrichr: interactive and collaborative HTML5 gene list enrichment analysis tool. *BMC Bioinformatics*. 2013;14:128. doi: 10.1186/1471-2105-14-128

139. Kuleshov MV, Jones MR, Rouillard AD, Fernandez NF, Duan Q, Wang Z, Koplev S, Jenkins SL, Jagodnik KM, Lachmann A, McDermott MG, Monteiro CD, Gundersen GW, Ma'ayan A. Enrichr: a comprehensive gene set enrichment analysis web server 2016 update. *Nucleic Acids Res*. 2016;44:W90-7. doi: 10.1093/nar/gkw377

140. Xie Z, Bailey A, Kuleshov MV, Clarke DJB, Evangelista JE, Jenkins SL, Lachmann A, Wojciechowicz ML, Kropiwnicki E, Jagodnik KM, Jeon M, Ma'ayan A. Gene Set Knowledge Discovery with Enrichr. *Curr Protoc*. 2021;1:e90. doi: 10.1002/cpz1.90

141. DeHaven CD, Evans AM, Dai H, Lawton Kai A. Software Techniques for Enabling High-Throughput Analysis of Metabolomic Datasets. In: Roessner U, ed. *Software Techniques for Enabling High-Throughput Analysis of Metabolomic Datasets.* [Erscheinungsort nicht ermittelbar]: InTech, 2012

142. Katsuki S, Arnold W, Mittal C, Murad F. Stimulation of guanylate cyclase by sodium nitroprusside, nitroglycerin and nitric oxide in various tissue preparations and comparison to the effects of sodium azide and hydroxylamine. *J Cyclic Nucleotide Res*. 1977;3:23–35

143. Single-cell transcriptomics of 20 mouse organs creates a Tabula Muris. *Nature*. 2018;562:367–372. doi: 10.1038/s41586-018-0590-4

144. Schenkman JB, Wilson BJ, Cinti DL. Diethylaminoethyl 2,2-diphenylvalerate HCl (SKF 525-A)—In vivo and in vitro effects of metabolism by rat liver microsomes—Formation of an oxygenated complex. *Biochem Pharmacol*. 1972;21:2373–2383. doi: 10.1016/0006-2952(72)90389-9

145. Crewe HK, Notley LM, Wunsch RM, Lennard MS, Gillam EMJ. Metabolism of tamoxifen by recombinant human cytochrome P450 enzymes: formation of the 4-hydroxy, 4'-hydroxy and N-desmethyl metabolites and isomerization of trans-4-hydroxytamoxifen. *Drug Metab Dispos*. 2002;30:869–874. doi: 10.1124/dmd.30.8.869

146. Leloup AJA, van Hove CE, Moudt S de, Meyer GRY de, Keulenaer GW de, Fransen P. Vascular smooth muscle cell contraction and relaxation in the isolated aorta: a critical regulator of large artery compliance. *Physiol Rep*. 2019;7:e13934. doi: 10.14814/phy2.13934

147. Wong MS-K, Vanhoutte PM. COX-mediated endothelium-dependent contractions: from the past to recent discoveries. *Acta Pharmacol Sin*. 2010;31:1095–1102. doi: 10.1038/aps.2010.127

148. Toblli JE, DiGennaro F, Giani JF, Dominici FP. Nebivolol: impact on cardiac and endothelial function and clinical utility. *Vasc Health Risk Manag*. 2012;8:151–160. doi: 10.2147/VHRM.S20669

149. Ramanujam D, Sassi Y, Laggerbauer B, Engelhardt S. Viral Vector-Based Targeting of miR-21 in Cardiac Nonmyocyte Cells Reduces Pathologic Remodeling of the Heart. *Mol Ther*. 2016;24:1939–1948. doi: 10.1038/mt.2016.166

150. Hinkel R, Ramanujam D, Kaczmarek V, Howe A, Klett K, Beck C, Dueck A, Thum T, Laugwitz K-L, Maegdefessel L, Weber C, Kupatt C, Engelhardt S. AntimiR-21 Prevents Myocardial Dysfunction in a Pig Model of Ischemia/Reperfusion Injury. *Journal of the American College of Cardiology*. 2020;75:1788–1800. doi: 10.1016/j.jacc.2020.02.041

151. Hardwick JP. Cytochrome P450 omega hydroxylase (CYP4) function in fatty acid metabolism and metabolic diseases. *Biochem Pharmacol*. 2008;75:2263–2275. doi: 10.1016/j.bcp.2008.03.004

152. Lepesheva GI, Hargrove TY, Kleshchenko Y, Nes WD, Villalta F, Waterman MR. CYP51: A major drug target in the cytochrome P450 superfamily. *Lipids*. 2008;43:1117–1125. doi: 10.1007/s11745-008-3225-y

153. Chuang SS, Helvig C, Taimi M, Ramshaw HA, Collop AH, Amad M, White JA, Petkovich M, Jones G, Korczak B. CYP2U1, a novel human thymus- and brain-specific cytochrome P450, catalyzes omega- and (omega-1)-hydroxylation of fatty acids. *J Biol Chem*. 2004;279:6305–6314. doi: 10.1074/jbc.M311830200

154. Preissner SC, Hoffmann MF, Preissner R, Dunkel M, Gewiess A, Preissner S. Polymorphic cytochrome P450 enzymes (CYPs) and their role in personalized therapy. *PLoS One*. 2013;8:e82562. doi: 10.1371/journal.pone.0082562

155. Nebert DW, Wikvall K, Miller WL. Human cytochromes P450 in health and disease. *Philos Trans R Soc Lond B Biol Sci*. 2013;368:20120431. doi: 10.1098/rstb.2012.0431

156. Doevendans P. Cardiovascular phenotyping in mice. *Cardiovasc Res*. 1998;39:34–49. doi: 10.1016/S0008-6363(98)00073-X

157. Azevedo PS, Polegato BF, Minicucci MF, Paiva SAR, Zornoff LAM. Cardiac Remodeling: Concepts, Clinical Impact, Pathophysiological Mechanisms and Pharmacologic Treatment. *Arq Bras Cardiol*. 2016;106:62–69. doi: 10.5935/abc.20160005

158. Shaik S, Pandey H, Thirumalasetti SK, Nakamura N. Characteristics and Functions of the Yip1 Domain Family (YIPF), Multi-Span Transmembrane Proteins Mainly Localized to the Golgi Apparatus. *Front Cell Dev Biol*. 2019;7:130. doi: 10.3389/fcell.2019.00130

159. Mahoney SJ, Dempsey JM, Blenis J. Chapter 2 Cell Signaling in Protein Synthesis. In: Hershey JWB, ed. *Chapter 2 Cell Signaling in Protein Synthesis.* Amsterdam, Boston: Elsevier/Academic Press, 2009:53–107

160. Guan B-J, Krokowski D, Majumder M, Schmotzer CL, Kimball SR, Merrick WC, Koromilas AE, Hatzoglou M. Translational control during endoplasmic reticulum stress beyond phosphorylation of the translation initiation factor eIF2α. *J Biol Chem*. 2014;289:12593–12611. doi: 10.1074/jbc.M113.543215

161. Morano M, Zacharzowski U, Maier M, Lange PE, Alexi-Meskishvili V, Haase H, Morano I. Regulation of human heart contractility by essential myosin light chain isoforms. *J Clin Invest*. 1996;98:467–473. doi: 10.1172/JCI118813

162. Sun D, Ojaimi C, Wu H, Kaley G, an Huang. CYP2C29 produces superoxide in response to shear stress. *Microcirculation*. 2012;19:696–704. doi: 10.1111/j.1549-8719.2012.00202.x

163. Kubli DA, Quinsay MN, Huang C, Lee Y, Gustafsson AB. Bnip3 functions as a mitochondrial sensor of oxidative stress during myocardial ischemia and reperfusion. *Am J Physiol Heart Circ Physiol*. 2008;295:H2025-31. doi: 10.1152/ajpheart.00552.2008

164. Fu Y, Wang X, Zhang L, Ren Y, Hao L. Allograft inflammatory factor-1 enhances inflammation and oxidative stress via the NF-κB pathway in diabetic kidney disease. *Biochem Biophys Res Commun*. 2022;614:63–69. doi: 10.1016/j.bbrc.2022.04.089

165. Kokoszka JE, Coskun P, Esposito LA, Wallace DC. Increased mitochondrial oxidative stress in the Sod2 (+/-) mouse results in the age-related decline of mitochondrial function culminating in increased apoptosis. *Proc Natl Acad Sci U S A*. 2001;98:2278–2283. doi: 10.1073/pnas.051627098

166. Taylor J, Fischer A. Endothelial cells dictate cardiac fuel source. *Aging (Albany NY)*. 2019;11:1083–1084. doi: 10.18532/aging.101825

167. Abumrad NA, Cabodevilla AG, Samovski D, Pietka T, Basu D, Goldberg IJ. Endothelial Cell Receptors in Tissue Lipid Uptake and Metabolism. *Circ Res*. 2021;128:433–450. doi: 10.1161/CIRCRESAHA.120.318003

168. Gross GJ, Hsu A, Falck JR, Nithipatikom K. Mechanisms by which epoxyeicosatrienoic acids (EETs) elicit cardioprotection in rat hearts. *J Mol Cell Cardiol*. 2007;42:687–691. doi: 10.1016/j.yjmcc.2006.11.020

169. Taegtmeyer H, Sen S, Vela D. Return to the fetal gene program: a suggested metabolic link to gene expression in the heart. *Ann N Y Acad Sci*. 2010;1188:191–198. doi: 10.1111/j.1749-6632.2009.05100.x

170. Jabs M, Rose AJ, Lehmann LH, Taylor J, Moll I, Sijmonsma TP, Herberich SE, Sauer SW, Poschet G, Federico G, Mogler C, Weis E-M, Augustin HG, Yan M, Gretz N, Schmid RM, Adams RH, Gröne H-J, Hell R, Okun JG, Backs J, Nawroth PP, Herzig S, Fischer A. Inhibition of Endothelial Notch Signaling Impairs Fatty Acid Transport and Leads to Metabolic and Vascular Remodeling of the Adult Heart. *Circulation*. 2018;137:2592–2608. doi: 10.1161/CIRCULATIONAHA.117.029733

171. Minamiyama Y, Imaoka S, Takemura S, Okada S, Inoue M, Funae Y. Escape from tolerance of organic nitrate by induction of cytochrome P450. *Free Radical Biology and Medicine*. 2001;31:1498–1508. doi: 10.1016/S0891-5849(01)00733-X

172. Minamiyama Y, Takemura S, Yamasaki K, Hai S, Hirohashi K, Funae Y, Okada S. Continuous administration of organic nitrate decreases hepatic cytochrome P450. *J Pharmacol Exp Ther*. 2004;308:729–735. doi: 10.1124/jpet.103.057877

173. Feelisch M, Kelm M. Biotransformation of organic nitrates to nitric oxide by vascular smooth muscle and endothelial cells. *Biochem Biophys Res Commun*. 1991;180:286–293. doi: 10.1016/S0006-291X(05)81290-2

174. Suk-Jae C, Ho-Leung F. Relationship between nitroglycerin-induced vascular relaxation and nitric oxide production. *Biochem Pharmacol*. 1993;45:157–163. doi: 10.1016/0006-2952(93)90388-D

175. McDonald BJ, Bennett BM. Biotransformation of glyceryl trinitrate by rat aortic cytochrome P450. *Biochem Pharmacol*. 1993;45:268–270. doi: 10.1016/0006-2952(93)90403-J

176. Beretta M, Wölkart G, Schernthaner M, Griesberger M, Neubauer R, Schmidt K, Sacherer M, Heinzel FR, Kohlwein SD, Mayer B. Vascular bioactivation of nitroglycerin is catalyzed by cytosolic aldehyde dehydrogenase-2. *Circ Res*. 2012;110:385–393. doi: 10.1161/CIRCRESAHA.111.245837

177. Opelt M, Eroglu E, Waldeck-Weiermair M, Russwurm M, Koesling D, Malli R, Graier WF, Fassett JT, Schrammel A, Mayer B. Formation of Nitric Oxide by Aldehyde Dehydrogenase-2 Is Necessary and Sufficient for Vascular Bioactivation of Nitroglycerin. *J Biol Chem*. 2016;291:24076–24084. doi: 10.1074/jbc.M116.752071

178. Griesberger M, Kollau A, Wölkart G, Wenzl MV, Beretta M, Russwurm M, Koesling D, Schmidt K, Gorren ACF, Mayer B. Bioactivation of pentaerythrityl tetranitrate by mitochondrial aldehyde dehydrogenase. *Mol Pharmacol*. 2011;79:541–548. doi: 10.1124/mol.110.069138

179. McGuire JJ, Anderson DJ, McDonald BJ, Narayanasami R, Bennett BM. Inhibition of NADPH-cytochrome P450 reductase and glyceryl trinitrate biotransformation by diphenyleneiodonium sulfate. *Biochem Pharmacol*. 1998;56:881–893. doi: 10.1016/s0006-2952(98)00216-0

180. Govoni M, Tocchetti P, Lundberg JO. Metabolism and pathways for denitration of organic nitrates in the human liver. *J Pharmacol Exp Ther*. 2013;346:96–104. doi: 10.1124/jpet.113.203356

181. Kim-Shapiro DB, Schechter AN, Gladwin MT. Unraveling the reactions of nitric oxide, nitrite, and hemoglobin in physiology and therapeutics. *Arterioscler Thromb Vasc Biol*. 2006;26:697–705. doi: 10.1161/01.ATV.0000204350.44226.9a

182. Lundberg JO, Weitzberg E. Nitric oxide signaling in health and disease. *Cell*. 2022;185:2853–2878. doi: 10.1016/j.cell.2022.06.010

183. Cosby K, Partovi KS, Crawford JH, Patel RP, Reiter CD, Martyr S, Yang BK, Waclawiw MA, Zalos G, Xu X, Huang KT, Shields H, Kim-Shapiro DB, Schechter AN, Cannon RO, Gladwin MT. Nitrite reduction to nitric oxide by deoxyhemoglobin vasodilates the human circulation. *Nat Med*. 2003;9:1498–1505. doi: 10.1038/nm954

184. Dejam A, Hunter CJ, Pelletier MM, Hsu LL, Machado RF, Shiva S, Power GG, Kelm M, Gladwin MT, Schechter AN. Erythrocytes are the major intravascular storage sites of nitrite in human blood. *Blood*. 2005;106:734–739. doi: 10.1182/blood-2005-02-0567

185. Goswami T, Jasti B, Li X. Sublingual drug delivery. *Crit Rev Ther Drug Carrier Syst*. 2008;25:449–484. doi: 10.1615/critrevtherdrugcarriersyst.v25.i5.20

186. Wishart DS, Knox C, Guo AC, Cheng D, Shrivastava S, Tzur D, Gautam B, Hassanali M. DrugBank: a knowledgebase for drugs, drug actions and drug targets. *Nucleic Acids Res*. 2008;36:D901-6. doi: 10.1093/nar/gkm958

187. Wishart DS, Feunang YD, Guo AC, Lo EJ, Marcu A, Grant JR, Sajed T, Johnson D, Li C, Sayeeda Z, Assempour N, Iynkkaran I, Liu Y, Maciejewski A, Gale N, Wilson A, Chin L, Cummings R, Le D, Pon A, Knox C, Wilson M. DrugBank 5.0: a major update to the DrugBank database for 2018. *Nucleic Acids Res*. 2018;46:D1074-D1082. doi: 10.1093/nar/gkx1037

188. Law V, Knox C, Djoumbou Y, Jewison T, Guo AC, Liu Y, Maciejewski A, Arndt D, Wilson M, Neveu V, Tang A, Gabriel G, Ly C, Adamjee S, Dame ZT, Han B, Zhou Y, Wishart DS. DrugBank 4.0: shedding new light on drug metabolism. *Nucleic Acids Res*. 2014;42:D1091-7. doi: 10.1093/nar/gkt1068

189. Knox C, Law V, Jewison T, Liu P, Ly S, Frolkis A, Pon A, Banco K, Mak C, Neveu V, Djoumbou Y, Eisner R, Guo AC, Wishart DS. DrugBank 3.0: a comprehensive resource for 'omics' research on drugs. *Nucleic Acids Res*. 2011;39:D1035-41. doi: 10.1093/nar/gkq1126

190. Wishart DS, Knox C, Guo AC, Shrivastava S, Hassanali M, Stothard P, Chang Z, Woolsey J. DrugBank: a comprehensive resource for in silico drug discovery and exploration. *Nucleic Acids Res*. 2006;34:D668-72. doi: 10.1093/nar/gkj067

191. Mülsch A, Busse R, Bassenge E. Desensitization of guanylate cyclase in nitrate tolerance does not impair endothelium-dependent responses. *European Journal of Pharmacology*. 1988;158:191–198. doi: 10.1016/0014-2999(88)90066-0

192. Molina CR, Andresen JW, Rapoport RM, Waldman S, Murad F. Effect of in vivo nitroglycerin therapy on endothelium-dependent and independent vascular relaxation and cyclic GMP accumulation in rat aorta. *J Cardiovasc Pharmacol*. 1987;10:371–378. doi: 10.1097/00005344-198710000-00001

193. Axelsson KL, Andersson RG. Tolerance towards nitroglycerin, induced in vivo, is correlated to a reduced cGMP response and an alteration in cGMP turnover. *European Journal of Pharmacology*. 1983;88:71–79. doi: 10.1016/0014-2999(83)90393-X

194. Sydow K, Daiber A, Oelze M, Chen Z, August M, Wendt M, Ullrich V, Mülsch A, Schulz E, Keaney JF, Stamler JS, Münzel T. Central role of mitochondrial aldehyde dehydrogenase and reactive oxygen species in nitroglycerin tolerance and cross-tolerance. *J Clin Invest*. 2004;113:482–489. doi: 10.1172/JCI19267

195. Ignarro LJ, Napoli C, Loscalzo J. Nitric oxide donors and cardiovascular agents modulating the bioactivity of nitric oxide: an overview. *Circ Res*. 2002;90:21–28. doi: 10.1161/hh0102.102330

196. Minamiyama Y, Takemura S, Nishino Y, Okada S. Organic nitrate tolerance is induced by degradation of some cytochrome P450 isoforms. *Redox Rep*. 2002;7:339–342. doi: 10.1179/135100002125000947

197. Thum T, Borlak J. Gene expression in distinct regions of the heart. *The Lancet*. 2000;355:979–983. doi: 10.1016/S0140-6736(00)99016-0

198. Choudhary D, Jansson I, Schenkman JB, Sarfarazi M, Stoilov I. Comparative expression profiling of 40 mouse cytochrome P450 genes in embryonic and adult tissues. *Archives of Biochemistry and Biophysics*. 2003;414:91–100. doi: 10.1016/s0003-9861(03)00174-7

199. Nithipatikom K, Gross ER, Endsley MP, Moore JM, Isbell MA, Falck JR, Campbell WB, Gross GJ. Inhibition of cytochrome P450omega-hydroxylase: a novel endogenous cardioprotective pathway. *Circ Res*. 2004;95:e65-71. doi: 10.1161/01.RES.0000146277.62128.6f

200. Lu T, Hoshi T, Weintraub NL, Spector AA, Lee HC. Activation of ATP-sensitive K(+) channels by epoxyeicosatrienoic acids in rat cardiac ventricular myocytes. *The Journal of Physiology*. 2001;537:811–827. doi: 10.1111/j.1469-7793.2001.00811.x

201. Cazade M, Bidaud I, Hansen PB, Lory P, Chemin J. 5,6-EET potently inhibits T-type calcium channels: implication in the regulation of the vascular tone. *Pflugers Arch*. 2014;466:1759–1768. doi: 10.1007/s00424-013-1411-0

202. Xu D, Li N, He Y, Timofeyev V, Lu L, Tsai H-J, Kim I-H, Tuteja D, Mateo RKP, Singapuri A, Davis BB, Low R, Hammock BD, Chiamvimonvat N. Prevention and reversal of cardiac hypertrophy by soluble epoxide hydrolase inhibitors. *Proc Natl Acad Sci U S A*. 2006;103:18733–18738. doi: 10.1073/pnas.0609158103

203. Wanders RJA, Komen J, Kemp S. Fatty acid omega-oxidation as a rescue pathway for fatty acid oxidation disorders in humans. *FEBS J*. 2011;278:182–194. doi: 10.1111/j.1742-4658.2010.07947.x

204. Mehrotra D, Wu J, Papangeli I, Chun HJ. Endothelium as a gatekeeper of fatty acid transport. *Trends Endocrinol Metab*. 2014;25:99–106. doi: 10.1016/j.tem.2013.11.001

205. Son N-H, Basu D, Samovski D, Pietka TA, Peche VS, Willecke F, Fang X, Yu S-Q, Scerbo D, Chang HR, Sun F, Bagdasarov S, Drosatos K, Yeh ST, Mullick AE, Shoghi KI, Gumaste N, Kim K, Huggins L-A, Lhakhang T, Abumrad NA, Goldberg IJ. Endothelial cell CD36 optimizes tissue fatty acid uptake. *J Clin Invest;*128:4329–4342. doi: 10.1172/JCI99315

206. Ibrahim A, Yucel N, Kim B, Arany Z. Local Mitochondrial ATP Production Regulates Endothelial Fatty Acid Uptake and Transport. *Cell Metab*. 2020;32:309-319.e7. doi: 10.1016/j.cmet.2020.05.018

207. Hagberg CE, Falkevall A, Wang X, Larsson E, Huusko J, Nilsson I, van Meeteren LA, Samen E, Lu L, Vanwildemeersch M, Klar J, Genove G, Pietras K, Stone-Elander S, Claesson-Welsh L, Ylä-Herttuala S, Lindahl P, Eriksson U. Vascular endothelial growth factor B controls endothelial fatty acid uptake. *Nature*. 2010;464:917–921. doi: 10.1038/nature08945

208. Bisaccia G, Ricci F, Gallina S, Di Baldassarre A, Ghinassi B. Mitochondrial Dysfunction and Heart Disease: Critical Appraisal of an Overlooked Association. *Int J Mol Sci*. 2021;22. doi: 10.3390/ijms22020614

209. Cohn JN, Ferrari R, Sharpe N. Cardiac remodeling—concepts and clinical implications: a consensus paper from an international forum on cardiac remodeling. *Journal of the American College of Cardiology*. 2000;35:569–582. doi: 10.1016/S0735-1097(99)00630-0

210. Schwarz DS, Blower MD. The endoplasmic reticulum: structure, function and response to cellular signaling. *Cell Mol Life Sci*. 2016;73:79–94. doi: 10.1007/s00018-015-2052-6

211. Barnaba C, Martinez MJ, Taylor E, Barden AO, Brozik JA. Single-Protein Tracking Reveals That NADPH Mediates the Insertion of Cytochrome P450 Reductase into a Biomimetic of the Endoplasmic Reticulum. *J Am Chem Soc*. 2017;139:5420–5430. doi: 10.1021/jacs.7b00663

212. Negishi M, Fujii-Kuriyama Y, Tashiro Y, Imai Y. Site of biosynthesis of cytochrome P450 in hepatocytes of phenobarbital treated rats. *Biochem Biophys Res Commun*. 1976;71:1153–1160. doi: 10.1016/0006-291X(76)90774-9

213. Almanza A, Carlesso A, Chintha C, Creedican S, Doultsinos D, Leuzzi B, Luís A, McCarthy N, Montibeller L, More S, Papaioannou A, Püschel F, Sassano ML, Skoko J, Agostinis P, Belleroche J de, Eriksson LA, Fulda S, Gorman AM, Healy S, Kozlov A, Muñoz-Pinedo C, Rehm M, Chevet E, Samali A. Endoplasmic reticulum stress signalling - from basic mechanisms to clinical applications. *FEBS J*. 2019;286:241–278. doi: 10.1111/febs.14608

214. Bertolotti A, Zhang Y, Hendershot LM, Harding HP, Ron D. Dynamic interaction of BiP and ER stress transducers in the unfolded-protein response. *Nat Cell Biol*. 2000;2:326–332. doi: 10.1038/35014014

215. Shen J, Chen X, Hendershot L, Prywes R. ER stress regulation of ATF6 localization by dissociation of BiP/GRP78 binding and unmasking of Golgi localization signals. *Dev Cell*. 2002;3:99–111. doi: 10.1016/s1534-5807(02)00203-4

216. Travers KJ, Patil CK, Wodicka L, Lockhart DJ, Weissman JS, Walter P. Functional and genomic analyses reveal an essential coordination between the unfolded protein response and ER-associated degradation. *Cell*. 2000;101:249–258. doi: 10.1016/s0092-8674(00)80835-1

217. Iwakoshi NN, Lee A-H, Glimcher LH. The X-box binding protein-1 transcription factor is required for plasma cell differentiation and the unfolded protein response. *Immunol Rev*. 2003;194:29–38. doi: 10.1034/j.1600-065x.2003.00057.x

218. Schaub MC, Tuchschmid CR, Srihari T, Hirzel HO. Myosin isoenzymes in human hypertrophic hearts. Shift in atrial myosin heavy chains and in ventricular myosin light chains. *Eur Heart J*. 1984;5 Suppl F:85–93. doi: 10.1093/eurheartj/5.suppl_f.85

219. Schaub MC, Hefti MA, Zuellig RA, Morano I. Modulation of contractility in human cardiac hypertrophy by myosin essential light chain isoforms. *Cardiovasc Res*. 1998;37:381–404. doi: 10.1016/S0008-6363(97)00258-7

220. Ritter O, Bottez N, Burkard N, Schulte HD, Neyses L. A molecular mechanism improving the contractile state in human myocardial hypertrophy. *Exp Clin Cardiol*. 2002;7:151–157

221. Babu GJ, Bhupathy P, Petrashevskaya NN, Wang H, Raman S, Wheeler D, Jagatheesan G, Wieczorek D, Schwartz A, Janssen PML, Ziolo MT, Periasamy M. Targeted overexpression of sarcolipin in the mouse heart decreases sarcoplasmic reticulum calcium transport and cardiac contractility. *Journal of Biological Chemistry*. 2006;281:3972–3979. doi: 10.1074/jbc.M508998200

222. Babu GJ, Zheng Z, Natarajan P, Wheeler D, Janssen PM, Periasamy M. Overexpression of sarcolipin decreases myocyte contractility and calcium transient. *Cardiovasc Res*. 2005;65:177–186. doi: 10.1016/j.cardiores.2004.08.012

223. MacLennan DH, Asahi M, Tupling AR. The regulation of SERCA-type pumps by phospholamban and sarcolipin. *Ann N Y Acad Sci*. 2003;986:472–480. doi: 10.1111/j.1749-6632.2003.tb07231.x

224. Pashmforoush M, Lu JT, Chen H, Amand TS, Kondo R, Pradervand S, Evans SM, Clark B, Feramisco JR, Giles W, Ho SY, Benson DW, Silberbach M, Shou W, Chien KR. Nkx2-5 pathways and congenital heart disease; loss of ventricular myocyte lineage specification leads to progressive cardiomyopathy and complete heart block. *Cell*. 2004;117:373–386. doi: 10.1016/s0092-8674(04)00405-2

225. Lacolley P, Regnault V, Laurent S. Mechanisms of Arterial Stiffening: From Mechanotransduction to Epigenetics. *Arterioscler Thromb Vasc Biol*. 2020;40:1055–1062. doi: 10.1161/ATVBAHA.119.313129

226. DeLoach SS, Townsend RR. Vascular stiffness: its measurement and significance for epidemiologic and outcome studies. *Clin J Am Soc Nephrol*. 2008;3:184–192. doi: 10.2215/CJN.03340807

10 Abbreviations

Table 21. List of abbreviations

Symbol	Name
11,12-EET	11,12-epoxyeicosatrienoic acid
14,15-EET	14,15-epoxyeicosatrienoic acid
20-HETE	20-hydroxyeicosatetraenoic acid
5,6-EET	5,6-epoxyeicosatrienoic acid
8,9-EET	8,9-epoxyeicosatrienoic acid
AA	Arachidonic acid
ABS	Antley-Bixler syndrome
ACTA2	α-smooth muscle actin
ALC1	Atrial light chain-1
ALDH2	Mitochondrial aldehyde dehydrogenase 2
Ang1	Angiopoietin-1
ATP	Adenosine triphosphate
BKCa	Large conductance calcium-activated potassium channel
Ca^{2+}	Calcium
CF	Cardiac fibroblast
cGMP	Cyclic GMP
CM	Cardiomyocyte
CoA	Coenzyme A
COX	Cyclooxygenase
CTL	Control
CYP450	Cytochrome P450
$Cytb_5$	Cytochrome b5
DHETE	Dihydroxyeicosatetraenoic acid
EC	Endothelial cell
EC_{50}	Half maximal effective concentration
$ecPOR^{-/-}$	Endothelial cell specific knockout of POR
EDHF	Endothelium-dependent hyperpolariing factor
EET	Epoxyeicosatrienoic acid
EGF	Epidermal growth factor
eNOS	Endothelial nitric oxide synthase

ER	Endoplasmic reticulum
ERK1/2	Extracellular signal-regulated kinase
ET-1	Endothelin-1
ET_B	Endothelin B receptor
FAD	Flavin adenine dinucleotide
FATP	Fatty acid transport protein
FMN	Flavin mononucleotide
H&E	Hematoxylin & eosin
HETE	Hydroxyeicosarrienoic acid
HO	Hemeoxygenase
IK	Intermediate-conductance calcium-dependent potassium channel
IR	Ischemia-reperfusion
ISDN	Isosorbide dinitrate
ISMN	Isosorbide mononitrate
K^+	Potassium
LEC	Lung endothelial cell
LOX	Lipooxygenase
LV	Left ventrcile
MI	Myocardial infarction
MLCK	Myosin light chain kinase
MLCP	Myosin light chain phosphatase
NADPH	Nicotinamide adenine dinucleotide phosphate
NO	Nitric oxide
NO_2^-	Nitrite
NOA	Nitric oxide analyser
NOS	Nitric oxide synthase
NRG-1	Neuregulin-1
NTG	Nitroglycerin
ORAB	O-ring aortic banding
PETN	Pentaerythritol tetranitrate
PKA	Protein kinase A
PKC	Protein kinase C
PKG	Protein kinase G

PLA2	Phospholipase A2
POR	Cytochrome P450 reductase
$POR^{-/-}$	Global deletion of POR
PORD	POR deficiency
PP1	Protein phosphatase 1
PUFA	Polyunsaturated fatty acid
RFL-6	Fibroblast derived from fetal rat lung
ROS	Reactive oxygene species
sEH	Soluble epoxide hydrolase
sGC	Soluble guanylyl cyclase
SK	Small condutance calcium-dependent potassium channel
SLN	Sarcolipin
SMC	Smooth muscle cell
$smcPOR^{-/-}$	Smooth muscle cell specific knockout of POR
SNP	Single nucleotide polymorphism
SR	Sarcoplasmic reticulum
TAC	Transverse aortic constriction
TLR4	Toll-like repcetor 4
TNF-α	Tumor necrosis factor α
TRPV4	Transient receptor potential channel
UPR	Unfolded protein response
VEGF	Vascular growth factor
VEGFR2	Vascular growth factor receptor 2
VSMC	Vascular smooth muscle cell
WB	Western blotting
WGA	Wheat germ agglutinin

11 List of figures

12 List of Tables

13 Appendix

13.1 Supplementary data

13.1.1 Differentially expressed genes RNA-sequencing analysis ecPOR

Table 22. DEGs CTL vs ecPOR$^{-/-}$; p-value ≤ 0.05; 24 up-regulated DEGs in cardiac ECs

Gene ID	Symbol	log2FoldChange	p-value
ENSMUSG00000028825	Rhd	1.751	3.77E-02
ENSMUSG00000011254	Thg1l	1.237	3.98E-03
ENSMUSG00000090733	Rps27	1.007	2.96E-01
ENSMUSG00000028029	Aimp1	0.636	2.19E-03
ENSMUSG00000049960	Mrps16	0.587	8.25E-01
ENSMUSG00000035202	Lars2	0.537	7.87E-03
ENSMUSG00000024713	Pcsk5	0.522	1.48E-02
ENSMUSG00000038900	Rpl12	0.499	1.25E-02
ENSMUSG00000032518	Rpsa	0.475	3.60E-01
ENSMUSG00000058006	Mdn1	0.458	1.26E-02
ENSMUSG00000074129	Rpl13a	0.458	3.99E-05
ENSMUSG00000028234	Rps20	0.420	1.13E-01
ENSMUSG00000009927	Rps25	0.410	6.71E-01
ENSMUSG00000046364	Rpl27a	0.395	1.52E-02
ENSMUSG00000036698	Ago2	0.351	4.67E-02
ENSMUSG00000039001	Rps21	0.348	7.00E-01
ENSMUSG00000073702	Rpl31	0.320	1.39E-02
ENSMUSG00000058600	Rpl30	0.294	1.79E-02
ENSMUSG00000047215	Rpl9	0.288	1.40E-02
ENSMUSG00000008682	Rpl10	0.254	1.59E-02
ENSMUSG00000000740	Rpl13	0.245	4.46E-02
ENSMUSG00000060938	Rpl26	0.243	3.43E-02
ENSMUSG00000062647	Rpl7a	0.223	3.35E-02
ENSMUSG00000012405	Rpl15	0.215	4.86E-02

Table 23. DEGs CTL vs ecPOR$^{-/-}$; p-value ≤ 0.05; 28 down-regulated DEGs in cardiac ECs

Gene ID	Symbol	log2FoldChange	p-value
ENSMUSG00000029657	Hsph1	-1.371	6.45E-05
ENSMUSG00000025757	Hspa4l	-1.277	1.89E-08
ENSMUSG00000063524	Eno1	-0.929	1.66E-05
ENSMUSG00000007659	Bcl2l1	-0.631	2.05E-03

ENSMUSG00000038074	Fkbp14	-0.557	1.99E-03
ENSMUSG00000023944	Hsp90ab1	-0.454	5.02E-03
ENSMUSG00000044337	Ackr3	-0.451	9.06E-03
ENSMUSG00000051675	Trim32	-0.434	1.70E-02
ENSMUSG00000056952	Tatdn2	-0.428	4.01E-02
ENSMUSG00000031770	Herpud1	-0.422	1.34E-02
ENSMUSG00000025980	Hspd1	-0.422	4.19E-04
ENSMUSG00000015656	Hspa8	-0.416	3.35E-02
ENSMUSG00000028410	Dnaja1	-0.397	1.55E-02
ENSMUSG00000051495	Irf2bp2	-0.390	2.11E-02
ENSMUSG00000068039	Tcp1	-0.363	1.57E-03
ENSMUSG00000007476	Lrrc8a	-0.347	1.89E-02
ENSMUSG00000024807	Syvn1	-0.340	7.15E-04
ENSMUSG00000020484	Xbp1	-0.307	1.74E-02
ENSMUSG00000038084	Opa1	-0.298	3.09E-02
ENSMUSG00000024777	Ppp2r5b	-0.297	9.73E-04
ENSMUSG00000007739	Cct4	-0.290	1.59E-02
ENSMUSG00000026864	Hspa5	-0.283	4.63E-02
ENSMUSG00000025613	Cct8	-0.280	2.14E-02
ENSMUSG00000022234	Cct5	-0.273	1.62E-02
ENSMUSG00000032553	Srprb	-0.272	3.91E-02
ENSMUSG00000026203	Dnajb2	-0.266	3.86E-02
ENSMUSG00000030894	Tpp1	-0.230	9.71E-03
ENSMUSG00000009291	Pttg1ip	-0.184	2.26E-02

Table 24. DEGs CTL vs ecPOR$^{-/-}$; p-value ≤ 0.05; 34 up-regulated DEGs in left ventricle

Gene ID	Symbol	log2FoldChange	p-value
ENSMUSG00000042045	Sln	13.182	5.20E-08
ENSMUSG00000022878	Adipoq	3.377	7.19E-03
ENSMUSG00000041220	Elovl6	2.223	3.92E-02
ENSMUSG00000022868	Ahsg	2.138	3.21E-03
ENSMUSG00000039145	Camk1d	1.652	8.08E-03
ENSMUSG00000063952	Brpf3	1.445	1.93E-03
ENSMUSG00000026833	Olfm1	1.348	1.83E-03
ENSMUSG00000026833	Olfm1	1.348	1.83E-03
ENSMUSG00000031488	Rab11fip1	1.316	4.00E-02
ENSMUSG00000020914	Top2a	1.205	3.24E-02

ENSMUSG00000020532	Acaca	1.029	8.25E-03
ENSMUSG00000050556	Kcnb1	0.921	2.55E-02
ENSMUSG00000056427	Slit3	0.896	1.75E-02
ENSMUSG00000047414	Flrt2	0.857	7.56E-03
ENSMUSG00000031636	Pdlim3	0.809	4.63E-02
ENSMUSG00000045312	Lhfpl2	0.610	4.30E-03
ENSMUSG00000032380	Dapk2	0.609	3.71E-02
ENSMUSG00000026193	Fn1	0.604	6.70E-03
ENSMUSG00000048583	Igf2	0.599	4.85E-02
ENSMUSG00000033685	Ucp2	0.592	2.88E-02
ENSMUSG00000023067	Cdkn1a	0.568	2.10E-02
ENSMUSG00000050295	Foxc1	0.568	4.52E-02
ENSMUSG00000020917	Acly	0.496	2.72E-02
ENSMUSG00000028456	Unc13b	0.486	2.42E-02
ENSMUSG00000015143	Actn1	0.478	2.71E-02
ENSMUSG00000027962	Vcam1	0.469	2.45E-02
ENSMUSG00000020644	Id2	0.434	4.62E-02
ENSMUSG00000040289	Hey1	0.348	1.78E-02
ENSMUSG00000064210	Ano6	0.307	1.50E-02
ENSMUSG00000076431	Sox4	0.297	1.47E-02
ENSMUSG00000054808	Actn4	0.252	1.27E-02
ENSMUSG00000075254	Heg1	0.249	1.97E-02
ENSMUSG00000030342	Cd9	0.245	4.90E-02

Table 25. DEGs CTL vs ecPOR$^{-/-}$; p-value ≤ 0.05; 46 down-regulated DEGs in left ventricle

Gene ID	Symbol	log2FoldChange	p-value
ENSMUSG00000037772	Mrpl23	-0.418	2.53E-02
ENSMUSG00000022551	Cyc1	-0.403	1.57E-02
ENSMUSG00000019863	Qrsl1	-0.387	6.23E-03
ENSMUSG00000037152	Ndufc1	-0.379	2.05E-02
ENSMUSG00000020153	Ndufs7	-0.364	9.66E-03
ENSMUSG00000030037	Mrpl53	-0.356	2.73E-02
ENSMUSG00000034932	Mrpl54	-0.345	3.80E-02
ENSMUSG00000036860	Mrpl55	-0.343	1.96E-02
ENSMUSG00000022820	Ndufb4	-0.343	4.24E-02
ENSMUSG00000071014	Ndufb6	-0.336	3.62E-02
ENSMUSG00000028648	Ndufs5	-0.336	2.45E-02

ENSMUSG00000023089	Ndufa5	-0.336	1.75E-02
ENSMUSG00000020514	Mrpl22	-0.336	3.20E-02
ENSMUSG00000002416	Ndufb2	-0.334	4.72E-02
ENSMUSG00000059534	Uqcr10	-0.332	1.83E-02
ENSMUSG00000017778	Cox7c	-0.326	2.32E-02
ENSMUSG00000026895	Ndufa8	-0.322	2.19E-02
ENSMUSG00000038880	Mrps34	-0.318	3.49E-02
ENSMUSG00000071654	Uqcc3	-0.315	4.76E-02
ENSMUSG00000063882	Uqcrh	-0.314	2.33E-02
ENSMUSG00000021606	Ndufs6	-0.314	2.45E-02
ENSMUSG00000000088	Cox5a	-0.313	2.66E-02
ENSMUSG00000002379	Ndufa11	-0.307	4.19E-02
ENSMUSG00000038462	Uqcrfs1	-0.304	1.27E-02
ENSMUSG00000022354	Ndufb9	-0.302	3.55E-02
ENSMUSG00000026032	Ndufb3	-0.297	2.03E-02
ENSMUSG00000020163	Uqcr11	-0.297	3.70E-02
ENSMUSG00000005510	Ndufs3	-0.295	2.17E-02
ENSMUSG00000040048	Ndufb10	-0.293	3.54E-02
ENSMUSG00000014313	Cox6c	-0.292	4.03E-02
ENSMUSG00000030869	Ndufab1	-0.292	4.93E-02
ENSMUSG00000039640	Mrpl12	-0.289	2.90E-02
ENSMUSG00000041881	Ndufa7	-0.285	4.57E-02
ENSMUSG00000057388	Mrpl18	-0.282	3.41E-02
ENSMUSG00000030647	Ndufc2	-0.279	4.86E-02
ENSMUSG00000031818	Cox4i1	-0.279	4.23E-02
ENSMUSG00000004610	Etfb	-0.278	3.79E-02
ENSMUSG00000090247	Bloc1s1	-0.278	4.52E-02
ENSMUSG00000036199	Ndufa13	-0.277	3.25E-02
ENSMUSG00000046756	Mrps7	-0.276	4.90E-02
ENSMUSG00000037916	Ndufv1	-0.276	3.17E-02
ENSMUSG00000021520	Uqcrb	-0.244	4.73E-02
ENSMUSG00000013593	Ndufs2	-0.240	2.79E-02
ENSMUSG00000060679	Mrps9	-0.231	4.55E-02
ENSMUSG00000000171	Sdhd	-0.226	4.03E-02
ENSMUSG00000022437	Samm50	-0.223	3.65E-02

13.1.2 Differentially expressed genes associated to oxidative stress (GO:0006979) ecPOR

Table 26. DEGs CTL vs ecPOR$^{-/-}$; p-value ≤ 0.05; 29 up- and down-regulated DEGs associated to oxidative stress in cardiac ECs

Gene ID	Symbol	log2FoldChange	p-value
ENSMUSG00000031616	Ednra	2.072	4.12E-04
ENSMUSG00000030641	Ddias	1.820	1.41E-02
ENSMUSG00000026204	Ptprn	1.462	4.13E-02
ENSMUSG00000054580	Pla2r1	1.451	2.62E-02
ENSMUSG00000024087	Cyp1b1	1.256	7.06E-03
ENSMUSG00000011254	Thg1l	1.237	3.98E-03
ENSMUSG00000024620	Pdgfrb	1.003	3.37E-03
ENSMUSG00000033871	Ppargc1b	0.829	4.71E-03
ENSMUSG00000026674	Ddr2	0.812	1.95E-02
ENSMUSG00000055633	Zfp580	0.709	4.63E-02
ENSMUSG00000021944	Gata4	0.636	8.96E-03
ENSMUSG00000021215	Net1	0.604	3.91E-03
ENSMUSG00000056394	Lig1	0.583	2.27E-02
ENSMUSG00000021936	Mapk8	0.544	2.72E-04
ENSMUSG00000029231	Pdgfra	0.509	3.03E-02
ENSMUSG00000022292	Rrm2b	0.466	1.88E-02
ENSMUSG00000005981	Trap1	-0.196	2.34E-02
ENSMUSG00000005312	Ubqln1	-0.224	2.83E-02
ENSMUSG00000004936	Map2k1	-0.227	3.18E-02
ENSMUSG00000002147	Stat6	-0.230	8.49E-03
ENSMUSG00000078566	Bnip3	-0.290	2.04E-02
ENSMUSG00000020484	Xbp1	-0.307	1.74E-02
ENSMUSG00000022574	Naprt	-0.467	2.99E-02
ENSMUSG00000019889	Ptprk	-0.548	2.54E-03
ENSMUSG00000021559	Dapk1	-0.874	4.07E-04
ENSMUSG00000030786	Itgam	-0.960	3.53E-02
ENSMUSG00000024397	Aif1	-1.116	4.41E-02
ENSMUSG00000029657	Hsph1	-1.371	6.45E-05
ENSMUSG00000032942	Ucp3	-2.877	2.11E-03

Table 27. DEGs CTL vs ecPOR$^{-/-}$; p-value ≤ 0.05; 18 up- and down-regulated DEGs associated to oxidative stress in lef ventricle

Gene ID	Symbol	log2FoldChange	p-value
ENSMUSG00000033685	Ucp2	0.592	2.88E-02
ENSMUSG00000021215	Net1	0.570	8.40E-03
ENSMUSG00000057133	Chd6	0.473	4.53E-02
ENSMUSG00000028484	Psip1	0.312	3.89E-02
ENSMUSG00000029428	Stx2	0.256	3.74E-02
ENSMUSG00000013593	Ndufs2	-0.240	2.79E-02
ENSMUSG00000029433	Diablo	-0.240	4.36E-02
ENSMUSG00000060803	Gstp1	-0.262	4.36E-02
ENSMUSG00000005161	Prdx2	-0.269	4.53E-02
ENSMUSG00000063358	Mapk1	-0.291	1.58E-02
ENSMUSG00000024789	Jak2	-0.302	1.53E-02
ENSMUSG00000078566	Bnip3	-0.310	1.34E-02
ENSMUSG00000022820	Ndufb4	-0.343	4.24E-02
ENSMUSG00000002731	Prkra	-0.345	2.14E-02
ENSMUSG00000024927	Rela	-0.374	2.26E-03
ENSMUSG00000067847	Romo1	-0.385	2.60E-02
ENSMUSG00000006818	Sod2	-0.591	9.91E-03
ENSMUSG00000022556	Hsf1	-8.798	2.35E-03

Table 28. Statistically significant metabolites identified in ecPOR$^{-/-}$ by UPLC-MS/MS; p-value ≤ 0.05; 12 up- and down-regulated in cardiac tissue

Metabolite	Sub pathway	log2FoldChange	p-value
1-(1-enyl-palmitoyl)-2-oleoyl-GPE (P-16:0/18:1)*	Plasmalogen	-1.010	1.31E-02
1-docosahexaenoylglycerol (22:6)	Monoacylglycerol	1.446	4.91E-02
2'-deoxyinosine	Purine Metabolism, (Hypo)Xanthine/Inosine containing	1.220	1.65E-02
2'-O-methyluridine	Pyrimidine Metabolism, Uracil containing	1.512	2.04E-02
3-formylindole	Food Component/Plant	0.544	4.50E-02
docosapentaenoate (n6 DPA; 22:5n6)	Long Chain Polyunsaturated Fatty Acid (n3 and n6)	1.641	2.27E-02

gamma-glutamylleucine	Gamma-glutamyl Amino Acid	1.404	4.77E-02
oleoyl-linoleoyl-glycerol (18:1/18:2) [2]	Diacylglycerol	-0.978	3.49E-02
palmitoyl-linolenoyl-glycerol (16:0/18:3) [2]*	Diacylglycerol	2.801	1.26E-02
phenylacetylglycine	Acetylated Peptides	2.664	7.53E-03
pipecolate	Lysine Metabolism	-1.089	2.33E-02
X-17146		2.962	3.38E-02

13.2 Declaration

Except where stated otherwise by reference or acknowledgement, the work presented was generated by myself under the supervision of my supervisors Dr. Flávia Rezende and Prof. Dr. Ralf P. Brandes during my doctoral studies. NTG, PETN and ISDN were kindly provided by Prof. Dr. Andreas Daiber (Universitätklinik, Mainz, Germany). FACS-sorting of endothelial cells was carried out by Praveen Mathoor (Institute of Biochemistry I, Frankfurt, Germany). RNA-sequencing was carried out by Dr. Stefan Günther (Max-Planck-Institute for Heart and Lung Research, Bad Nauheim, Germany). The Wheat Germ Agglutinin staining was carried out by Dr. Deepak P. Ramanujam (Institute of Pharmacology and Toxicology, Technical University of Munich, Munich, Germany). Furthermore, untargeted metabolomics were carried out by Metabolon Inc. (Morrisville, North Carolina, USA). The transverse aortic constriction surgery was learned from Ina Broll (Institute of Experimental Cardiology, Heidelberg, Germany). All contributions from colleagues are explicitly referenced in the thesis.

The following parts of the thesis have been previously published:

Chapter	**Published in**
1	Lopez *et al.* (2021)[53] and Lopez *et al.* (2022)[122]
4	Lopez *et al.* (2021)[53] and Lopez *et al.* (2022)[122]
5.1	Lopez *et al.* (2021)[53]
5.2	Lopez *et al.* (2022)[122]
6.1	Lopez *et al.* (2021)[53]
6.2	Lopez *et al.* (2022)[122]

Figure number	**Published in**
16-27; 36	Lopez *et al.* (2021)[53]
28-35	Lopez *et al.* (2022)[122]

Table number	**Published in**
1	Lopez *et al.* (2021)[53]
20	Lopez *et al.* (2022)[122]

13.3 Acknowledgements

13.4 Publications

Boos F, Oo JA, Warwick T, Günther S, Izquierdo Ponce J, **Lopez M**, Rafii D, Buchmann G, Duc Pham M, Valasarajan C, Li T, Seredinski S, Haydar S, Kashefiolasl S, Plate KH, Behr R, Mietsch M, Krishnan K, Pullamsetty SS, Bibli S-I, Hinkeö R, Baker AH, Boon RA, Schulz MH, Wittig I, Miller FJ, Brandes RP, Leisegang MS. The endothelial-specific LINC00607 mediates endothelial angiogenic function. *In press*.

Lopez M, Malacarne PF, Ramanujam DP, Warwick T, Müller N, Hu J, Dewenter M, Weigert A, Günther S, Gilsbach R, Engelhardt S, Brandes RP, Rezende F. Endothelial deletion of the cytochrome P450 reductase leads to cardiac remodelling. *Front. Physiol*. 2022;13. doi: 10.3389/fphys.2022.1056369

Malacarne PF, Bezzenberger J, **Lopez M**, Warwick T, Müller N, Brandes RP, Rezende F. Epoxyeicosatrienoic Acid and Prostanoid Crosstalk at the Receptor and Intracellular Signaling Levels to Maintain Vascular Tone. *Int J Mol Sci*. 2022;23. doi: 10.3390/ijms23115939

Malacarne PF, Ratiu C, Gajos-Draus A, Müller N, **Lopez M**, Pflüger-Müller B, Ding X, Warwick T, Oo J, Siragusa M, Angioni C, Günther S, Weigert A, Geißlinger G, Lütjohann D, Schunck W-H, Fleming I, Brandes RP, Rezende F. Loss of Endothelial Cytochrome P450 Reductase Induces Vascular Dysfunction in Mice. *Hypertension*. 2022;79:1216–1226. doi: 10.1161/HYPERTENSIONAHA.121.18752

Lopez M, Malacarne PF, Gajos-Draus A, Ding X, Daiber A, Lundberg JO, Offermanns S, Brandes RP, Rezende F. Vascular Biotransformation of organic nitrates is independent of cytochrome P450 monooxygenases. *Br J Pharmacol*. 2021;178:1495–1506. doi: 10.1111/bph.15362

13.5 Curriculum vitae

13.6 Selbstständigkeitserklärung

Ich erkläre hiermit, dass ich die im Fachbereich Biochemie, Chemie und Pharmazie der Goethe-Universität Frankfurt am Main zur Promotionsprüfung eingereichte Arbeit mit dem Titel:

„The cytochrome P450 reductase enzyme contributes to normal cardiovascular function“

im Institut für Kardiovaskuläre Physiologie unter Betreuung und Anleitung von Herrn Prof. Dr. Ralf P. Brandes und Frau Dr. Flávia Rezende ohne sonstige Hilfe selbst durchgeführt und bei der Abfassung der Arbeit keine anderen als die in der Dissertation angeführten Hilfsmittel benutzt habe. Ich versichere, die Grundsätze der guten wissenschaftlichen Praxis beachtet, und nicht die Hilfe einer kommerziellen Promotionsvermittlung in Anspruch genommen zu haben.

Ich habe bisher an keiner in- oder ausländischen Universität ein Gesuch um Zulassung zur Promotion eingereicht. Die vorliegende Arbeit wurde bisher nicht als Dissertation eingereicht.

Vorliegende Ergebnisse der Arbeit sind zum Teil veröffentlicht in:

Lopez M, Malacarne PF, Gajos-Draus A, Ding X, Daiber A, Lundberg JO, Offermanns S, Brandes RP, Rezende F. Vascular Biotransformation of organic nitrates is independent of cytochrome P450 monooxygenases. *Br J Pharmacol*. 2021;178:1495–1506. doi: 10.1111/bph.15362

Lopez M, Malacarne PF, Ramanujam DP, Warwick T, Müller N, Hu J, Dewenter M, Weigert A, Günther S, Gilsbach R, Engelhardt S, Brandes RP, Rezende F. Endothelial deletion of the cytochrome P450 reductase leads to cardiac remodelling. *Front. Physiol*. 2022;13. doi: 10.3389/fphys.2022.1056369

Frankfurt am Main, April 2023

……

(Melina López Sciarra)